UiT
THE ARCTIC
UNIVERSITY
OF NORWAY

FACULTY OF SCIENCE AND TECHONOLOGY

Department of Geology

Relationship between fluid leakage and faulting along the western and northern margin of the Hammerfest Basin

Jessica Arvo

Master thesis in GEO-3900
May 2014

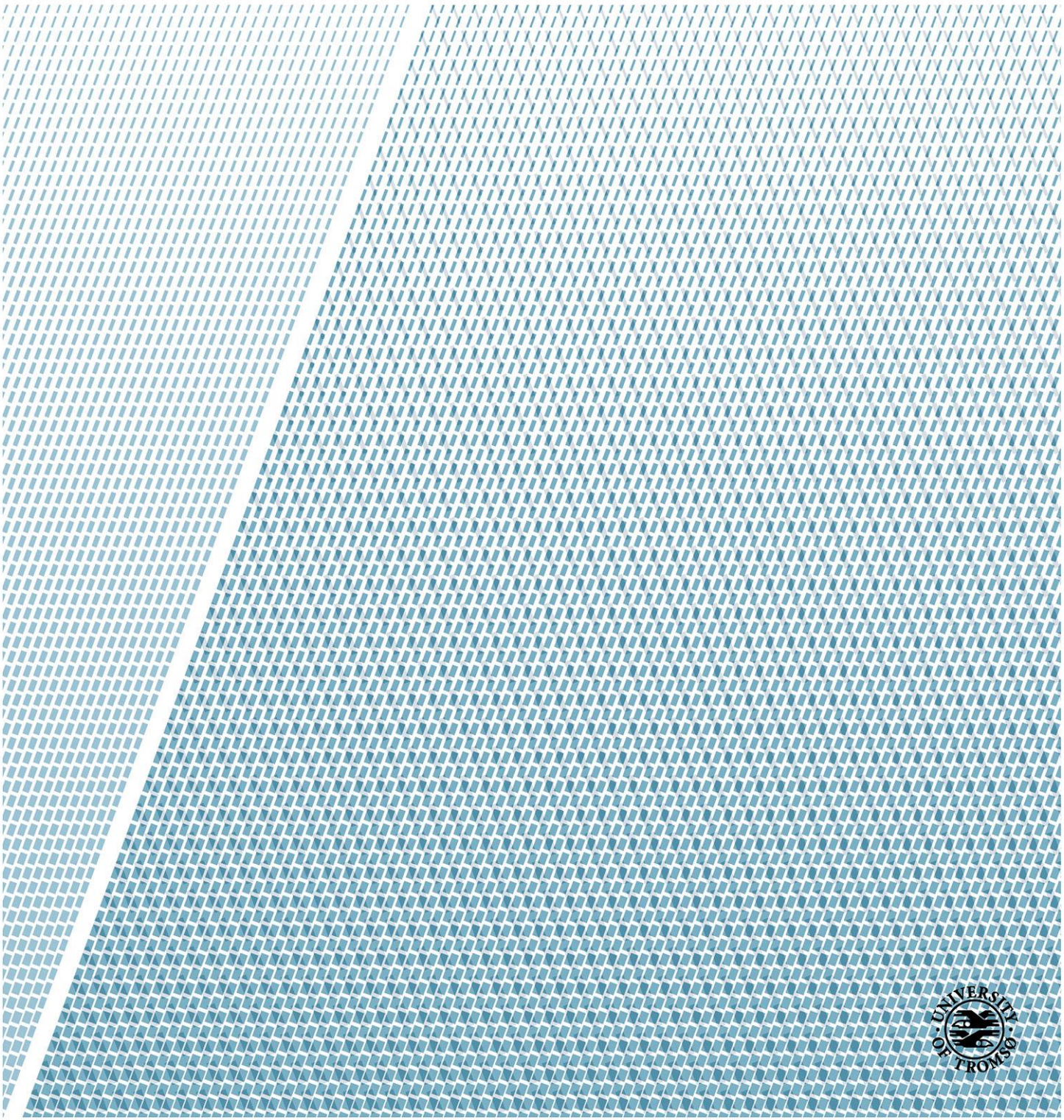

Abstract

This thesis focuses on establishing a causal relationship between potential fluid sources, fluid migration pathways, shallow gas accumulations and potential gas hydrates in the western part of the Hammerfest Basin, SW Barents Sea. Two 3D seismic surveys (LN0901 and ST8320R00) were used to map fluid flow, stratigraphy, structure, fluid flow and other fluid-related features along the western and northern border of the Hammerfest Basin. Furthermore well log data was used to supplement the seismic data and to provide stratigraphic framework of 3D seismic datasets. Widespread fluid flow features, shallow gas accumulation and has hydrates commonly occur in Tertiary succession on the Barents Sea Shelf. These features (especially gas hydrates) have had a growing interest during the last decade as a potential energy resource and as an agent in climate change. Shallow gas accumulations can cause, and have caused, major drilling and engineering hazards around the world. Both hydrates and shallow gas accumulations represent significant geohazards and is therefore important to better understand their occurrence formation mechanism and potential impact on exploration in the SW Barents Sea, a major Norwegian petroleum province.

In general three main types of faults are identified between the Hekkingen Formation and the Torsk Formation; these are 1) Large deep-seated faults, 2) Polygonal faults and 3) Smaller shallow faults. The large deep-seated faults are interpreted to be a result of early initiation and later reactivation in two main rift phases. During Late Jurassic- Early Cretaceous period (from c. 160 Ma) a first rift phase probably occurs. Continental rifting continues through the Cretaceous and into Cenozoic. In Plaeocene-Early Eocene another rift-phase occurs. Polygonal faults are interpreted to be a result of dewatering of Late Cretaceous deposits and penetrat into lower Paleocene strata. The smaller, shallow faults could be the result of later smaller tectonic activity and/or from unloading and isostatic rebound related to glacial growth and decay.

Likely evidence of vertical fluid migration through faults exists in form of acoustically masked areas close to the faults and high amplitude zones at depth where many of the deeper faults terminate towards shallower strata. Here, most of the vertical fluid migration seems to terminate in shallow gas accumulations in the Tertiary succession, just below URU. The Quaternary succession above mostly acts as sealing- and overburden rock for the shallow gas accumulations, which as a consequence often spread laterally beneath impermeable beds. However, in few instances, fluids may migrate laterally along updipping strata or even create

enough overpressure to create small pathways, e.g. pipes, to the seabed. Pockmarks are observed occasionally on the seafloor associated with the aforementioned fluid migration pathways. However, their formations might also be related to the dissociation of gas hydrates after the retreat of the ice sheet.

Acknowledgement

Da går det mot slutten av studie tiden og mange fine år som student er snart over. Da er det vel også på tide og bli voksen! Arbeidet har alltid vært like lett, og i den anledning til jeg takke de personene som har hatt med meg og gjøre den siste tiden.

Ganz besonders möchte ich meinem Berater, Stefan Bünz für die guten Rückmeldungen und die hilfreoche Leistung im koorrigieren meiser Arbeit danken. Sie hatten immer Zeit gefunden, mir hilfreich beizustehen. Nochmals vielen dank für alles, ich habe viel gelemt in diesen Monaten.

Malin fortjener en stor takk som har lest gjennom oppgaven utallige ganger og alltid vært positiv og flink til å motivere.

Jeg vil også takke alle de fantastiske studentene som jeg har blitt kjent med og alle de gode lunsj pausene på "brakka". En ekstra takk til Karoline som har vært en god støttespiller gjennom det siste året, og for alle gode samtaler, både faglige og ikke faglige.

Det har vært mange lange kvelder og krevende jobb for å gjennomføre masteren, og jeg er veldig takknemlig for å ha fått en så god venn som Trude og dele all slitet og de morsomme stundene sammen med meg.

En takk går til Martine som har tatt vare på meg gjennom denne perioden meg lange dager på skolen og vært så snill og laget middag til meg når jeg selv ikke gadd.

Til slutt vil jeg til takke pappa for gjennomlesing og retting av engelsk, og mamma som alltid har vært tilgjengelig på telefon og motivert meg videre når det har gått tyngst.

Nå gleder jeg meg til et nytt kapitel i livet.

Jessica Arvo

Tromsø, Mai 2014

Contents

1.1 Obectives 1
1.2 Fluid migration systems 2
1.3 Dynamics and physical laws 4
1.4 Seismic indications of fluid flow 5
1.5 Migration models 7
1.5.1 Lateral fluid migration 7
1.5.2 Vertical fluid migration 7
1.6 Gas hydrates and shallow gas 12
1.7 Pockmarks 13
2.1 Introduction 15
2.2 Tectonic settings of the SW Barents Sea 16
2.2.1 Geological history 16
2.2.3 Hammerfest Basin 23
2.3 Stratigraphy 23
2.4 Source rock 26
2.5 The effect of the uplift and erosion from Cenocoic 27
3.1 Dataset 29
3.1.1 3D seismic dataset 30
3.2 Seismic resolution 31
3.2.1 Vertical resolution 31
3.2.2 Horizontal resolution 32
3.3 Wells 34
3.4 Artefacts 37
3.5 Methods 38
3.5.1 Seismic attributes 38
3.5.2 Stability modeling of gas hydrates 38
4.1 Seismic stratigraphy 41
4.1.2 Upper Regional Unconformity (URU) 45
4.2 Faults 46
4.2.1 Deep, larger-scaled faults 46
4.2.2 Shallower fault-systems 48
4.3 Shallow gas accumulation 52

4.3.1 Amplitude anomaly 1 53
4.3.2 Amplitude anomaly 2 54
4.3.3 Amplitude anomaly 3 54
4.3.4 Amplitude anomaly 4 57
4.3.5 Amplitude anomaly 5 57
4.3.6 Amplitude anomaly 6 58
4.4 Vertical fluid migration 60
4.4.1 Small vertical fluid zone 60
4.4.2 Potential fault related leakage zones 63
4.5 Morphological circular to sub-circular depressions on the seabed 69
5.1 Faults 78
5.2 Vertical migration of fluids 82
5.2.1 Potential source rock 82
5.2.2 Fluid flow along chimneys 86
5.2.3 Fluid flow along faults 87
5.3 Lateral mechanism 89
5.3.1 Lateral fluid migration and fluid accumulation 91
5.3 Presence of gas hydrates 91
5.3.1 GHSZ modeling 92
5.5 Indication of fluid leakage on the seafloor 96
5.5.1Formation of the depressions 96
5.6 Model of fluid migration and accumulation 100
6. Clonclusion 103
7. References 105

1. Introduction

1.1 Obectives

The main objective for this master thesis is to map and determine the shallow gas accumulations and structural features along the western and northern border of the Hammerfest Basin (figure 1-1). The study is based on analysis of two 3D seismic cubes from the area (LN0901 and ST8320R00). Previous studies of the SW Barents Sea (Andreassen et al., 2007a; Chand et al., 2008; Vadakkepuliyambatta et al., 2013) indicates that fluid migration occurs along faults. In certain circumstances overpressure can have caused gas expansion which lead to leakage from the accumulations area. The fluid migration can lead to formation of acoustic masking and structures on the seafloor, as pockmarks (Hovland, 2003).

The Barents Sea has undergone uplift and glacial erosion which may have affected the pressure regime in the area, which might be interesting when studying the fluid migration.

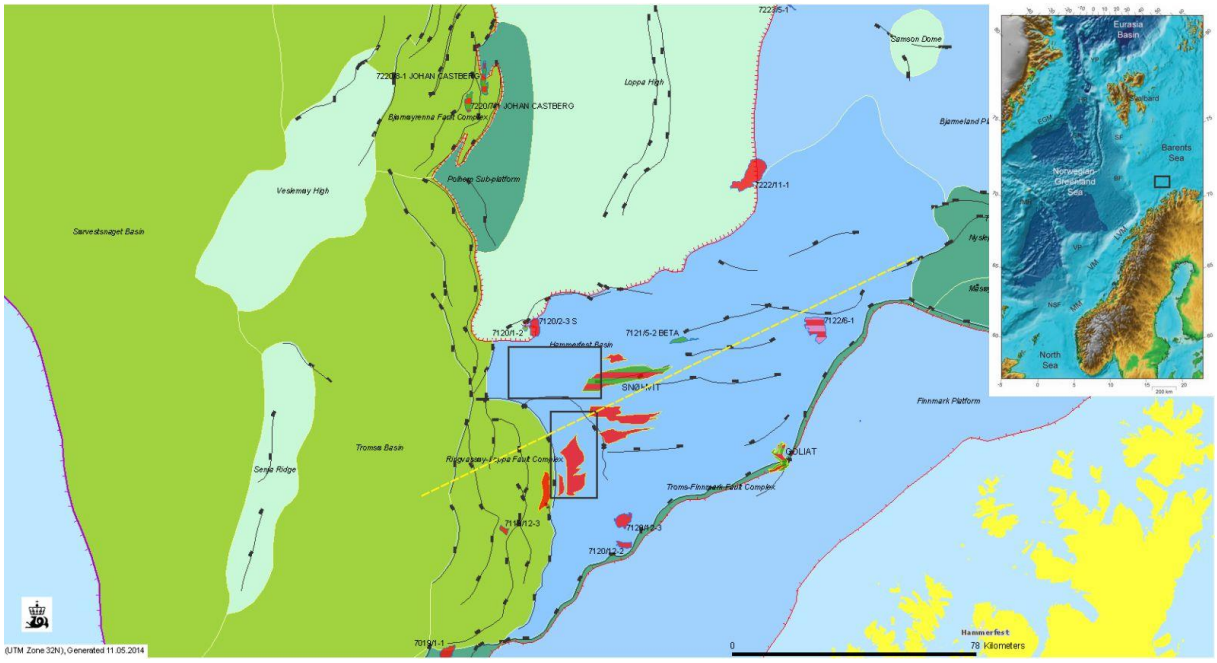

Figure 1- 1. . The SW Barents Sea with structural elements, the study area within the north-western part of the Hammerfest Basin shown in the two black triangles. Figure from Faleide et al. (2008) and NPDs fact pages (2014). The yellow, dotted line shows the position of the geological evolution described in chapter 2 (figure 2-5).

1.2 Fluid migration systems

Fluids are often trapped in pore spaces between sediments and rocks, which will affect the fluids when sedimentation and compaction occurs. The fluids may change phase between gases, liquids or solutions (Guzzetta and Cinquegrana, 1987). In the subsurface the compaction and sedimentation will increase with depth which would influence the liquids to be displaced upward because the density is lower than the surrounding solids. The liquid can also be entrapped during emplacement in rock bodies (like water in sediments) (Guzzetta & Cinquegrana, 1987).

The fluid flow at the subsurface occurs mainly from complex fault systems, salt diapirs and will mainly be trapped in the highest point of a permeable rock unit (Selley, 1998).

Fluid migration is defined when petroleum migrates from the source rock to the reservoir rock. This process is defined when petroleum is transported as a separated phase and mainly driven by buoyancy of petroleum relative to water (Bjørklykke, 2010). The solubility for most oil compounds is very low but for gas it will be much higher especially if it obtains methane. Oil, gas and water occur in porous, permeable reservoir rocks. It is stratified according to their relative density which will provide the opportunity to migrate free, both vertically and laterally (Selley, 1998).

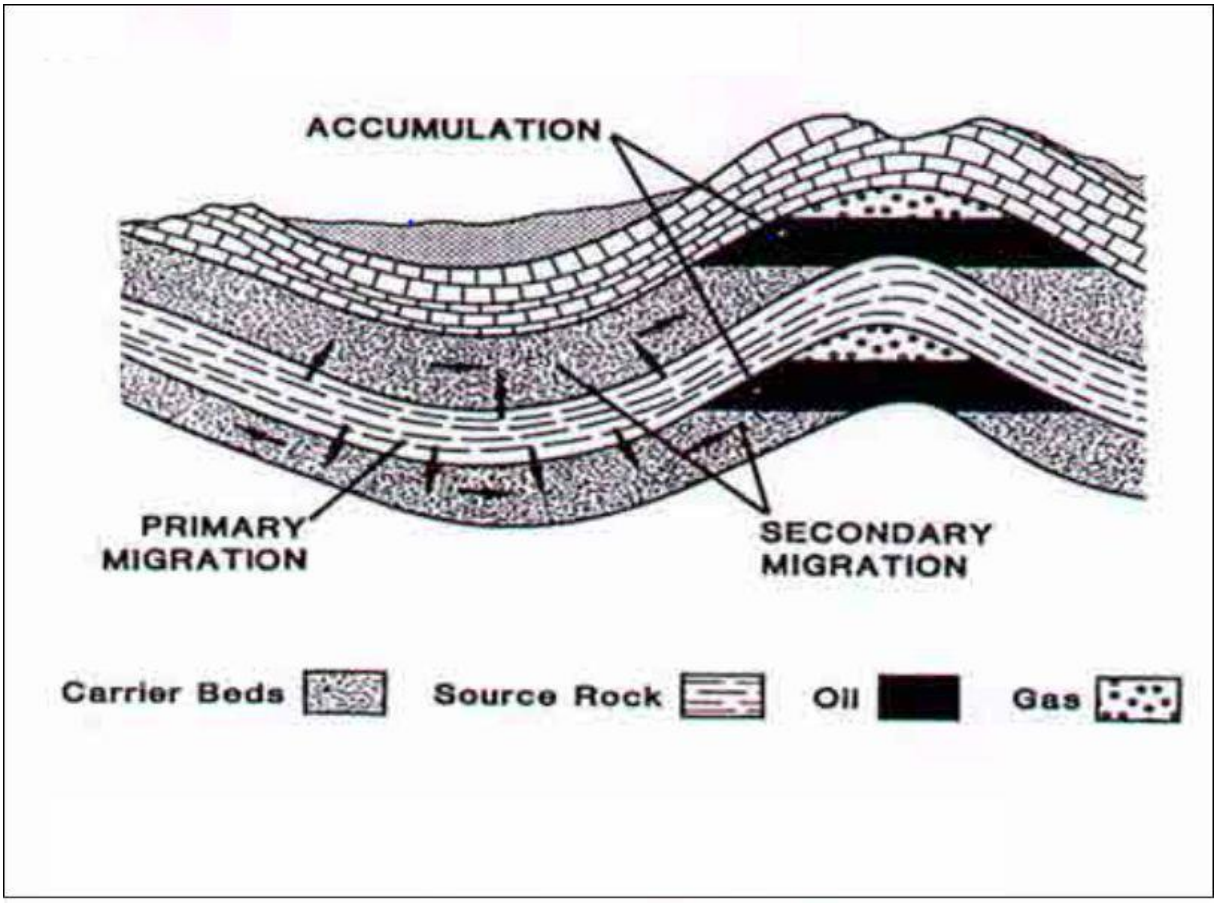

Figure 1- 2. The figure shows fluid migration from source rock to reservoir. Primary migration occurs when the kerogen converts to hydrocarbons and migrates directly out of the source rock. Secundary migration occurs along the permeable units. Because of the difference in denisty the gas will be lying on the top above the oil/water in a reservoir. The figure is from Tissot and Welte (1984)

There are three types of petroleum migration, two of which are most important. Primary migration (figure 1-2) occurs when hydrocarbons emigrate from low permeable source rocks into carrier beds. The kerogen expands when it's transformed into fluid of oil or gas because the density of the primary kerogen will be higher than the remaining solids in the kerogen. Even if this doesn't cause a big volume expansion, it will be contribute to an overpressure due to the main factor which is the change in the void ratio when solid kreogen is altered to fluid petroleum (Bjørklykke, 2010; Selley, 1998)

Secondary migration (figure 1-2) occurs when hydrocarbons flows from the source rock to the reservoir rock. This must be understood in terms of two-phase flow and in some cases three-phase flow (Bjørklykke, 2010). This migration will occur by buoyancy due to the different densities of the fluids and the response from the differential pressure. The secondary migration occurs when the petroleum is identifiable as crude oil and gas (Selley, 1998). When the expulsion of the primary migration from the source rock has achieved, the oil and gas will

flow upwards caused by buoyancy, where high oil saturation will increase the relative permeability. Secondary migration will be occurring if there is continuous pathway from the primary migration. The pathway will be established by the petroleum saturation, where the flow is prevented from high capillary entry pressure or low permeability (Bjørklykke, 2010). Most of the migration of oil and gas occurs in separate phases and flows by the driving force of the buoyancy of the hydrocarbon phase in water. The migration will always be dependent on the size of pore throats along continuous pathways for hydrocarbon migration (Bjørklykke, 2010).

1.3 Dynamics and physical laws

The physical properties of sedimentary rocks will change accord to burial depth due to temperature and pressure increase, while the porosity and permeability decreases. Compaction depends on the lithology of the sedimentary rocks where sandstones density increases almost linearly with depth. During deposition of fine grained sediments such as clay, porosity value tends to be high just after deposition and compact mostly in the first 1000 m. From 3000 m and deeper, further compaction is digenesis of clay minerals. When porosity decreases with depth, fluid flows is likely to occur (Berndt, 2005; Bjørlykke, 2010).

The principle of how fluids move in the subsurface is called Darcy's law (Equation 1) which describes how fluids flow through a permeable medium in response to a hydraulic potential field (Berndt, 2005). The law defines how much fluid is able to flow between two points of a rock, which depends on the properties of the conduct fluid, the rocks properties, and the pore-water pressure difference between the two ends of the flow (Berndt, 2005). Darcy's law explains the fluid flow in the subsurface except when the underlying assumption of the flow through a bulk medium with a given conductivity is not valid. In the subsurface the rocks are deposited as layers, and the fluid flow between these layers is conducted by the permeability (Berndt, 2005).

Darcy's law:

$$F = k \times \frac{\nabla P}{\mu} \qquad \text{(Equation 1)}$$

$F = \left[\frac{m^3}{s}\right]$ Fluid flux $\qquad k = [m^2]$ permeability

$\nabla P = [Pa]$ Pressure gradient $\qquad \mu = \left[\frac{N \times s}{m^2}\right]$ viscosity

It is important to understand what causes the rise to pressure difference since Darcy's law depends on the presence of hydraulic heads (Berndt, 2005).

1.4 Seismic indications of fluid flow

Seismic reflection occur when there is a change in acoustic impedance, which is a product of the compressional wave velocity (V) and density (p) (Andreassen et al., 2007a). Seismic reflections occur where there is a change in the sedimentation conditions and where there is a lithology change, as well as a variation in the pore content (Veeken, 2007). For example there will be a dramatic reduction in Vp when gas is presence in the sediment pore space (Veeken, 2007).

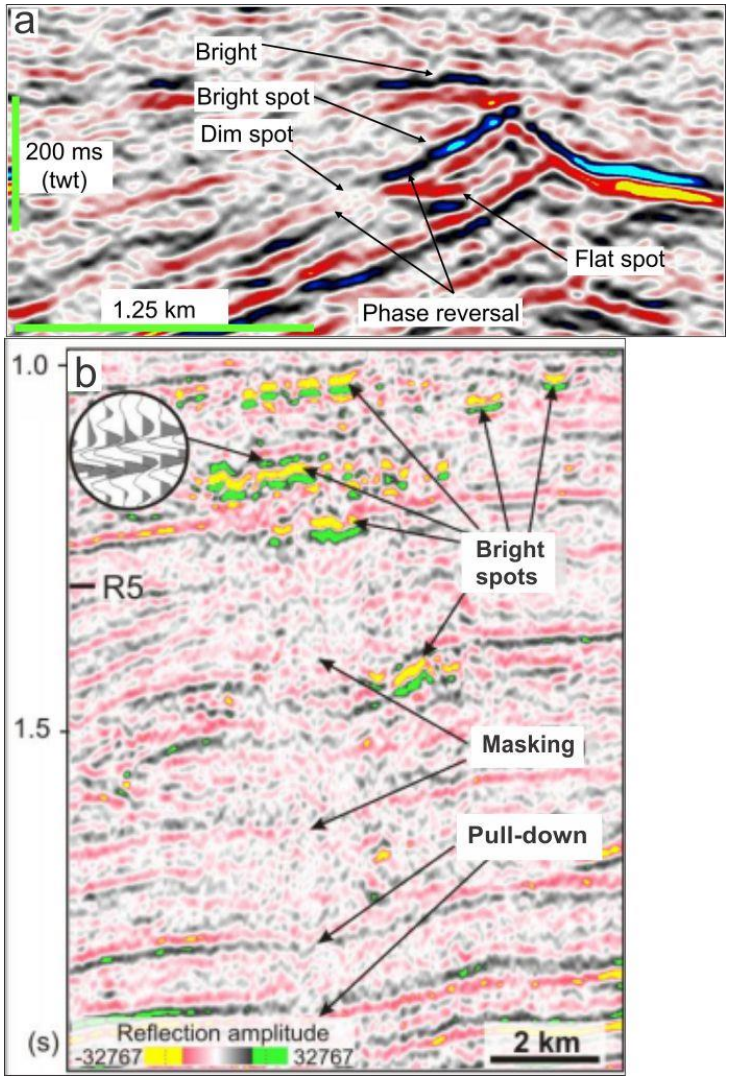

Figure 1- 3. a and b show bright spots, dim spots, flat spot, phase reversal, acoustic masking and push-down. Figure a) is from Løseth et al. (2009). Figure b) is from Andreassen et al. (2007a)

An acoustic impedance contrast will occur if the gas column is thick enough. This contrast can be between gas-/oil or the gas-/water-filled portions of a reservoir and a reflection commonly called a flat spot will result (figure 1-3; Badley, 1985). Flat spots can be a good indicator for hydrocarbon/water contact because of its flatness (Andreassen et al., 2007a).

Bright spots (figure1-3) are reflections that occur by the presence of gas which have high amplitude and reversed phase compared with the seafloor reflection (Andreassen et al., 2007a). The high amplitude reflections occur where there is gas on top of unlithified and relatively high-porosity sediments. Gas in pore spaces, especially in porous sediments, causes a reduction in the acoustic velocity and a lower density (Andreassen et al., 2007a).

Dim spots are seismic reflection with anomalously low amplitude (figure 1-3). Zones where the reflections are weaker/lower than the adjacent areas are where reflection continuity and amplitude are reduced. Such zones can be localized above hydrocarbon accumulations (Andreassen et al., 2007a; Løseth et al., 2009).

Pull-down can occur as underlying reflectors when the gas column is sufficiently thick (figure 1-3). The decrease of the velocity in gas makes it seem like the reflector beneath lies lower than it actually does. This effect is most likely in areas where the gas accumulation is high. The opposite effect, pull-ups, occurs in areas where there is an increase in the velocity (Badley, 1985).

Gas chimneys are zones where patchy appearance of gas will give irregularly distributed low-velocity (figure 1-4). Seismic data has shown that low-velocity gas patches are irregularly distributed in low permeable shales (Arntsen et al., 2007; Løseth et al., 2009). Based on studies, gas chimneys occur where there are fracture cap rocks. Since gas chimneys are associated with low-velocity anomalies, pull-downs may be observed beneath the chimneys, and bright and dim anomalies are often observed above gas chimneys (Løseth et al., 2009). Gas chimneys have been interpreted as hydrocarbon leakage pathways (Arntsen et al., 2007).

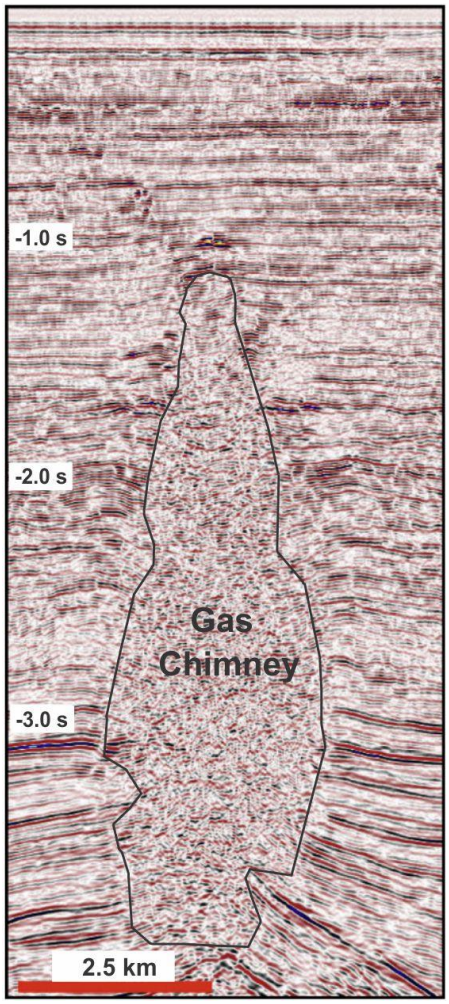

Figure 1- 4. Seismic expression of a vertical obelix-shaped wipe-out zone located over a salt dome which is interpreted as a gas chimney. The wipe-out zone has a sharp outer boundary shown as the black outer body. Figure is modified from Løseth et al. (2009).

1.5 Migration models

Migration pathways are controlled largely by structural morphology (Hindle, 1997). The migration pathway is determined by the interrelationship of sediment fill, sedimentation rate, tectonics and fluid flow (Hindle, 1997). Petroleum fluids move from high to low fluid potential. These fluid potential are caused by variation in excess water pressure and the natural buoyancy of the less dense petroleum in a medium that is filled with denser water and capillary pressure differences (England et al., 1987).

1.5.1 Lateral fluid migration

Fluid migration will only occur laterally trough rocks if the applied pressure is greater than the opposing capillary pressure. Petroleum will only migrate laterally if the carrier bed is permeable (England et al., 1987). Lateral petroleum migration can occur over tens to hundreds of kilometers between source rock and trap between accumulation and the surface (Trasher et al., 1996).

1.5.2 Vertical fluid migration

The two main driving forces for hydrocarbons after they have left the source rock are buoyancy and groundwater flow. The buoyancy force is dependent on the density difference between the petroleum phase and the water phase. The buoyancy phase increases as the density difference increases. This buoyancy force drives the hydrocarbons vertically upwards (Hindle, 1997).

If fluids flow vertically through a seal, they act as a seal bypass system (SBS). These systems allow fluids to bypass the pore network. Cartwright et al., (2007) have exhibited a range of examples of SBS-affecting contrasting types of sealing sequences using three-dimensional seismic data. These examples show evidence of vertical flow through the seal sequence, with internally leakage at higher levels or the surface (Cartwright et al., 2007). SBS is classified into three groups of vertical fluid migration: (1) fault related, (2) intrusion related, and (3) pipe related (Cartwright et al., 2007).

1.5.2.1 Fault related fluid flow

Faults are mainly caused from tectonic activity or from deposition of sediments where water-rich sediments are overlain by impermeable sediments. The faults may provide permeable vertical pathways through the otherwise impermeable strata (Laberg et al., 1998; Wirprut & Zoback, 2000; Gay et al., 2006; Ostanin et al., 2012). It is important to know petrophysical properties of faults to gather information for how the faults will be acting as seals or fluid migration pathways for hydrocarbons (Fisher & Knipe, 2001). The permeability of the fault-

rocks is very important for the internal structure and external geometry. The composition of each component plays an important role in controlling the patterns and rates of fluid flow in and around the fault zone (Caine et al., 1996). Faults zones may contain large interconnected fractures that act as good pathways for vertical fluid flows. They may be useful as traps or may be cemented as good seals (Løseth et al., 2009). Fault zones are the main conduits for fluid many places worldwide, especially in the deeper subsurface where there is consolidated to completely lithified rocks (Ligtenberg, 2005).

Large-scaled faults often form one or several boundaries in a petroleum field where hydrocarbons can be trapped or open joints for fluid migration (Fisher & Knipe, 2001). The larger-scaled deep faults can often be a pathway for fluid migration to the shallower fault complex (figure 1-5). In seismic data, reflections show highly chaotic and low-amplitude close the faults zones, indicating the migration of gas through the sediments. If there is high amplitude anomalies along the fault plane indicates the presence of gas (Løseth et al., 2009; Cartwright et al., 2007; Ligtenberg, 2005;
Vadakkepuliyambatta et al., 2013).

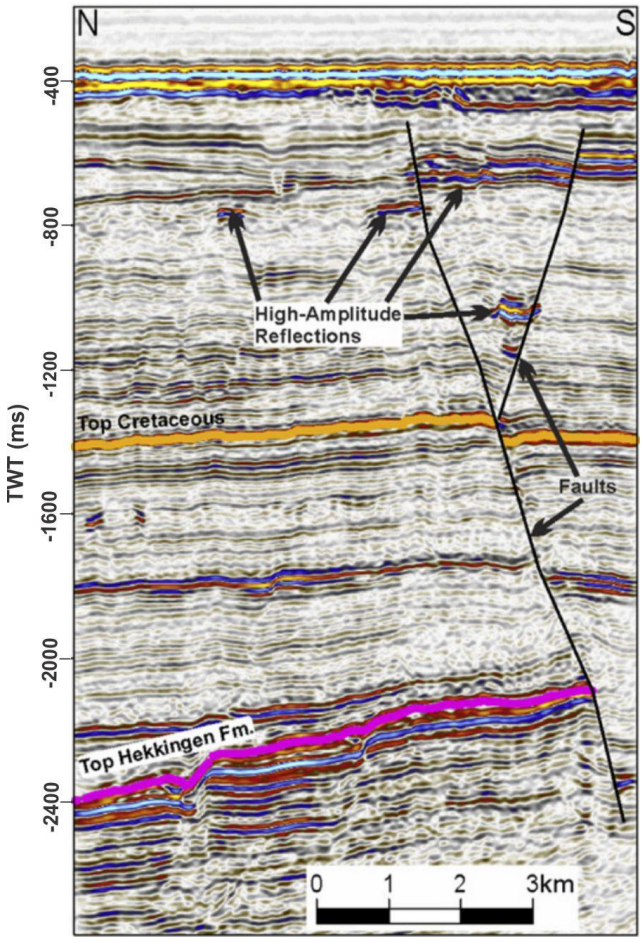

Figure 1- 5. Seismic section shows fluid leakage along faults, from deeper to shallower section and terminates into high amplitude anomaly from the northwestern part of the Hammerfest basin. From Vadakkepuliyambratta et al. (2013).

Polygonal faults are a result of compaction during burial and fluid migration within a certain layer (Berndt, 2005). These fault structures often terminate in pipe structures, which conducts the expelled pore fluids towards the surface (Berndt, 2005; Berndt et al., 2003). Polygonal faults either influence the fluid propagation in the sediments or representing preferred fluid pathway as they are zones with high vertical connectivity (Berndt, 2005; Cartwright, 1998; Ostanin et al., 2012). They are shown to be the result of sediment contraction and fluid expulsion (Berndt, 2005). Small fractures are important for potential hydrocarbon conduits (Smith, 1966), but is difficult to enhance on seismic data and therefore faults that are seismically resolvable confined as fluid-migration pathways (Cartwright et al., 2007). Normally the permeability of the fault zone rocks is lower than their host rocks, and there will be a low steady flow leakage. At shallow depth faults may become sealed by gas hydrates if shallow faults occur within the gas hydrate stability zone (Knipe, 1997; Chand et al., 2008; Ostanin et al., 2012). Direct evidence of leakage from faults are pockmark craters that are aligned vertically above the upper tips of the fault planes (Heggland, 1997; Ligtenberg, 2005; Cartwright et al., 2007).

1.5.2.2 Intrusions

Intrusive structures occur when the intrusion breaks the sealing sequence. There are four examples of different types of intrusions; sandstone intrusions, ingenious intrusions, mud diapirs and salt diapirs (Cartwright et al., 2007).

Magmatic- and sandstone intrusion are the two main types of sheet intrusions (Polteau et al., 2008). Intrusions of fluidized injected sands can get up to several kilometers long of sandstones dikes and sills in petroleum systems (Cartwright et al., 2007; Polteau et al., 2008). These intrusions of sand may form hydrocarbon reservoir or high-porosity fluid migration pathways. They often cut horizontal sedimentary strata and create a local doming of the overburden sediments (Polteau et al., 2008). They can intrude high-quality sealing sequences and provide a secondary migration pathway. After formation of a sandstone intrusion they might be open as a highly permeable conduit for many millions years, before the pore space gets cemented (Cartwright et al., 2007).

The igneous intrusions have lower permeability than the host sealing facies, but the intrusion of hot magma into cold and wet sediments causes a major change in the host rocks properties (Cartwright et al., 2007). The intrusions are related to voluminous magmatism in undeformed sedimentary basins and may act as water reservoir and barriers (Ploteau et al., 2008). There

Fracturing will occur under the intrusion, due to the metamorphism and contraction fracturing longer term cooling of the intrusive body itself will occur (Cartwright et al., 2007). The fracturing that is developed will modify fluid-flow behavior around the intrusion during and after the intrusion event (Cartwright et al., 2007).

"Mud diapirs are bodies of muddy sediment driven upwards by buoyancy forces arising from the bulk density contrast between an over pressured muddy mass and an overburden of greater density" (Hovland, 2003) mud diapirs are associated with mud volcanoes (Cartwright et al., 2007). The intrusion or extrusion of mud is a phenomena where fluid rich, fine grained sediments ascend within a lithologic succession due to their buoyancy (Kopf, 2002). The thickness of a mud diapir can be up to several kilometers in sedimentary sequence. They occur mainly in areas with convergent plate margins, where the sediment is affected by lateral compression and are often associated with faulting at fault intersections (Hovland, 2003). At a convergent plate margin the sedimentation rate is normally very high and fluid rich sediments are buried (Kopf, 2002). Salt diapir growth often associated with forced folding, radial and concentric faulting. These deformations can exert a major impact on fluid-flow regimes and seal integrity (Cartwright et al., 2007). Salt buried beneath denser overburden will therefore be buoyant. Salt diaprism due to differential loading may be induced by gravitational forces. The salt will only move if the driving force exceeds the resistance to flow (Hudec & Jackson, 2007). Salt diaprism can create structural traps influencing reservoir distribution, and the salt itself can be a good seal to fluid migration. The growth of a diaprism is mostly episodic and often follows the cycles established by regional tectonics. Fluid flow which is associated with salt disprism occurs via complex fracture networks and are also likely to be episodic (Hudec & Jackson, 2007; Cartwright et al., 2007).

1.5.2.3 Gas chimneys and pipes

Fluid migration path often appear gas chimneys which are vertical- to near-vertical zone of fluid flux (figure 1-4) (Ligtenberg, 2003). The shape of gas chimneys can vary from diffuse shadows, funnels, pipes (figure 1-6), to distinct cigars or obelixes (Løseth et al., 2009). They occur when there is transported gas from reservoirs into caprock through a connected fracture network followed by diffusion (Arntsen et al., 2007). As mentioned in chapter 1.4, gas chimneys can be associated with upward fluid migration. They can be caused by gas released from upward moving water due to pressure release and are frequently linked to features such as faults, pockmarks, mud volcanoes and carbonate formations (Heggland, 1998; Løseth et al., 2009). The general texture of the internal structure of gas chimneys shows a chaotic reflection

pattern of low energy (figure 1-4; Heggland, 2008). Often only the large gas chimneys can be seen in the seismic (Ligtenberg, 2003). Gas chimneys often terminate in the shallower stratigraphy, with high amplitude anomalies at their upper limit which can indicate the presence of gas (Vadakkepuliyambatta et al., 2013).

Pipes are best defined as columnar zones of disturbed reflections that may or may not be associated with sub vertically stacked amplitude anomalies (Cartwright et al., 2007). They normally form a high-permeable vertical zone also known as a "seal bypass system" (Cartwright et al., 2007) where fluids and gas can be transported faster than in a network of normal permeable sediments (Løseth et al., 2011). Pipes are commonly circular or sub-circular in plan-form and are therefore easy to identify in 3-D seismic volumes (figure 1-6). Pipes are laterally narrow, about 20-300 m wide, circular zones and show up-bending, low-amplitude reflections (Berndt et al., 2003). Evidenced caused by fluid flow can be the creation of pockmarks (Hovland, 2003).

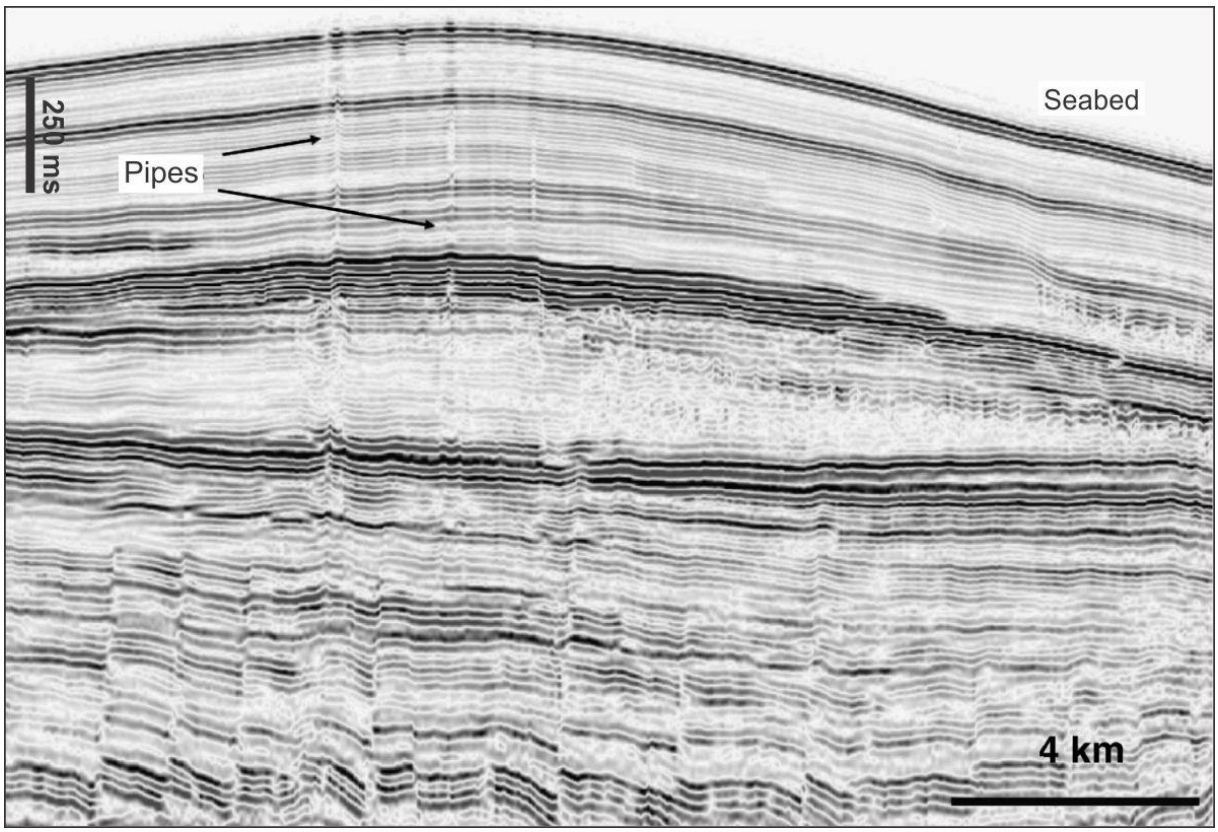

Figure 1- 6. Seismic expression of pipes arising from a low-relief anticlinal structure. Figure from Berndt et al. (2003).

1.6 Gas hydrates and shallow gas

Gas hydrates are crystalline compounds that contains methane or other low molecular weight gases (figure 1-7), which occur when water forms a cage like structure around smaller guest molecules (Sloan, 1998a). The hydrate formation occurs in low-temperature and high-pressure environment. The stability of gas hydrates depends on the pressure, temperature and gas concentration in the surrounding pore water as well as the water activity (Liu and Flemings, 2006; Sloan, 1998a). Methane is most common gas in hydrates, but heavier hydrocarbons, carbon dioxide and hydrogen sulphide may occur. There are three forms of hydrate structure I, II and H, where structure I is the most common in nature (Sloan, 1998a, Chand & Minshull, 2003).

Figure 1- 7. Gas hydrate from a core sample from Gulf of Mexico in 2002. They are not stable in atmospheric conditions so they are stored under right temperature and pressure condition to be preserved. Figure from Barth et al. (2006).

Gas hydrates are stable in the upper few hundred meters of the geosphere on the continental margin. This zone is called the gas-hydrate stability zone (GHSZ) (figure 1-8). The bottom zone of the GHSZ is dependent on the geothermal gradient, bottom water temperature, pressure, gas composition, pore water salinity and the physical and chemical properties of the host rock (Bunz et al., 2003). An increase in either temperature or pressure will release gas from the hydrates. As gas hydrates may cement sediments and increase their shear resistance, a more stable slope may occur. A change in GHSZ may also modify the stability of the slope, and as a result, gas-hydrates dissolution may cause slope failure. Dissolution of hydrates can be caused by liquefaction and the gas hydrates can become underconsolidated, resulting in gas

being caught beneath the hydrates of an unestablished weak layer of overpressurised sediments (Bunz et al., 2003). Gas-hydrates occasionally detected in seismic reflection data due to bottom-simulating reflectors (BSR) (figure 1-8), which have high amplitudes and reversed polarity that is sub-parallel to the seafloor. The BSR occur in seismic due to an acoustic impedance contrast between the hydrate-bearing sediments and free gas trapped in the sediments beneath the gas hydrates. Hydrate-bearing may be without the occurrence of BSR if no gas caught underneath (Chand & Minshull, 2003, Bunz et al., 2003).

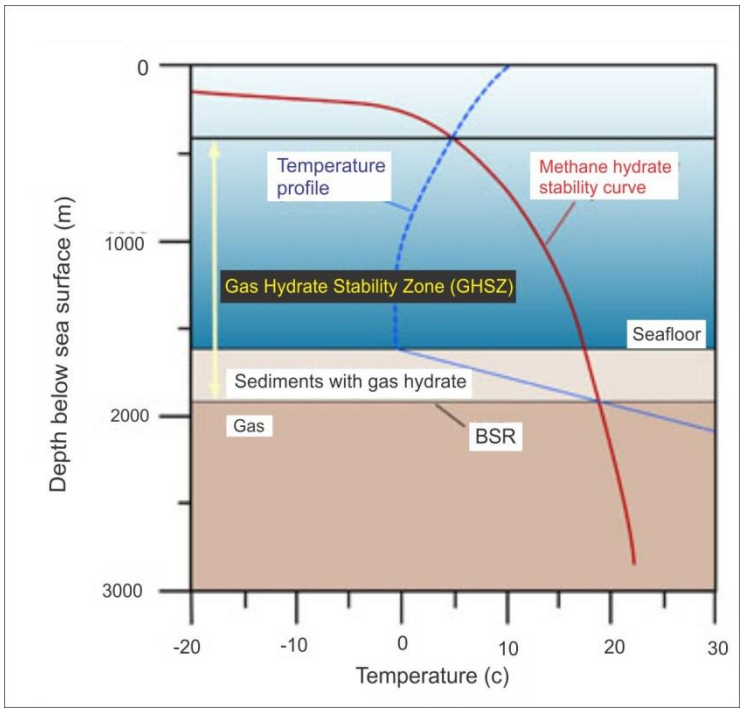

Figure 1- 8. Phase diagram for has hydrates. As long as the gas hydrates are within the gas hydrate phase diagram, along the red line, they are stable. Fluids with occur outside this stable zone will occur as free gas or water. At the bottom of the stability zone a BSR can be formed. Figure modified from Chand & Minshull (2003).

On seismic data gas hydrates are often associated with seismic wipe-outs, reflector terminations, seeps and acoustic turbidity (Hovland & Judd, 1988). Wipe-out and pipes have low reflectivity and are associated with gas migration or vertical fluids. These zones can reach the seafloor and are often connected with pockmarks (Chand & Minshull, 2003). In deeper parts of seismic sections there are reflectors that are characterized by pull-ups and pull-downs. Faults act as conduits for fluid flow and heat which may disturb the BSRs. In these areas there may be active gas venting, pockmarks and chemosynthetic organisms. Gas hydrates normally do not extend to the seafloor because the concentration of gas is less than the solubility in the shallowest sediments (Chand & Minshull, 2003).

1.7 Pockmarks

Pockmarks are crater-like depressions found on the seabed (figure 1-9) they can be related to focus fluid flow and are normally found in low permeable, fine-grained sediments. The size and shape of pockmarks can vary greatly and have been subdivided into six morphological

classes. They range in diameter from 0.5 m to 45 m in depth and vary in size from 1 to 700 meters,and can occur as single or appear as chains on the seafloor. There are different types of pockmarks which characterize their size, location, internal character and composite structure when individual pockmarks merge into each other (Ligtenberg, 2005; Hovland et al., 2002; Løseth et al., 2009).

Pockmarks are commonly located in areas where gas is associated with sediments in near-surface environments and where gas chimneys break the seafloor (Cathles et al., 2010). Pockmarks can be a result from present or past fluid migration along fault structures (Hovland & Judd 1988; Ligtenberg, 2003). Groups of pockmarks can be found in circular to semi-circular patterns which can be related to diagenesis and cementation of the sediments into impermeable rocks directly above fluid flow (Ligtenberg, 2005). Pockmarks can also occur in buried sediments, and these can be useful indicators of fluid flow in the past and possibly represent hydrocarbons in the deeper subsurface (Heggland, 1998; Ligtenberg, 2005).

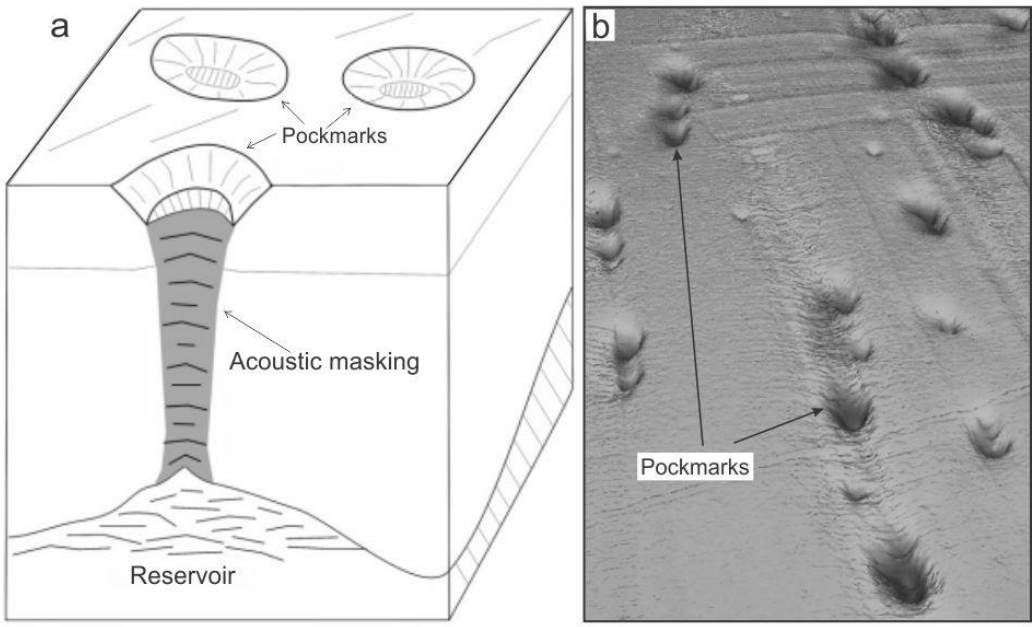

Figure 1- 9. ***a***: Pockmarks occur on the top of the acoustic masking structure where it breaks the seabed. *b*: Appearance of pockmarks on the seabed. Figure *a* is modified from Hovland (1989) and figure *b* is from Judd and Hovland (2007).

2. Study area

2.1 Introduction

The Barents Sea is a region that is bordered in the north by the Norwegian and Russian coast, the Novaya Zemlya, Franz Josef Land and Svalbard archipelagos, and the eastern margin of the deep Atlantic Ocean (figure 2-1) (Dore, 1995). This is an area of about 1.3 million km² with a water depth averaging about 300 m. (Dore, 1995). The Barents Sea is one of the world's largest epicontinental seas, which is underlain by a thick sediment pile, likely of Palaeozoic and Mesozoic age and major structural features in the area are defined. From multichannel reflection data gathering taken in the early 1970s hydrocarbon potential in the area was discovered (Gabrielsen, 1984). Since then there have been collected thousands of multichannel seismic reflections and seismic profiles. Most of the discoveries and wells that have been drilled have occurred in the Hammerfest basin. The largest gas field discovery on the Norwegian side of the Barents Sea is the Snøhvit field (Faleide et al. 1993; Dore 1995).

Figure 2- 1. The Barents Sea position is north for Norway and by the northern coast of Russia (Wikipedia, 2014). The red rectangle shows the position of the study area.

2.2 Tectonic settings of the SW Barents Sea

Lower to Middle Devonian sedimentary strata is preserved in a large north-south oriented graben (Gudlaugsson et al., 1998). In the Middle to Late Devonian the Late Caledonian compressional system changed to a left-lateral shear regime and strike-slip movements. These tectonic regimes were dominant for structural development in the Barents Sea (Faleide et al., 1984).

As a result of the opening of the Norwegian-Greenland Sea and the Eurasian Basin during the Late Paleocene development predominately in the western Barents Sea a weak sheared margin occurred (Faleide et al., 1984). This extension led to a major north-east Atlantic rift. These altered rift zones in the Barents Sea influence the fault zones of later periods to follow the weak zones (Gudlaugsson et al., 1998)

In the Middle Oligocene the western margin developed rifted passive margins that caused a shift in the pole of plate rotation. When parts of the Barents Sea were uplifted little tectonic activity was developed (Faleide et al., 1984).

2.2.1 Geological history

Paleozoic

The Barents Sea consist of several platforms and basins which were mainly formed during two periods of major collisions and subsequently sundered by continental separation. The first event of collision, the Caledonian orogeny occurred about 400 Ma (figure 2-2). This collision represented the closure of the Iapetus Ocean, a major paleo seaway (Dore, 1995). The Paleozoic period was highlighted by convergent plate boundaries, the two continents Laurasia and Baltica collided and merged into the Laurasia continent (Fossen et al., 2006; Dore, 1995). In the SW Barents Sea there have been formed structures which are orientated NE-SW, caused by the Caledonian sedimentary systems, partly controlled by active horst-graben tectonics and basin formation (Smelror et al., 2009). There is an N-S trending alignment caused by horst and graben development located on a strike-slip transfer on the western Barents shelf including western Spitsbergen and Bjørnøya Basin. Further east, in the Nordkapp Basin, Bjarmeland platform and surrounding areas the alignments| trend is NE-SW and associated with transitional transform/extensional movements (Smelror et al., 2009). In the late Palaeozoic most of the Barents Sea was affected by the crustal extension. In this period the extensions were characterized by westward migration of the rifting, formation of well-defined rifts and pull-apart basins in the south west, and in the north a development belt

of strike-slip faults trends (Faleide et al., 1993; Smelror et al., 2009). The collision of the Caledonian orogeny stopped and it collapsed when the eastern plate started to retreat (Fossen et al., 2006).

In the late Devonian the Caledonian compressional regime changed to a left-lateral shear regime with large strike-slipe movements (figure 2-2) (Harland, 1970; Ziegler, 1978; Faleide et al., 1984) The SW parts of the Barents shelf consists of complex system of highlands, alluvial and fluvial plains, marshes and predominantly easterly propagating deltas (Smelror et al., 2009).

The extension of the plate boundaries lead to erosion and deposition of large amounts of sediments in local basins. There where thick deposits of carbonates and evaporates associated with clastic sediments (Fossen et al., 2009; Faleide et al., 1984).

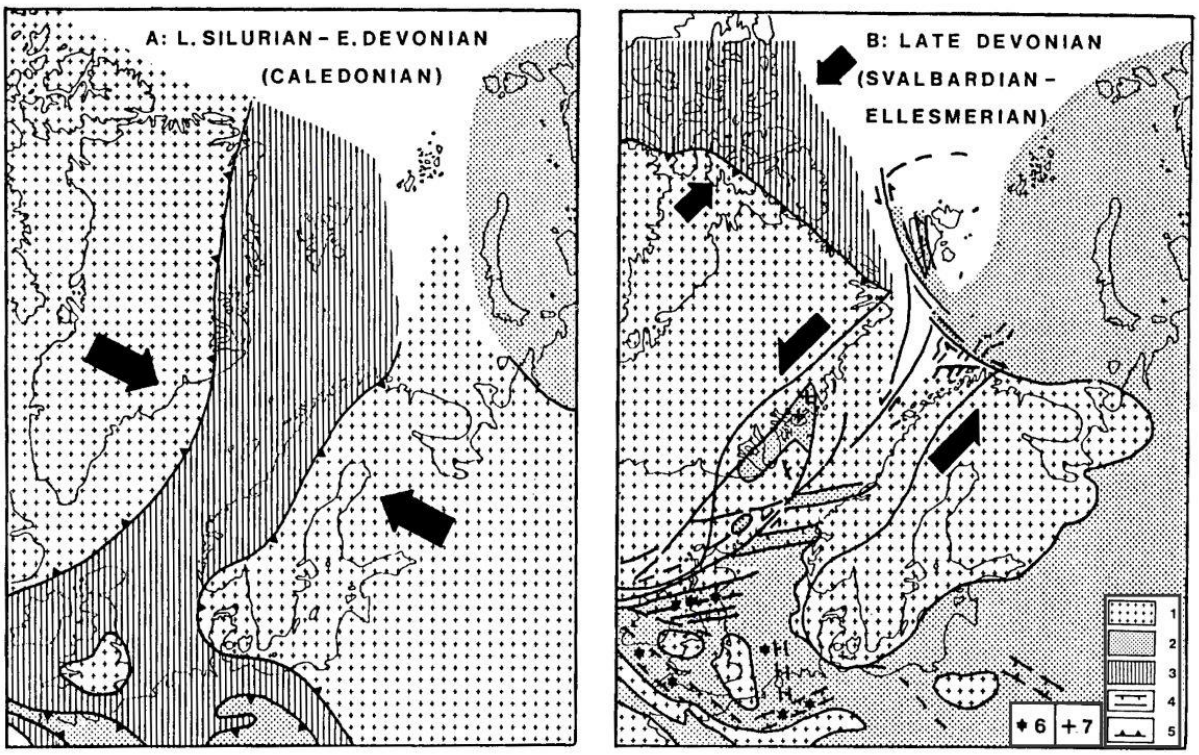

Figure 2- 2. Main stages of the Paleozoic tectonics. A) Late Silurian-Early Devonian orogeny. B) Late Devonian compressional regime and extensional faulting in the north. From Faleide et al. (1984).

Mesozoic

During the Triassic the marine connection to the south was closed causing the formation of the Uralian orogenic belt. The tectonic activity in the early Mesozoic was very quiet in Svalbard and Bjørnøya and a regional subsidence lead to deep marine environments and clastic marine sedimentation (Smelror et al., 2009, Faleide et al., 1984). Minor movements occurred on the Bjarmeland- and Finnmark platforms, and more active faults where found on the western margin where the Loppa High was uplifted and eroded causing rifting in the west of the high (Smelror et al., 2009).

In the Middle-Late Jurassic there was a period (Kimmerian) with calm regional extension between Greenland and Norway, and minor strike-slip adjustments along old alignments. The extension led to progressively subsidence of rotational fault blocks in the Kimmerian. This major phase is divided into three events, the Early (Rhaetian), Mid (Aalenian-Bajocian) and Late (Volgian-Valanginian) Kimmerian, whereas the latest event was most important. In the Early Jurassic there was a break in sedimentation areas bordering the Barents Sea followed by a regional transgression in Bathonian-Callovian (Faleide et al., 1984; Faleide et al., 1993).

In the Late Jurassic to Early Cretaceous, the Sverdrup Basin subsided relatively slowly, and dolerite intrusions and basaltic lava flows renewed the tectonic instability. This period with major rifting and tectonically instability (figure 2-3*a*) induced a lowstand in relative sea level which affected the entire North Atlantic (Faleide et al., 1984; Faleide et al., 1993). There were at least three tectonic phases that affected the Barents Sea during the Early Cretaceous. The termination of doming during early Barremian marked the end of active rifting in the Hammerfest Basin (Faleide et al., 1993). The Barremian (Kolje Formation) thickens towards the west and Ringvassøy-Loppa Fault Complex. The Early Cretaceous in the SW Barents Sea is characterized by extensional faulting with large downthrows to the west (Faleide et al., 1993).

In the Late Cretaceous major rifting with continental breakup occurred along the North Atlantic rift and in the Amundsen Basin to the north (figure 2-3*b,c*). This rifting event affected a dextral stress field that was set up along the Senja-Hornsund alignment (figure 2-3*c*) and during the Paleogene this mega-fracture acted as a relay zone between the spreading centers (Smelror et al., 2009).

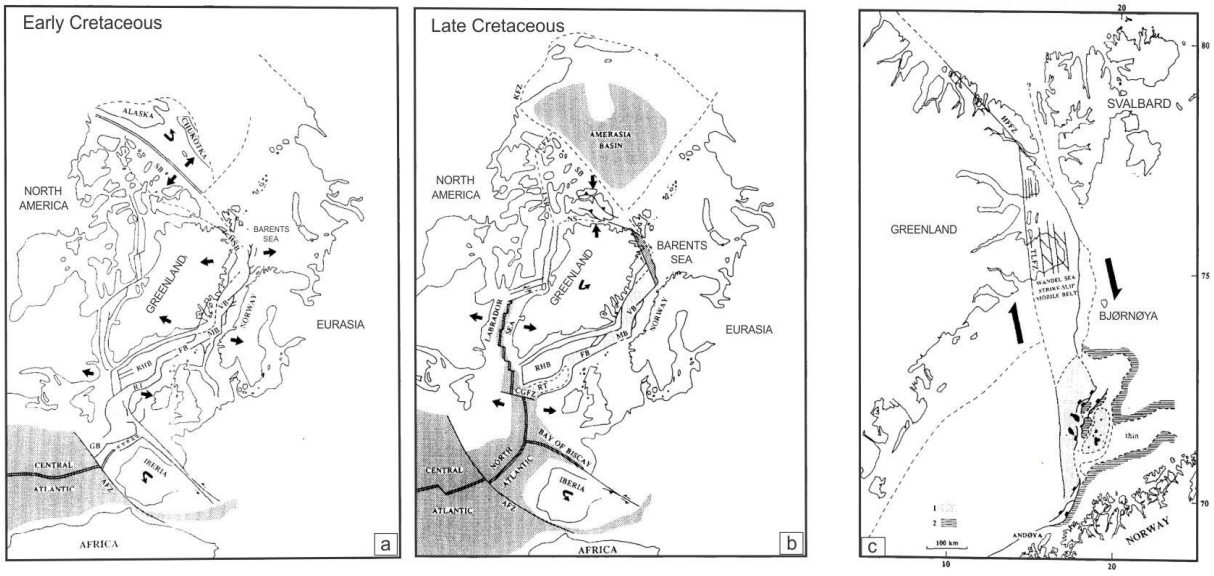

Figure 2- 3. a) Early Cretaceous tectonic with extensional regime. b) Late Cretaceous tectonic setting with regional stress field. c) Late Cretaceous faulting and sediment distribution in the SW Barents Sea. From Faleide et al. (1993).

Cenozoic

In the transition Palaeocene-Eocene there was a major change in the direction of motion of Greenland relative to North America (figure 2-4*a,b*), which occurred at the same time as the Tertiary spreading of the seafloor between the Norwegian-Greenland Sea and the Eurasia Basin (figure 2-4*a*). The reorganization of the spreading patterns occurred in the Mid Eocene and the spreading expanded further north into the southern limits of the Hornsund Fault Zone (HFZ) (figure 2-4*a,b*) (Smelror et al., 2009; Faleide et al., 1984; Faleide et al., 1993). Regional shear between the Norwegian Sea and Eurasia Basin began the formation of the continental margins of the Barents Sea and Svalbard, and the opening of the southern Greenland Sea (figure 2-4*b*) (Faleide et al., 1993). The direction of the opening was at a small angle relative to the Senja Fracture Zone (SFZ) and the Hornsund Fault zone (figure 2-4*a,b*). The opening influenced the Senja Fracture Zone as it developed during the Eocene opening of the Norwegian-Greenland Sea (figure 2-4*c,d*), first by continent-continent shear followed by continent-ocean shear and has now been passive since the earliest Oligocene time (Faleide et al., 2008). In the Norwegian-Greenland Sea the relative direction of the plate movement changed to west-north-west causing the crustal stretching of the seafloor spreading towards the northern Greenland Sea (figure 2-4*d*) (Faleide et al., 1993). During the opening there was a transpression that caused folding and thrusting in western Spitsbergen (Faleide et al., 1993).

This period was characterized by crustal cooling and thermal subsidence following the earlier periods of extension and crustal thinning (Nøttvedt et al., 2008). Along the main rift axis

where the crust was subjected to maximum extension and thinning into the deep, regional depressions such as the Møre, Vøring, Harstad, Tromsø and Sørvestsnaget Basins were formed. Extreme degrees of crustal thinning occurred and promoted several kilometers of thermal subsidence which caused continuous sediment infilling from the basin margins (Nøttvedt et al., 2008). Throughout the Eocene time deep marine conditions persisted and deposition of significant sandy submarine fans occurred during the Middle Eocene (Ryseth et al., 2003; Faleide et al., 2008).

During the Tertiary, major parts of the Barents Sea was uplifted and acted as a source area for the clastic wedge along the western margin (Faleide et al., 1984). In the Late Pliocene the Barents shelf was occupied by glacial deposits of the Northern Hemisphere glaciations. During the Pliocene-Pleistocene period the entire Barents shelf was uplifted and eroded and major amounts of sediments where deposited (Smelror et al., 2009).

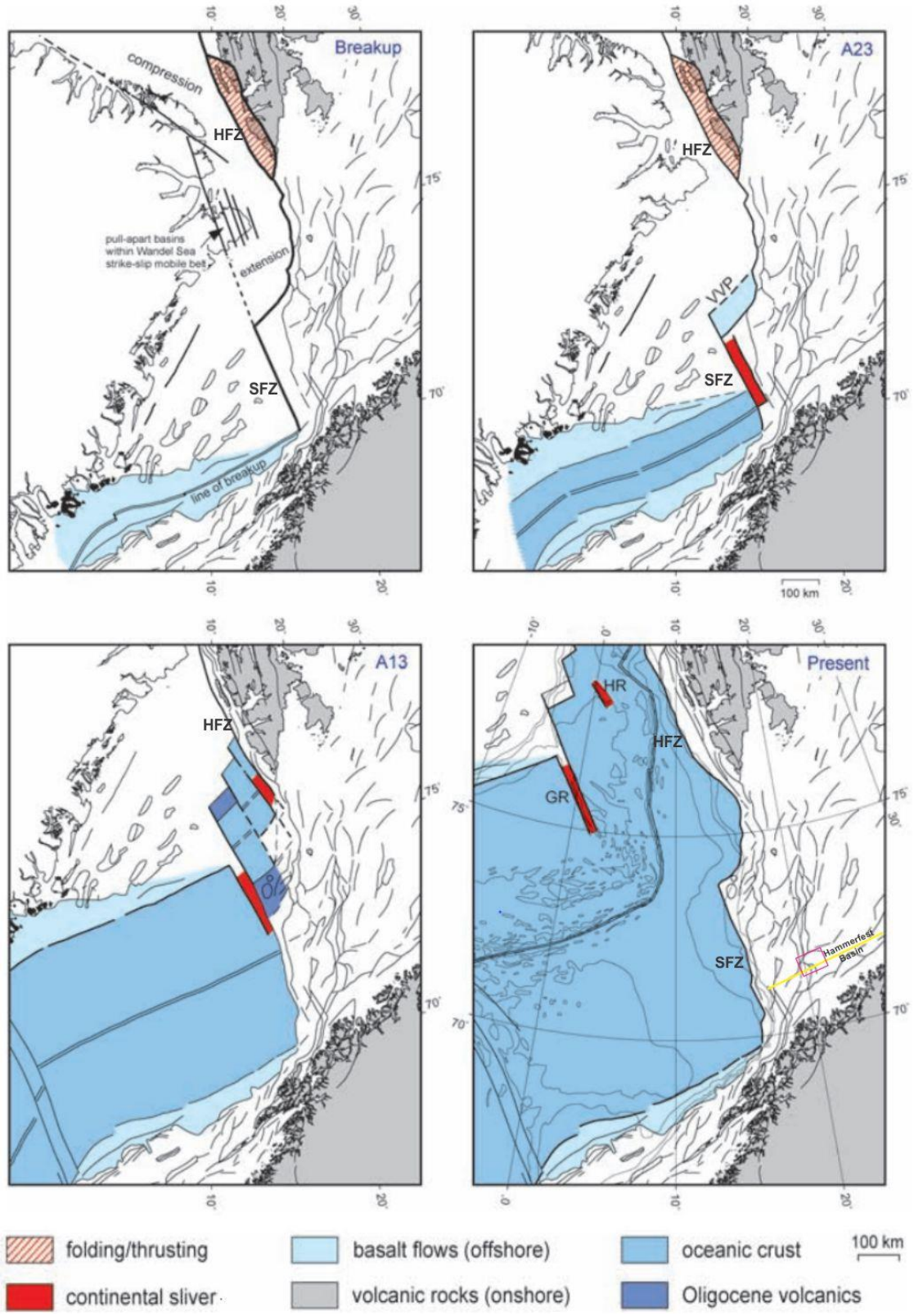

Figure 2- 4. a) Early Tertiary tectonic setting. b) Structual configuration at the time of break up (Paleocene-Eocene transition) between north-east Greenland and the Barents Sea. c) Mid-Tertiary (Oligocene) tectonic setting. d) Areas along western Barents Sea-Svalbard continental margin affected by the post-Eocene oblique extension. From Faleide et al. (2008).

The structural evolution of the Hammerfest Basin is illustrated graphical in figure 2-5, where the tectonic evolution of SW Barents Sea and mainly Hammerfest Basin is revised chronologically from Paleozoic to Cenozoic time.

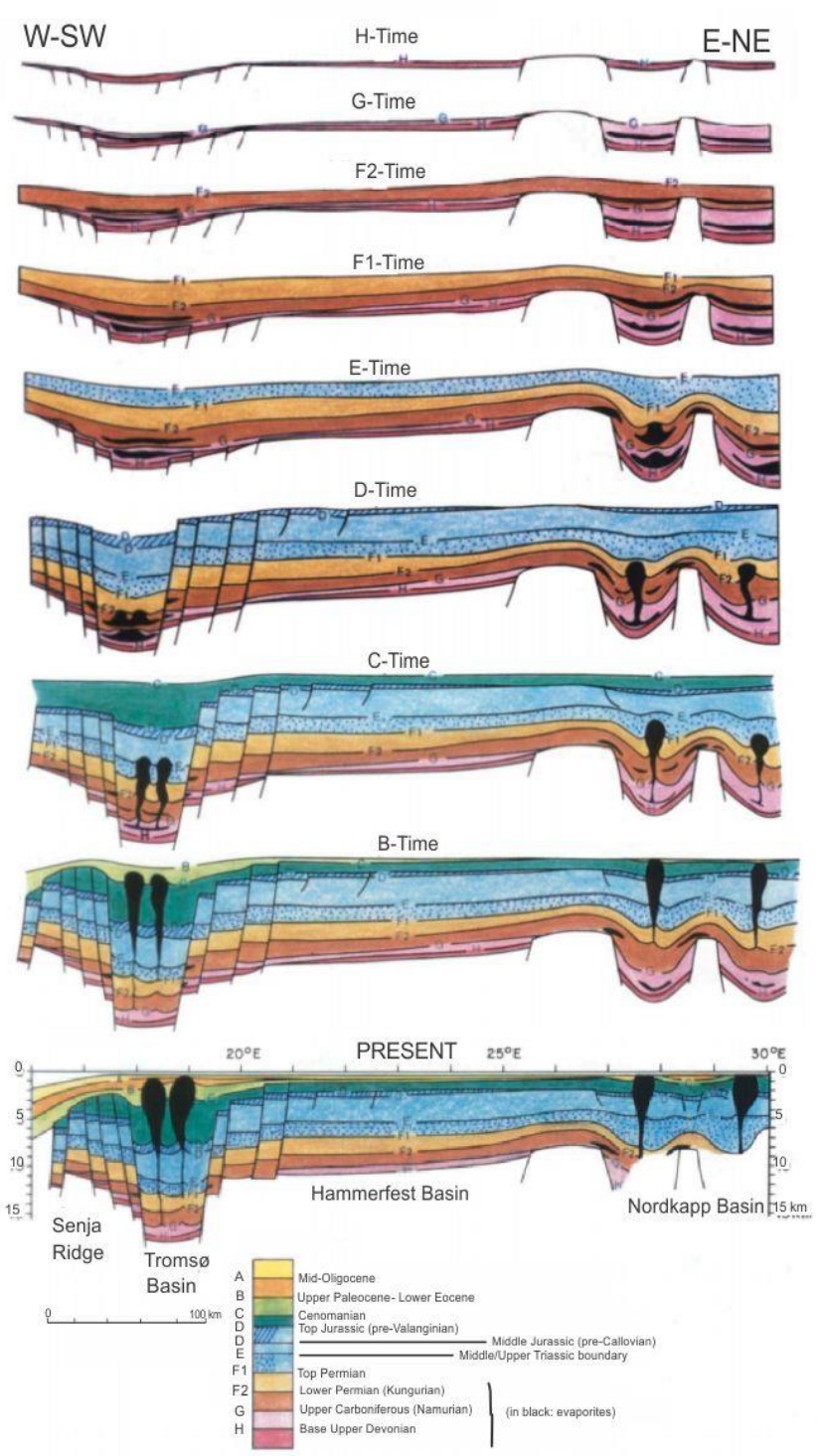

Figure 2- 5. Tectonic to sedimentology evolution of structures in the SW Barents Sea. Figure is modified from Faleide et el. (1984).

2.2.3 Hammerfest Basin

The Hammerfest Basin is relatively shallow. It is situated between 70°50'N, 20°E, 71°15'N, 20°E, 72°15'N, 23°15'E and 71°40'N, 24°10'E (Gabrielsen et al., 1990). The Hammerfest basin borders to the Finnmark platform in the south by the Troms-Finnmark Fault Complex, and the Loppa High and Bjarmeland platform in the north by the Asterian Fault Complex. In the west it limits to the Tromsø Basin which is defined by the southern segment of the Ringvassøy-Loppa Fault Complex. The basin has an elongated east-northeast striking graben-like feature that is 150 km long and 70 m wide. The Ringvasøy-Loppa Fault Complex has a north trending rotated fault block which marks the transition to the much deeper Tromsø Basin in the west (Faleide et al., 1984; Knutsen and Vorren, 1991; Gabrieslen et al., 1990). Most of the basins extending E-W are fault-controlled and were most likely established in the Late Carboniferous period. The internal structure of the basin is characterized by a central dome located along the basin axis and by the complex pattern of dominantly E-W- and WNW-ESE-trending faults, all of these features formed during the Late Jurassic tectonism (Larssen et al., 2005). The eastern part of the Basin is generally less influenced of faulting and is characterized as a sag basin (Gabrielsen et al., 1990).

2.3 Stratigraphy

The Hammerfest Basin contains a 5 km succession above the basement (Linjordet and Olsen, 1992) The Paleozoic succession has hardly been preserved in the Hammerfest Basin. From a total of 29 wells that have been drilled, there have only been two that have penetrated the Upper Paleozoic succession (well 7120/9-2 in the basin penetrated about 117 m below the top Permian and well 7120/12-2 on the southern margins penetrated a 1000 m thick upper Permian sequence resting on lower Permian dolomites and red beds and basement) (Larssen et al., 2002). The sedimentation succession that has been preserved in the Basin is from Permian to Holocene (Larssen et al., 2002). A sequence of glacigenic sediments overly the URU with a thickness between 0 to 300 m (Vorren et al., 1991).

During the Triassic there were deposit in the Hammerfest Basin sediments from the Fennoscandian Shield and the Urals. During the maximum regression in the Mid-Triassic clinoforms extended over the Finnmark Platform, Hammerfest Basin as well as to the Bjarmeland Platform. Sands, siltstones and shales were deposited in delta-fronts along the paleocoastline. This deposition is known as the Kobbe Formation and snadd Formation (figure 2-6) (Smelror 2009; Mørk & Elvebakk 1999; Riis et al. 2008).

From Lower-Triassic north in the Hammerfest Basin there are deposited shales with delta-fronts above the formation (figure 2-6). In the eastern parts there are coarse-grained fluvial deposits, while in the west it is dominated by marine sediments (Worsley et al. 1988).

The Tubåen Formation deposited during the Early Jurassic represents tidal inlets, estuaries and lagoons, which contain coal layers and marine shales (figure 2-6) (Smelror 2009; Linjordet & Olsen 1992). During Mid-Jurassic deposition of sandstones, siltstones and minor shale occurs in the Stø Formation (figure 2-6). This Formation has deposits which are excellent reservoir qualities (Smelror et al., 2009).

Mid-Lower Jurassic deposits occur as hiatus and major areas of Hammerfest Basin, the Bathonian sequence are gone (Worsley et al., 1988; Smelror et al., 2009).

The Cretaceous strata consist mainly of claystones with thin siltstones and sandstones stringers in the middle part of the succession. Dolomite and limestone stringers occur in the lower and middle part of the succession, and limestones are interbedded with claystones in the upper part (figure 2-6) (Linjordet and Olsen, 2008; Smelror et al., 2009). These sediments where mainly deposited in a marine shelf environment (Linjordet and Olsen, 2008).

The Kviting Formation is characterized as a carbonate platform (figure 2-6) that occurs in the eastern parts of the Hammerfest Basin, this shows a gradual change to the Kveite Formation in the western parts (Worsley et al., 1988). A hiatus between Cretaceous and Tertiary (Linjordet and Olsen, 2008).

A transgression occurred in the Early Paleocene which caused higher regions such as Loppa High and Troms- and Finnmark Platform to flood over. Sediments where then transported south-southeast from Loppa High into Hammerfest Basin where they were deposited (Vorren et al., 1991). As aTertiary sediments in the Hammerfest Basin get thicker towards the west, and thinner towards the north and Loppa High (Vorren et al., 1991). There is a thick layer of mid-Paleocene volcanic ash, 5-10 m, which rests directly on the upper Cretaceous strata in the Hammerfest Basin (Knutsen and Vorren, 1991).

The average temperature towards the Lower Pliocene decreases and several glaciations occurred. The temperature kept on decreasing towards the Early Pleistocene and caused the formation of major marine glaciers. The processes from the glaciers caused intensive erosion and eustatic uplift of the shelf and deposit of sediments along the western part of the Barents margin (Faleide et al., 1996).

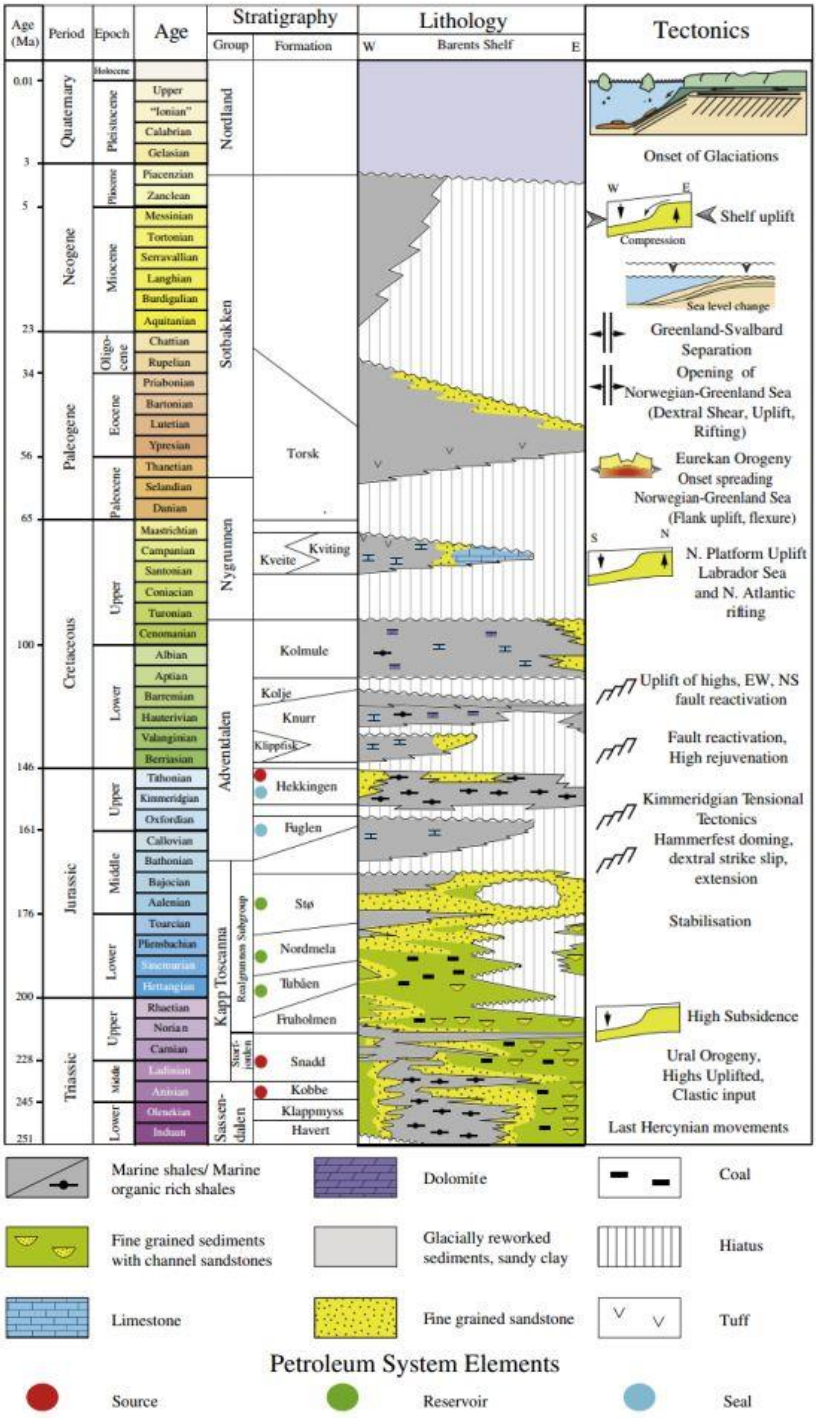

Figure 2- 6. Lithostratigraphic chart of the Barents Sea area, with major tectonic events in the area. Correlation between time, eras and age used in the literature, groups and formations from the Barents Sea. From Ostanin et al. (2012).

2.4 Source rock

Source rock is a sedimentary unit that is capable of generating hydrocarbons that can migrate into a reservoir. To preserve a source rock it has to a contain amount of organic matter (kerogen) under deposition in an environment that inhibits oxidation. Kerogen is formed by incomplete decomposition of organic matter and later maturation at high pressure and temperature in the subsurface (Dore, 1995; Selley, 2008). Oil is formed at lower temperature than gas. Terrestrial kerogen has a tendency to generate gas whereas marine kerogen tends to create oil (Dore, 1995).

There are lots of potential source horizons present in the Barents Sea. The best quality source rock consists of dark, organic rich shales which are from the Late Jurassic age (Dore, 1995). This formation is called the Hekkingen Formation (Worsley et al., 1988). They are present in large areas of the southern Barents Sea but in some cases these shales have not realized their full generation potential because of problems with maturation (Dore, 1995). The Hekkingen Formation is supposed to be mature along a narrow belt along the western margin of the Hammerfest Basin and along the western fringe of Loppa High. Further west this formation seemed to be too deeply buried and further east it is too shallow to mature properly (Dore, 1995).

There are three potential source rocks in the Hammefest Basin, the Late Jurassic anaerobic shales of the Hekkingen Formation, the Early Jurassic Nordmela Formation deposited under terrestrial conditions and the Triassic shales. The Hekkingen Formation is the best source rock, and has been documented in the Snøhvit Field by wells. Here there is good potential for light oil, condensate and gas. The Nordmela is rich on clay and has the potential to generate waxy hydrocarbons and gas. The Triassic shales have mainly gas potential (Linjordet and Olsen, 1992).

Lower-Middle Triassic potential source rocks are deposited in terrestrial environments in the Snadd- and Kobbe formation in the southern part of the Barents Sea. These deep formations have been difficult to collect data through wells so the quality of the source rock is more unsure (Ohm et al., 2008).

Major discoveries on the Norwegian sector consist of reservoirs from the Lower-Middle Jurassic sandstones. These sandstones where deposited in a coastal marine setting and normally have very favorable reservoir properties with high porosity and permeability (Dore, 1995). The traps that were formed on the Norwegian sector during the Jurassic are generally

fault-bounded positive blocks. The Triassic reservoirs properties are not as favorable as the Jurassic, as they are more sand-poor. The traps are fault-bounded with domal structures and are sealed with intra-Triassic shales (Dore, 1995).

2.5 The effect of the uplift and erosion from Cenocoic

The Cenozoic is characterized by large amounts of uplift and erosions in the basins and highs on the Barents shelf (Reemst and Cloetingh, 2008). The uplift of the Fennoscandia is associated generally with the uplift of the Barents Sea. The theory behind this has been speculated to have been caused by the pre-opening of the Atlantic margin elevation, mantle phase change, flexural response to sediment loading, intraplate stress, isostatic respons to sedimentary unloading or a combination of several of these phenomena (Dore and Jensen, 1996). Despite the arguments it appears that the uplift was tectonic in nature, probably occurring several times throughout the Cenozoic, with the latest and most important uplift occurring during the glacial period Pleistocene-Pliocene (Dore and Jensen, 1996). Late Cenozoic, the south-western Barents Sea was influenced by the glaciations and it impacted on the erosion and sedimentation of the area (Dore and Jensen, 1996).

The uplift and erosions have influenced the hydrocarbon generation, migration, entrapment and preservation (Dore and Jensen, 1996).

During the Cenozoic most of the Barents Sea was uplifted except of the western margin, where thick sedimentary succession from the Barents Sea hinterlands was deposited (Dore and Jensen, 1996). The uplift varies throughout the Barents Sea from around 500 to 3000 m where it increases form west to east. Minimum values are mainly found in the Hammerfest and Tromsø Basins. Further south, the uplift seems to decrease from the mainland towards the axial part of the North Sea rift system. The pre-existing hydrocarbon accumulations in hinge areas will have been tilted and might have caused spillage of oil and gas (figure 2-7). The result of uplift may have changed the structural attitude and as a result may have created potential hydrocarbon traps. If no further hydrocarbon where generated these traps would then be empty (Dore and Jensen, 1996; Reemst and Cloetingh, 2008). During uplift there will be removal of sedimentary overburden and consequent decrease in pressure which will cause the gas in a gas accumulation or gas cap to expand (Dore and Jensen, 1996). The seal of the traps will react negatively from the cause of the uplift (figure 2-7). Shales will become more brittle because of the pressure decrease and might fracture. The fracture of the seals may cause hydrocarbon spillage and the effect of uplift may lead to opening of faults with can cause a

migration pathway for hydrocarbons (figure 2-7). The formation of kereogen is formed during a long period of time and under specific temperature and pressure condition. During uplift these condition are influenced from kinetic theory where the source rocks will effectively cause hydrocarbon generation to cease (Dore and Jensen, 1996). Rapid deposition of sediments in basins caused an accelerated maturation of source rocks. Viking graben and Halten terrace show a phase of enhanced hydrocarbon generation and secondary migration in the last 4 m.y. as a result of rapid burial (Dore and Jensen, 1996). The uplift will bury the source rock deeper which causes them to be more thermally mature than expected from their present depth (Dore and Jensen, 1996).

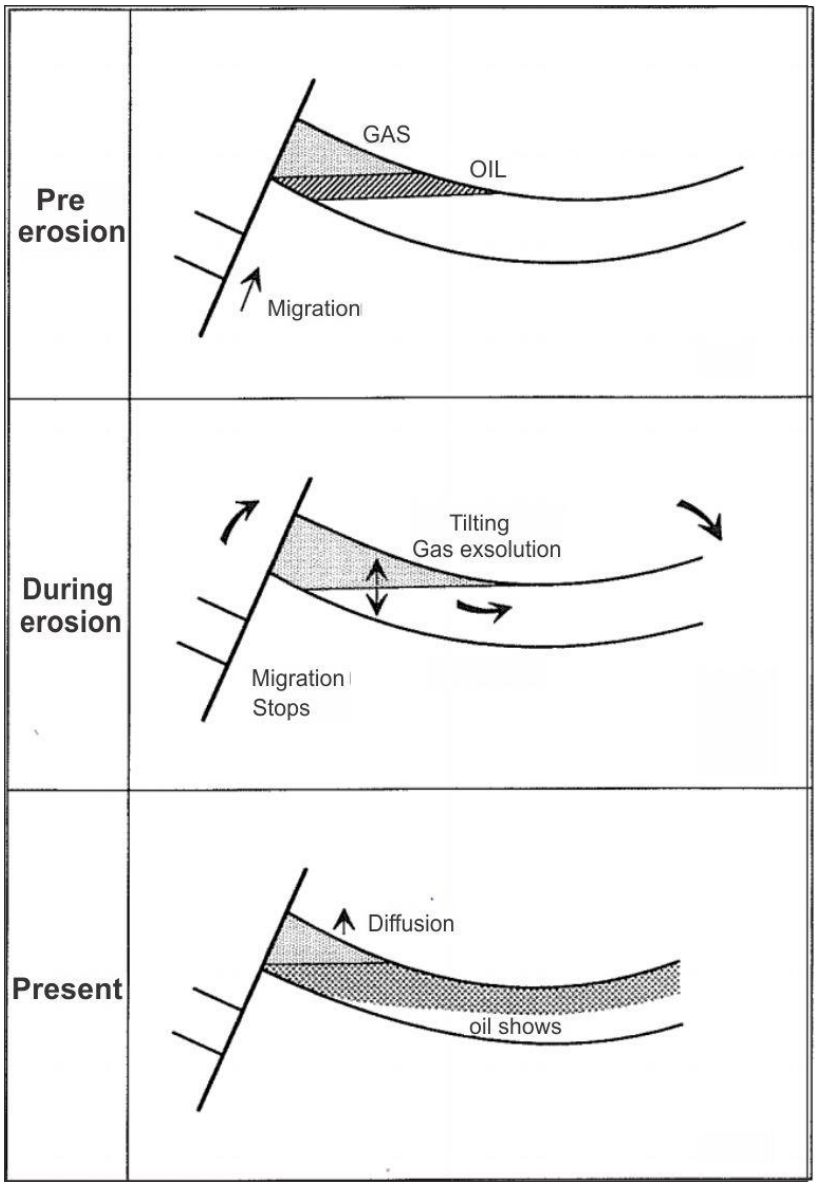

Figure 2- 7. Effects of erosion and uplift on hydrocarbon accumulation. During cooling the gas expands due to pressure and temperature drop and the oil will be pressed out. The diffusion of gas and oil will occur after erosion and uplift and migrates through the faults. Figure modified from Riis (1992).

3. Data and methods

3.1 Dataset

This study is primarily based on studies from two 3D seismic datasets. In addition, regional 2D seismic lines are used for correlation. The quality of 3D survey ST8320R00 is very poor and the interpretations appear with a lot of noise. For dataset LN0901 the quality is good.

Figure 3- 1. The map is obtained by using Petrel 2012. The White polygons indicate 3D datasets. The yellow lines indicate the 2D seismic used for correlation.

3.1.1 3D seismic dataset

The 3D data sets ST8320R00 and LN0901 have been processed to zero-phase, normal European polarity (SEG reverse) (figure 3-4) with a positive reflection coefficient (peak) corresponding to a decrease on acoustic impedance (soft reflections) (Sheriff, 2006).

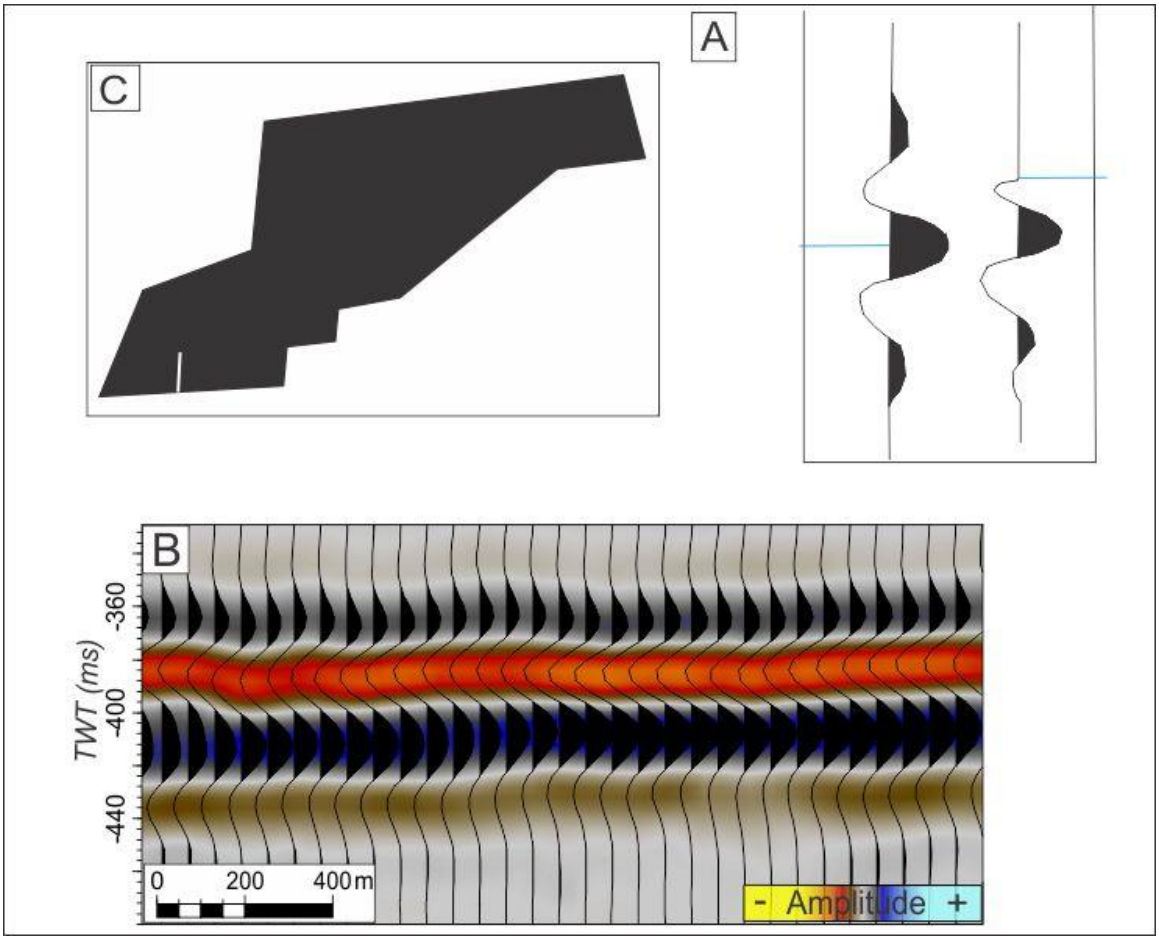

Figure 3- 2A: SEG standard polarity. For a positive reflection; 1) starts with a wave of minimum-phase (to the right) with a negative trough at the start of the reflection, 2) starts with a wave at zero-phase (to the left) with a sentral positve peak which is localized in the middle of of the reflection. Figure is modified from Sheriff (2006). B. Seismic cross section of survey LN0901 that shows that the datasets are processed to a zero-phase reversed signal. C. The white line indicates the localization to the seismic cross section in B**.**

Dominate frequencies for dataset LN0901 from the seafloor to 4000 ms two-way-time (TWT) show three peaks at 22 Hz, 24 Hz and 28 Hz (figure 3-3). The frequency spectrum is between 15-40 Hz at 0.6 amplitude (figure 3-3).

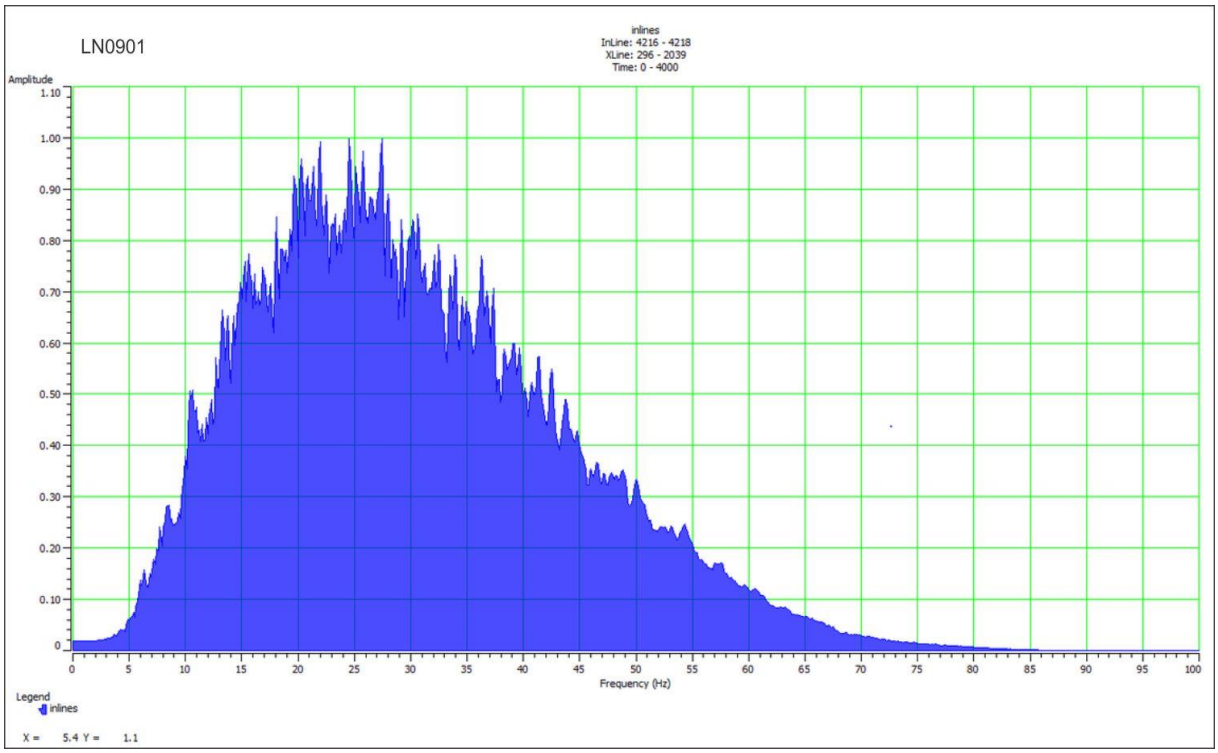

Figure 3- 3. Spectral analyses from inline 4216-4218 and Xline from 296-2036. The dataset LN0901 have three peaks with dominant frequencies of 22 Hz, 24 Hz and 28 Hz and a frequency spectrum of 15-40 Hz at amplitude 0.6.

3.2 Seismic resolution

Resolution has both vertical and horizontal aspects. The seismic data is always measured in terms of the seismic wavelength, which is given from the velocity and frequency. Seismic velocity increases with depth because the rocks are more compacted, and the frequency decreases with depth because of higher frequencies in seismic signals are more quickly attenuated (Brown, 1999). This results in an increase in the wavelength with depth and making the resolution poorer (Brown, 1999).

3.2.1 Vertical resolution

The vertical resolution is dependent of an acoustic impedance contrast in the seismic reflection, where the polarity of the incident wavelet is preserved on the reflected wavelet (Badley, 1985). The dissolution decides the wavelength. The wavelength (λ) is a function of the frequency (f) and velocity (v) (equation 2) (Badley, 1985). When the two-way transit time of a sediment layer reaches half of the wavelet width, and the sediment layer equals ¼ of the wavelength, this boundary is also known as the vertical resolution (equation 3) (Andreassen et al., 2007a; Badley 1985).

(equation 2) (equation 3)

Wavelength, $\lambda = v/f$ vertical resolution = λ¼

Wavelength (m) = λ, velocity (m/s) =v, dominated frequency = f

In shallow sections where the velocities are unusually low and frequencies are high, the wavelength is normally 40 m with a corresponding resolvable thickness of 10 m, the limited thickness of the sediment layer to produce a reflection of a about 1.3 m. In deeper sections, where the velocities are higher and the frequencies lower, the resolvable and detectable limits are higher (Badley, 1985).

3.2.2 Horizontal resolution

The horizontal resolution is determined by the fresnel zone. The fresnel zone is the portion of reflection energy which returns to the receivers within a half circle. For an unmigrated seismic section, this will be calculated by equation 4 (Badley, 1985).

(Equation 4)

$$rf = \frac{V}{2}\left(\frac{t}{f}\right)^{1/2}$$

rf = radius of the fresnel zone, V = average velocity, t = two-way travel time in seconds, f = dominant frequency in hertz.

The fresnel zone radius will increase with depth due to attenuation and increasing velocity (Badley, 1985).

The horizontal resolution is improved in the 3D seismic data from the 2D seismic data in two important respects. Firstly, the grid space is reduced from kilometers in 2D seismic profiling, to 25 m or less in 3D seismic surveys. Second, the effect of migration will be reduced in the fresnel zone to an ellipse perpendicular, to the line for 2D-migration and a small circle for the 3D-migration (figure 3-4). The ultimate limit for lateral resolution in 3D-migrated seismic data is the diameter of one-quarter of a wavelength indicated in figure 3-4 is for perfect migration (Brown, 1999).

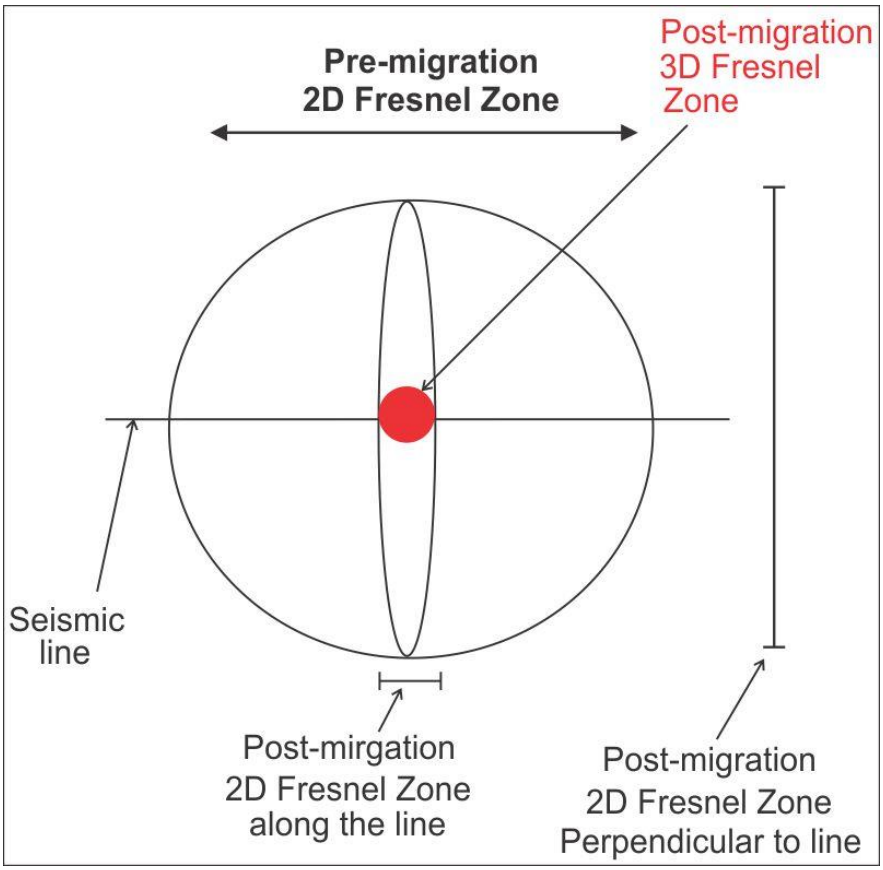

Figure 3- 4. Illustration of the Fresnal Zone size and form after 2D and 3D migration. The circle represents the Fresnal Zone before migration has occurred, the cigar shape after 2D migration and the red dot after 3D migration. Figure modified from Sheriff (2006)

The vertical and horizontal resolution for the two datasets in the study area has dominated frequency between 15-40 Hz with peaks between 22-28 Hz (see table 3.1)

Dominat frequency (Hz)	**Lithostratigraphy**	**Wavelength $\lambda = V/f$**	**Vertical resolution (m)**	**Horizontal resolution (m), before migration**	**Horizontal resolution (m), after migration**
22	Torsk Fm (1600m/s)	72,73	18,18	113,27	18,18
28	Torsk Fm	57,14	14,29	100,4	14,29
22	Hekkingen Fm (2600m/s)	118,18	29,55	448,62	29,55
28	Hekkingen Fm	92,86	23,22	396,66	23,22

Table 3.1: Vertical resolution is calculated from the equation λ=V/f, and the vertical resolution is = ¼λ. The velocity of the sedimentary sequence Torsk Fm (1600 m/s) and Hekkingen Fm (2600 m/s) is from table 3.2. The horizontal resolution before migration is calculated from the formula rf = V/2 $(t/f)^{½}$, the TWT (t) is for Torsk Fm 0.414 s and for Hekkingen Fm 2.6 s (table 3.2). Horizontal resolution after migration is ¼λ

3.3 Wells

The lithostratigraphy within the seismic has been calibrated and determined from several exploratory well data (7120/5-1, 7120/6-1, 7120/7-2, 7120/8-1, 7120/9-1). Well 7120/8-1 is located within the ST8320R00 dataset (figure 3-5). Well data from this well has therefore been used to calibrate the interpreted seismic horizons and units. All the formation tops gather from the well data, for this well can be identified with acceptable confidence to seismic correlation (figure 3-5, 4-1).

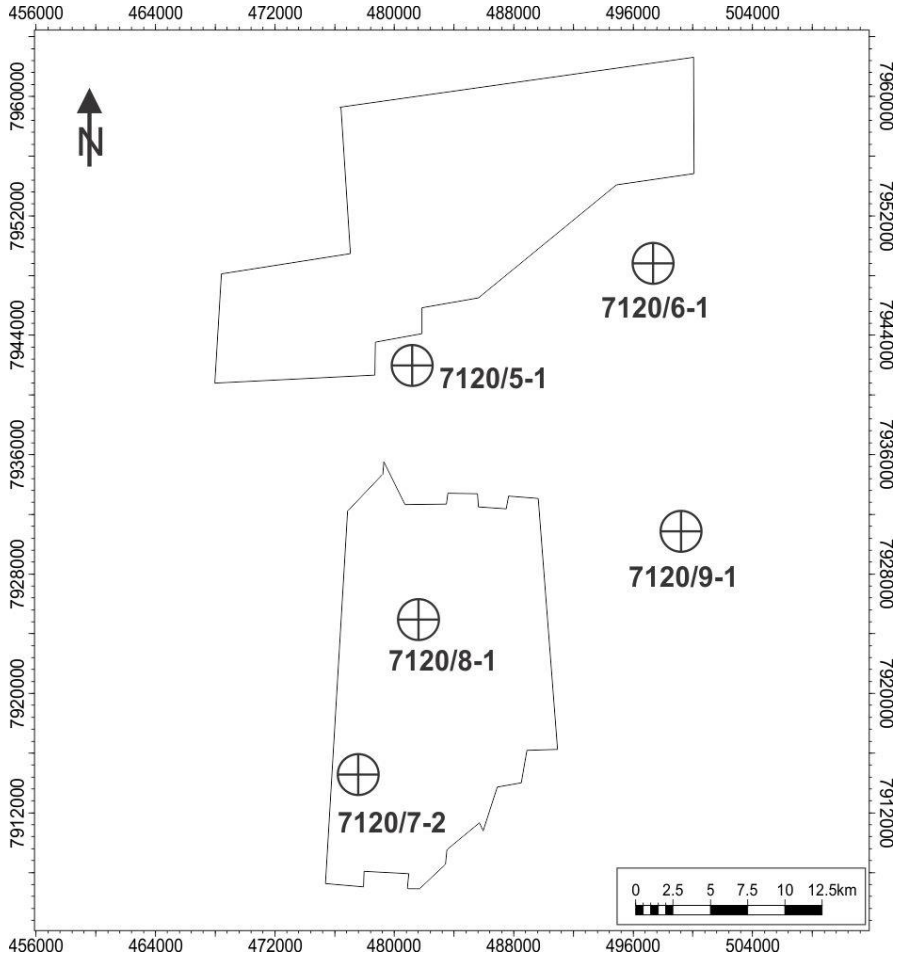

Figure 3- 5. 3D survey LN0901 and ST8320R00 with location of wells used in the thesis for correlation of interpreted horizons, calculation of velocities in the sediments and for gas composition for GHSZ.

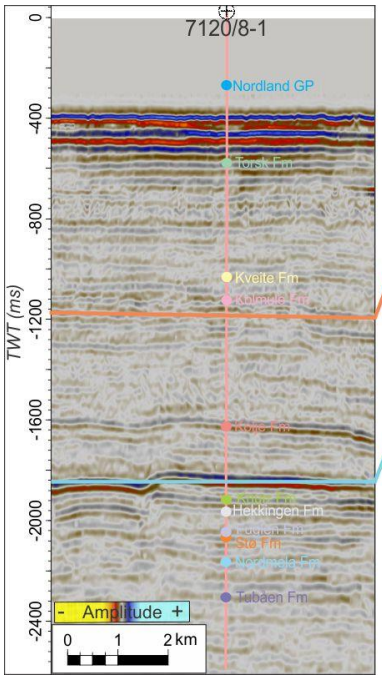

Top depth TWT (ms)	Top Depth (m)	Formation top	Age	
			Sub-Era	Periode
270	295	NORDLAND GP	Cenozoic	Neogene
578	603	TORSK FM		Paleogene
1031	1056	KVEITE FM		Cretaceous
1125	1150	KOLMULE FM		
1625	1650	KOLJE FM		
1917	1942	KNURR FM		
1965	1990	HEKKINGEN FM	Mesozoic	Jurassic
2061	2086	FUGLEN FM		
2067	2092	STØ FM		
2165	2190	NORDMELA FM		
2305	2330	TUBÅEN FM		

Figure 3- 6. Formation tops within the survey ST8320R00 of well 7120/8-1, and their ages (modified from NPD.no)

Seismic velocity data is important for determine rock and fluid properties in sedimentary basins. Experimental studies have found relatively clear relations between seismic velocity, porosity and clay content (Wyllie et al., 1958, 1958; Han et al., 1986; Stovoll et al., 2005). Stovoll et al. (2005) has determined and interpreted major velocity-depth trends within the Barents Sea with velocity data from 14 studied wells (figure 3-7). Figure 3-8 shows the velocity of the sediments at their present burial depth within the Barents Sea and the blue trend line shows a velocity increase with depth for northern North Sea, Haltenbanken and Barents. For calculating the velocity trend within the study area, three wells have been used (7120/5-1, 7120/8-1 and 7120/7-2, figure 3-4) and the average depth within the top depth is presented in table 3.2. The blue trend line has been used to calibrate the velocity within the different lithostratigraphy in the study area.

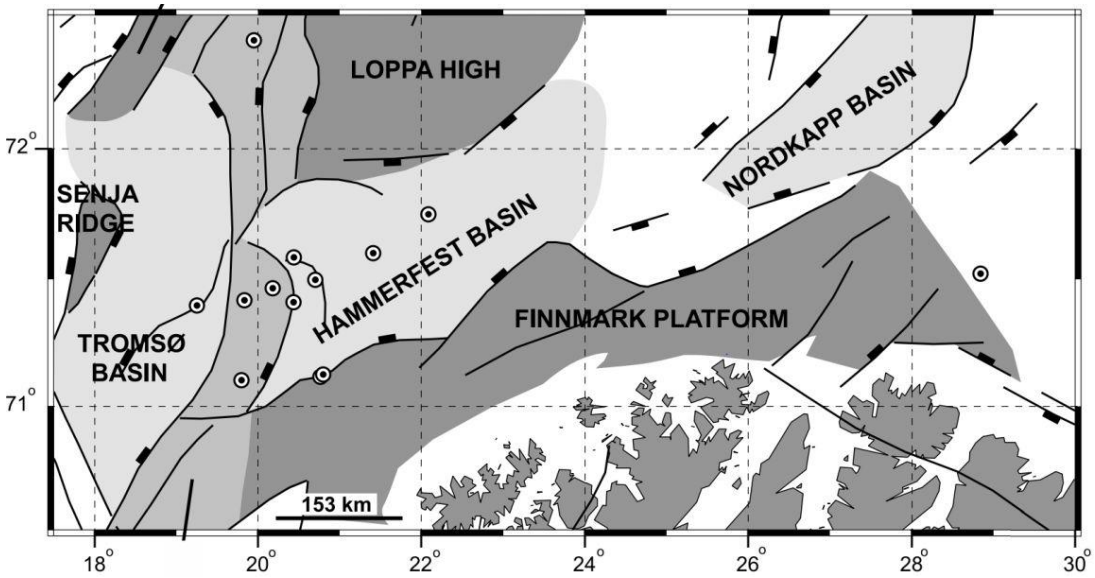

Figure 3- 7. Location map of the Barents Sea where the position of wells, marked by dotted circles, are used in figure 3-7. Figure from Storvoll et al. (2005).

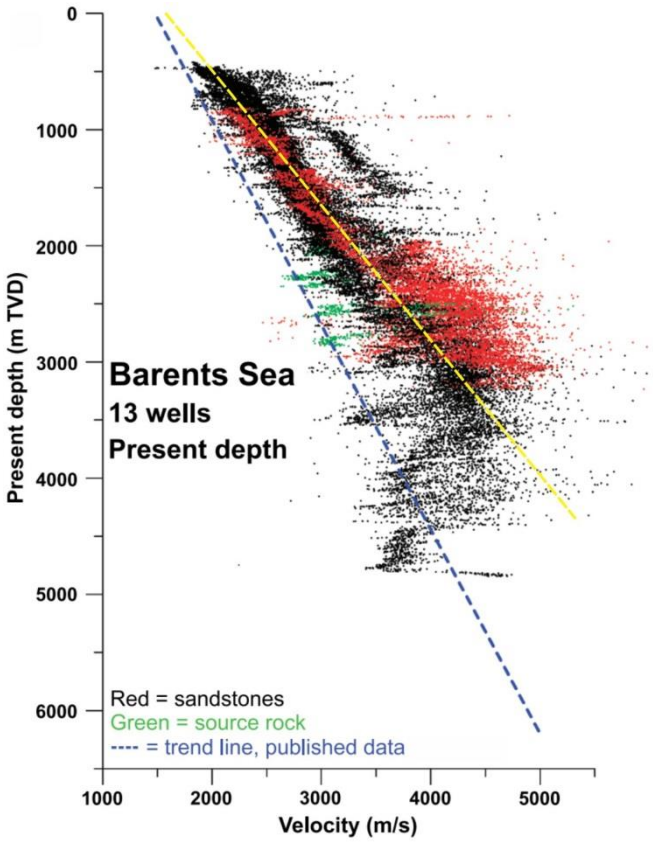

Figure 3- 8. Sonic velocity measurements (every 0.5-0.7 m with depth) from 13 wells (figure 3-6). The sandstones is highlighted in red, shales in black, and the organic Hekkingen Formation in greenwhich shows the average velocity from the 13 wells within the Barents Sea. The yellow dotted line shows the average velocity for the 13 wells.The estimated blue trend line shows the average velocity for Haltenbanken, northern North Sea and Barents Sea. The velocity measurements are at present burial depth (no corrections). From Storvoll et al. (2005).

Lithostratigraphy	Top depth (m)	Top depth TWT (ms)	Velocity Storvoll (2005) m/s
Nordland GP	292	269	-
Torsk Fm	465	441	-
Kviting/Kveite Fm	1062	1039	-2200
Kolmule Fm	1157	1134	-2200
Kolje Fm	1829	1806	-3200
Knurr Fm	2045	2022	-3200
Hekkingen Fm	2085	2062	-3200
Fuglen Fm	2166	2143	-3300
Stø Fm	2176	2153	-3300
Nordmela Fm	2291	2268	-3600
Tubåen Fm	2409	2386	-3700

Table 3.2. Lithostratigraphy from well (7120/5-1, 7120/8-1 and 7120/7-2). The average top depth TWT (ms) is from the seismic well data (yellow dotted line). Torsk FM and Nordland GP has not been calculated due to no obtained data within the depth. The average top depth is calculated from NPD.no. Velocity calculated from the blue trend line in figure 3-7.

3.4 Artefacts

Artificial features appearing in the dataset often created during acquisition or by processing are called artefacts (figure 3-9). In dataset ST8320R00, parallel lineation's with the orientation south-north (figure 3-9). These lineations occur within the same distance and throughout the dataset. The parallel lineations are interpreted as artefacts interpreted as systematically noise caused because it is difficult to achieve identical rates for each line that are collected (Bulat, 2005).

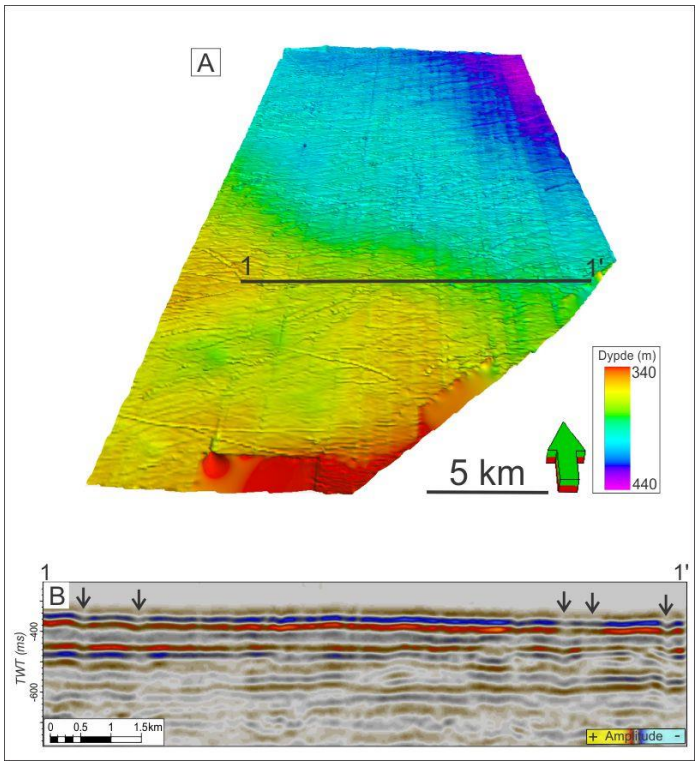

Figure 3- 9 A; Seabed horizon that shows the lineation noise. The black indicates localization B. B. Seismic profil that shows the lineation noise, the black arrows indiactes the noise that looks like vertical colums in the cross section.

3.5 Methods

The software 2012 by Schlumberger was used for interpretation and visualization tool. Petrel comprehends different tools which can be used for interpretation, generating of horizon attribute maps and volumes. And other geological information can be determined. Coreldraw X5 is used to edit the figures.

3.5.1 Seismic attributes

Seismic attributes is used to improve seismic interpretation and visualizations of geological structures and amplitude differences etc.

Structural smoothing smoothest the input signal guided by local structures to increase the continuity of seismic reflections. It can be used to illuminate noise from the data, and increase the signal/noise ratio. It is often used in front of variance, chaos and ant-tracking attributes (Schlumberger, 2011).

Chaos measures the "lack of organization" of the chaotic signal pattern in the dip and azimuth estimation method. The chaos attribute can be useful to identify faults and fractures but also classify salt diapirs, gas chimneys and channel infill (Schlumberger, 2011).

Variance (Edge method) is used to isolate edges from the input data set. This method estimates the variation in the continuity along a reflection and highlights the termination of several reflections caused by stratigraphic terminations or structures (faults). A result from this method can map zones of faults and acoustic masking (Schlumberger, 2011).

RMS (root mean square) computes the average amplitude value of a given volume window. All the value is calculated as square root values before the average is calculated, so no of the values will become negative. Some seismic amplitude will become brighter which makes it possible to see morphologic structures because the acoustic impedance contrast with the surrounding sediments becomes more visible (Schlumberger, 2011).

3.5.2 Stability modeling of gas hydrates

In the study area the gas hydrate stability zone (GHSZ) have been previously modeled. The CSMHYD program from Sloan (1998b) was used for the model (figure 3-10). The program estimates the pressure/temperature conditions for phase transition between free gas and gas hydrates. A change will occur in the GHSZ thickness caused by the different gas compositions. In the study area gas compositions are calculated from wells (7120/5-1, 7120/6-

1, 7120/8-1, 7120/7-2, 7120/9-1, figure 3-5; Vadakkepuliyambatta, 2014). The GHSZ thickness increases with a higher percentage of higher order hydrocarbons (Sloan 1998b).

The CSMHYD program was used to calculate which type of gas hydrates can be stable at specific depths in the study area. Temperature and pressure are assumed to follow the geothermal gradient.

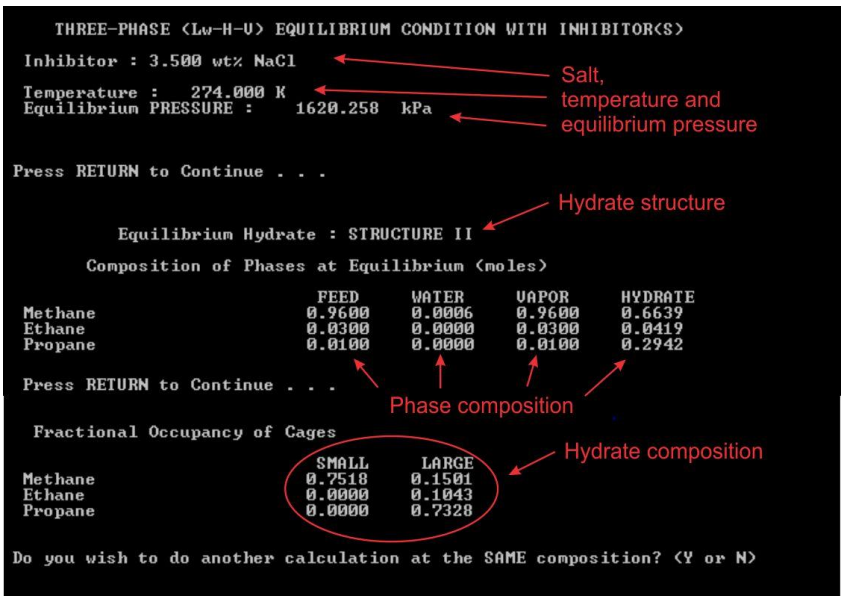

Figure 3- 10. Section from the program CSMHYD from Sloan (1998b). The program calculates the equilibrium pressure from a given temperature with possible inhibitor. Further, it calculates the composition of free gas-phase and solid hydrate-phase**.**

4. Results

Observations and interpretations made for the 3D seismic dataset LN0901 and ST8320R00 are presented in this chapter. The main focuses of seismic interpretation were to map stratigraphy, faults, fluid migration pathways, fluid accumulation and pockmarks on the seafloor.

4.1 Seismic stratigraphy

Prominent and strong amplitude-reflectors within the two seismic cubes are used to stratigraphically correlate the seismic with well 7120/8-1 (Figure 4-1). The well data was obtained from NPD's Petrobank and contains well tops from Top Sto to Top Torsk formation. Due to the scope of this thesis, Top Hekkingen is the deepest horizon studied here. These results can further be correlated with the work of Faleide et al. (1984), Worsley et al. (1988), Rodrigues Duran et al. (2013), Linjordet and Olsen (1992) and Dore et al. (1995) and contribute to a better stratigraphic understanding of the regional area. All reflections associated with the formation top can be identified in both of the 3D seismic datasets but URU can only be observed in some parts of survey LN0901.The basin deepens towards the west-northwest. The deep Tromsø basin is located even further to the west. This is observed in both of the surveys where there is a clear dipping strata in the deeper subsurface (figure 4-1 and figure 4-2).

The top of Hekkingen Formation occurs as a strong reflection with negative polarity relative to the seafloor (figure 4-1 and 4-2), within 1.9 to 2.3 s (TWT) in survey ST8320R00 and within 2 to 2.6 s (TWT) in survey LN0901. The seismic signature below the top Hekkingen Formation is discontinuous and shows weaker reflection amplitudes. For both of the 3D seimic surveys, the interpreted surface of top Hekkingen Formation is distinctly dipping towards the north-northwest, and several deeper-seated fault complexes influence the surface. The top of Hekkingen marks the Base Cretaceous Unconformity. Due to the faulting and the poor seismic quality of, particularly the ST8320R00 survey, the interpretation was more challenging and uncertain for this horizon (figure 4-1).

The Knurr Formation occurs above Hekkingen Formation and is also influenced by these fault complexes (figure 4-1 and 4-2). Above Hekkingen Formation a regional unconformity occurs

above the reflections which represent the Knurr Formation (figure 4-1 and 4-2). This formation has a negative reflection anomaly with strong amplitude and continuity. The formation occurs within 1.75 to 2.15 s (TWT) in dataset ST8320R00 and 1.9 to 2.3 s (TWT) in dataset LN0901. The interpreted surface of Knurr shows that the strata become deeper towards the west in survey LN0901 and towards the north-west for both of the surveys (figure 4-1 and 4-2). The Kolje and Kolmule Formations show chaotic internal reflections with mostly low but still some continuity, mostly observed in the ST8320R00 survey (figure 4-1). An exception is the top of Kolje which has higher continuity and reflection energy. The formation has a considerable thickness between 1.5 s to 2 s (TWT) in dataset ST8320R00 and between 1.7 s to 1.9 s (TWT) in dataset LN0901. The Kolje Formation shows influence from the deep-seated normal faults in both of the surveys and the horizon shows deepening towards the north, north-west. Within the Kolmule Formation there are areas within the LN0901 survey with polygonale faults (figure 4-8). The Kolmule Formation was formed during the upper part of the Lower Cretaceous and occurs within 0.9 s to 1.5 s (TWT) in dataset ST8320R00 and within 1.1 s to 1.6 in dataset LN0901.

The narrow Kviting/Kveite Formation occurs above the Kolmule Formation, where the top Kviting/Kveite represents the Upper Cretaceous. This strata is also dipping towards the northwest and occurs between 0.9 s to 1.4 s (TWT) in both of the datasets, where the formation is shallowest within the eastern part of the surveys. There are observed normal deep-seated faults which extend into this horizon (figure 4-1 and 4-2). This narrow formation shows reflection configuration which is characterized of continuous internal reflectors with mostly low amplitude.

The Torsk Formation occurs above the Kviting Formation. The Torsk Formation was formed during the Upper Paleocene. Lower sections of the Torsk Formation show internal chaotic reflections with low continuity and low reflection energy. In the upper part of the Torsk Formation clinoforms occur. The clinoforms progrades towards the northwest and several clinoforms have increasing seismic amplitudes stratigrapical upwards (figure 4-3). The top Kviting Formation marks the boundary between Tertiary and Mesozoic deposits.

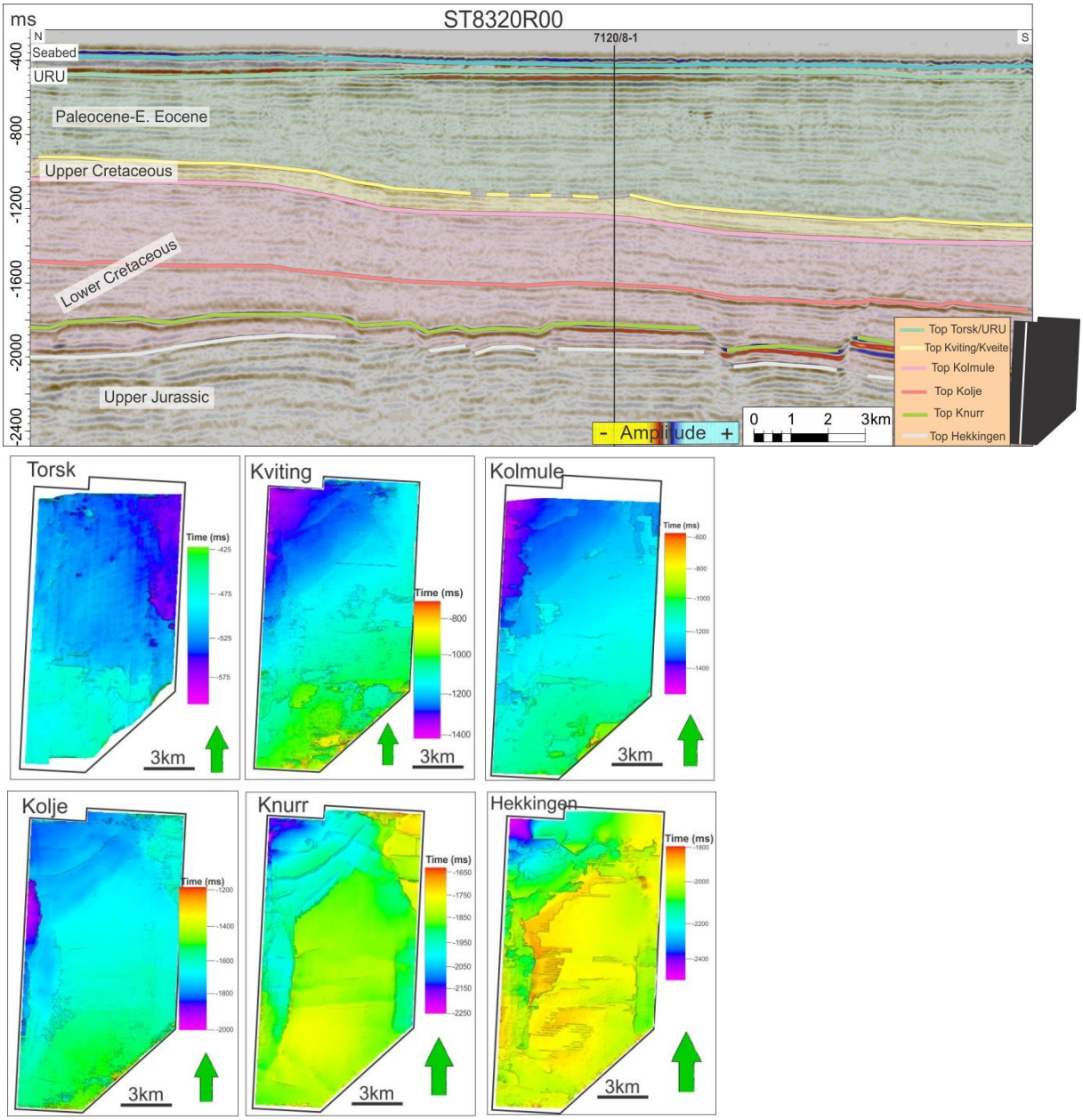

Figure 4- 1. Seismic cross section of the seismic survey ST8320R00 with the different stratigraphic sequences from Torsk to Hekkingen Formation. The red line in the polygon indicates the seismic line. Beneath, time-structure maps of all interpreted tops are shown.

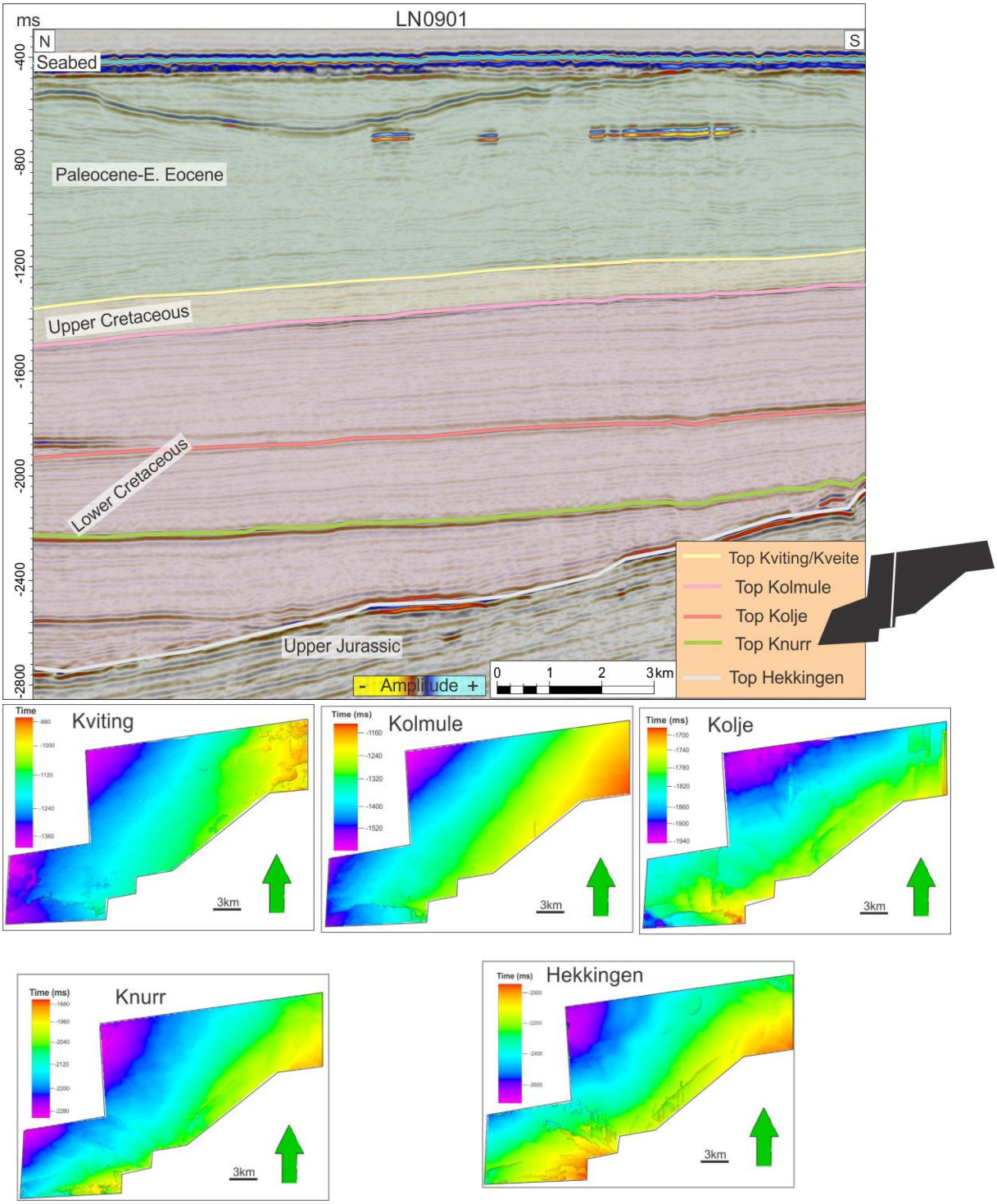

Figure 4- 2. Seismic cross section of the seismic survey LN0901 with the different stratigraphic sequences. The white line in the polygon indicates the seismic section. Beneath, time-structure maps of all interpreted formation tops are shown.

4.1.2 Upper Regional Unconformity (URU)

The Upper Regional Unconformity (figure 4-3) is a boundary that separates the preglacial Cenozoic bedrock from the overlaying glacegenic sediments. It represents the oldest glaciogenic surface that is overlain by late Pleistocene sediments, which have been deposited during several periods of erosion on the continental shelf (Andreassen et al., 2008; Ostanin et al., 2013; Vorren et al., 1989). The horizon interpreted to be the Upper Regional Unconformity can only be recognized all the way throughout the survey ST8320R00 (figure 4-1). In dataset LN0901 the URU coincides with the seafloor, but can only be located in the western and eastern part of the survey just below the seafloor (figure 4-3).

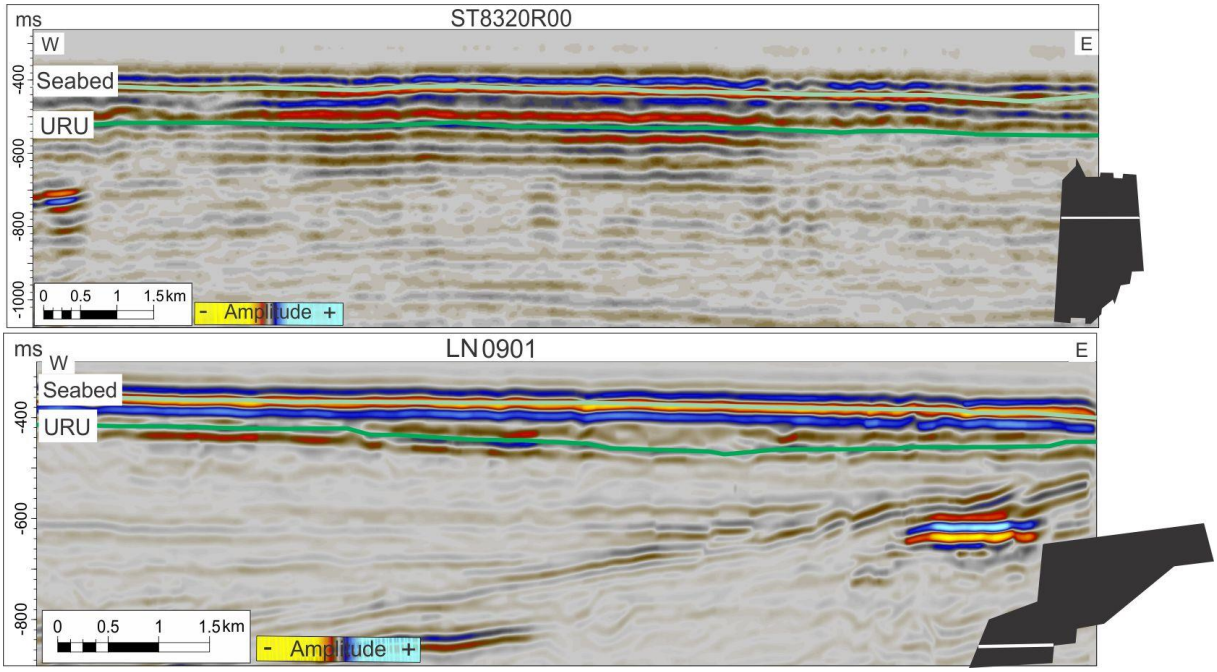

Figure 4- 3. Seismic cross section of the two datasets where URU is indicated by truncation of westward dipping strata below. It can mostly be recognized as a continuous reflection, but with significant variation in amplitude.

4.2 Faults

Mainly two categories of fault-systems are observed in the data; deeper-seated larger-scaled faults and shallower smaller-scaled faults. These occur within the upper 2.5 s (TWT) of the seismic surveys, characterized of three main sets of faults, affecting the Jurassic to Paloecene-Eocene, the Upper Cretaceous and intra Paleocene-Early Eocene. The deeper-seated faults are observed in both surveys, but the shallower faults have been difficult to trace in survey ST8320R00 due to of the poorer quality of the dataset.

4.2.1 Deep, larger-scaled faults

The fault complexes have mainly three different orientations: WNW-ESE to NNW-SSE, ENE-WSW to NNE-SSW and E-W (figure 4-4). All the faults are interpreted as relatively parallel normal faults with throws varying from 20-70 ms TWT. This may indicate several extensional episodes. In both datasets the faults have the largest throw within the Hekkingen Formation (figure 4-5 and 4-6). The Hekkingen Formation is located in a deeper level in survey LN0901 at 2200 ms (TWT) and in survey ST8320R00 at 2000 ms (TWT) (figure 4-4). The faults terminate at different stratigraphic levels between Lower Cretaceous to Early Eocene (figure 4-5 and 4-6). The fault blocks create a horst-graben structure.

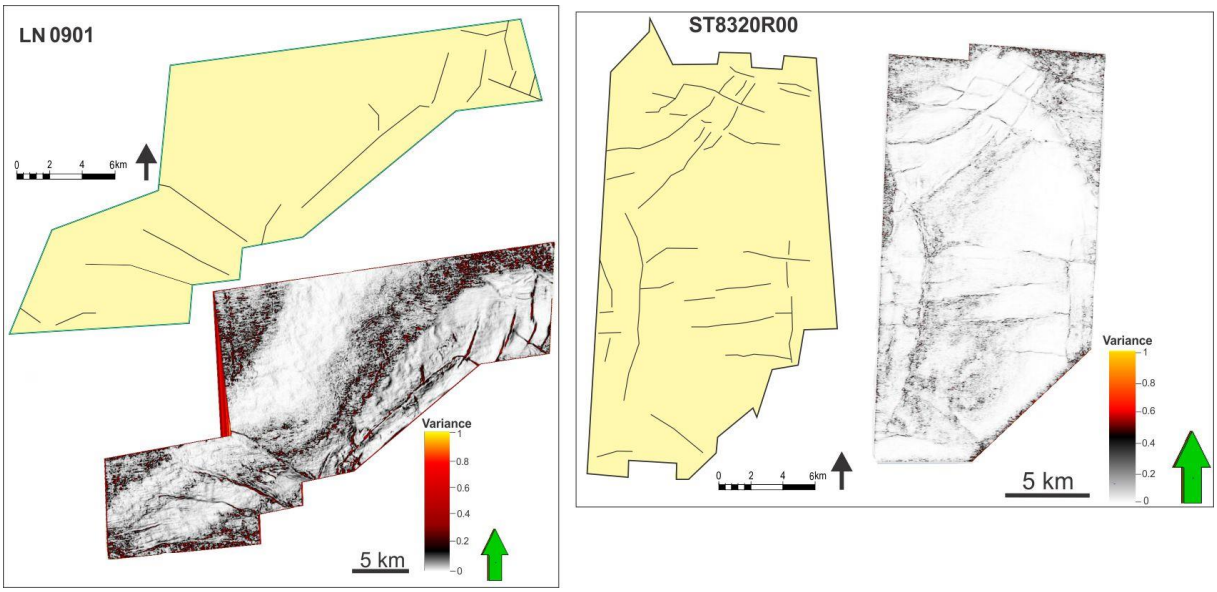

Figure 4- 4. Overview map of the deeper faults in dataset LN0901 and ST8320R00. Based on time section through variance cube at 2200 ms TWT for LN0901 and 2000 ms TWT for ST8320R00.

The WNW-ESE to NNW-SSE oriented faults is mainly located in the southwestern and north-eastern parts of survey LN0901 (figure 4-4). In the southwestern part only these deep-seated faults that are represented (figure 4-4). The throw of the faults is largest within the Hekkingen Formation and decreases in shallower levels (figure 4-6*b*). The upper termination of the faults occurs within the Upper Paleocene. The throw varies where they are measurable from 25 ms (TWT) up to 70 ms (TWT). The height of the throw is ~35 ms (TWT) which corresponds to 45.5 m (TVD) with an assumed velocity of 2600 m/s (chapter 3, table 3.2). For survey ST8320R00 this orientation of faults occurs within the southern and northern area (figure 4-4). The throw is most distinct within the Hekkingen and Knurr Formation and has an average throw of 40 ms (TWT) (figure 4-5*b*), which is 52 m TVD in converted value using a velocity of 2600 m/s (table 3.2). The faults extend into Upper Paleocene level (figure 4-5*b*).

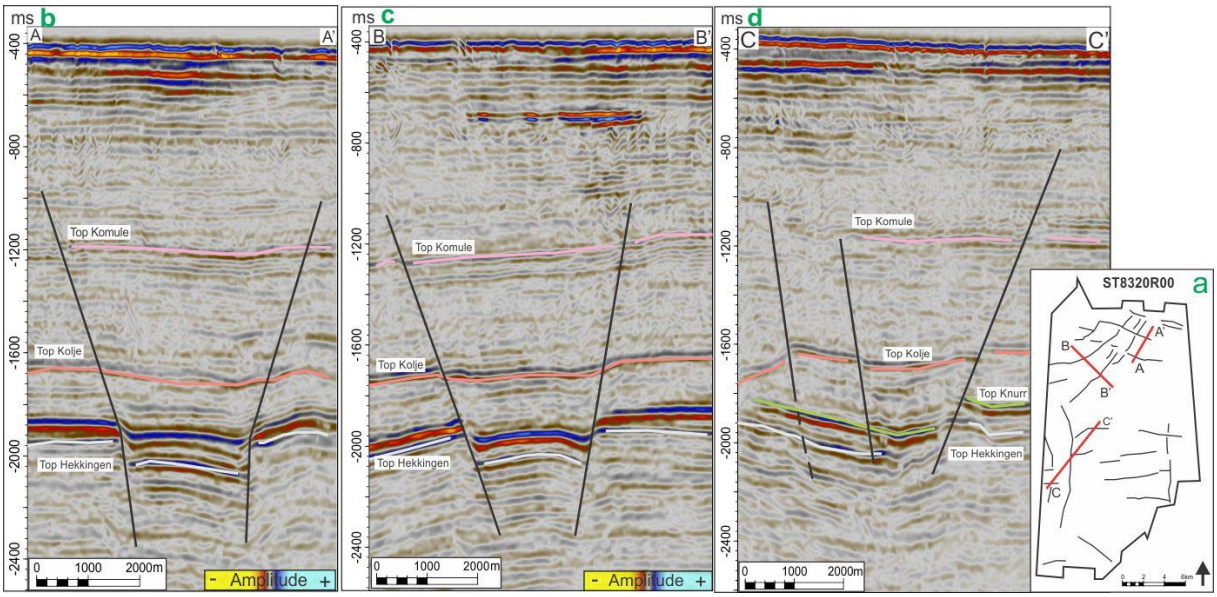

Figure 4- 5. a: Overview map of the faults where the red line indicates the seismic cross section. b: Seismic cross section "A-A". c: Seismic cross section "B-B". d: Seismic cross section "C-C".

The ENE-WSW to NNE-SSW oriented faults are located in the north-eastern area of survey LN0901 (figure 4-4). The throw is largest within the Hekkingen Formation within both the surveys (figure 4-5*c* and 4-6*c*). There is one larger fault in dataset LN0901 with this direction which extends from southwest to northeast with a length of 11 km (figure 4-6*a*). The faults terminate in the Lower Cretaceous strata. The longest fault has a throw of 60 ms (TWT) which is 78 m (TVD) with a conversion using 2600 m/s velocity (chapter 3, table 3.2). The average throws of the faults located in the north is 20 ms (TWT) which in

converted value is 26 m (TVD). Within survey ST8320R00 the faults occur mainly in the northern and eastern area (figure 4-4). The throw decreases into the shallower levels and terminates in the Upper Paleocene strata (figure 4-5*c*). The throws vary from 70 ms to 100 ms (TWT), with an average of 85 ms (TWT). The converted value is 85 m (TVD) with using velocity of 2600 m/s.

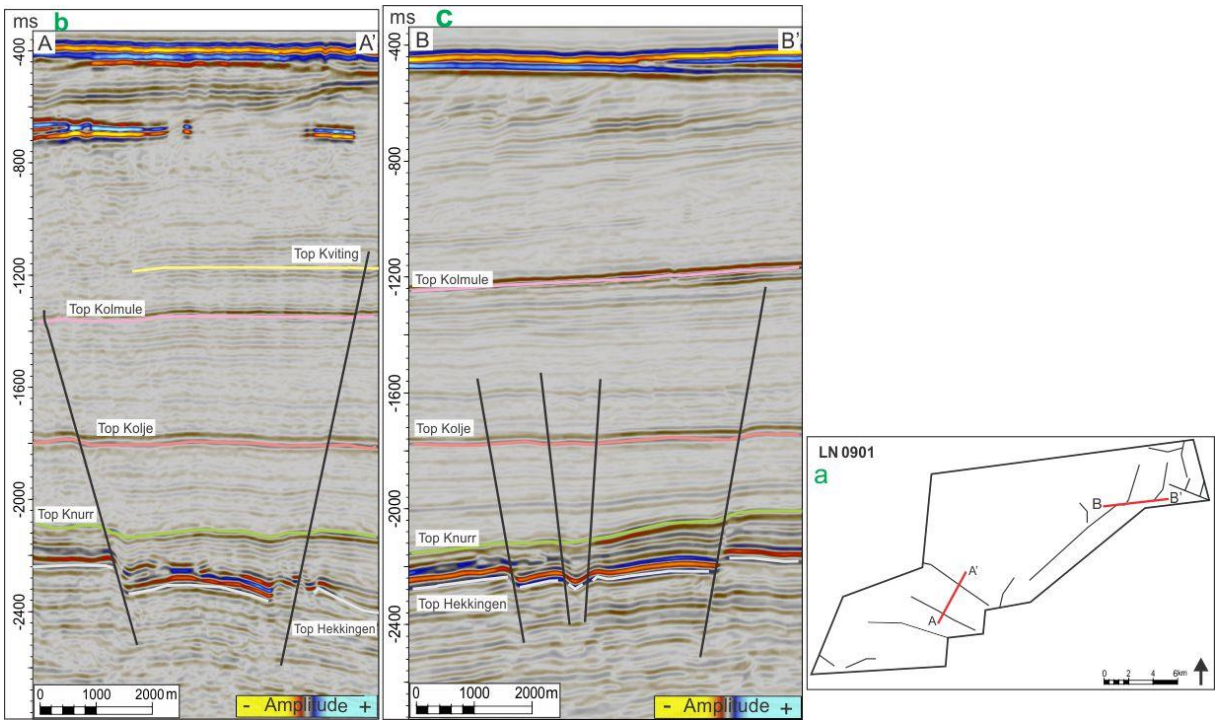

Figure 4- 6 a: Overview map for deep faults where the red line indicates the seismic cross section. b: Seismic cross section "A-A". c: Seismic cross section "B-B

The W-E oriented faults occur mainly in the middle and southern part of the ST8320R00 survey (figure 4-5*a*). The throw is largest (60 ms) within the Hekkingen Formation and varies along the faults (figure 4-5*d*). However the averages of the throws lie between 30-40 ms (TWT), which correspond to 30-40 m TVD. The throw decreases in the shallower layers (figure 4-5*d*). The faults extend into the Upper Paleocene stratigraphy (figure 4-4*d*). A central doming, located along the basin axis, forms internal faults of an orientation of E-W and WNW-ESE, reflecting predominantly the Late Jurassic tectonism (Larssen et al., 2002).

4.2.2 Shallower fault-systems

Polygonal faults

The central part of the LN0901 survey shows small, closely-spaced faults within the lower Cretaceous Kolmule Formation between ~1.75 s to 1.25 s (TWT) (figure 4-7). The polygonal faults show small vertical throws of 10 to 20 ms TWT. In plan view, the faults show curved to

rectangular shape throughout the mapped area (figure 4-8). These faults are interpreted to be polygonal faults comparable to interpretations in the Hammerfest Basin (Ostanin et al., 2012) and on the mid-Norwegian margin (Cartwrgiht and Dewburst, 1998). They are developed in passive margin basins, in sequences controlled by lateral and vertical lithological variations, which can be of fine grained clay with smectice or as carbonate chalks (Cartwright and Dewburst, 1998; Ostanin et al., 2012). The polygonal faults are possibly related to the Late Cretaceous uplift, and the interval might have been thicker prior to the uplift and erosion (Ostanin et al., 2013). There are three different dominant directions on the polygonal faults; WNW-ESE, NE-SW and E-W orientation (figure 4-8).

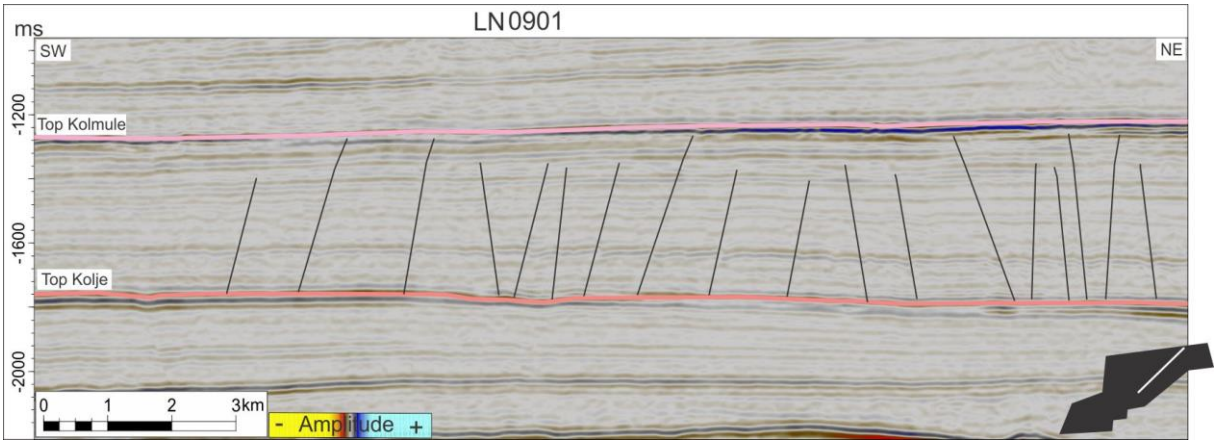

Figure 4- 7. Seismic cross section that shows the polygonal faults within the white line in the polygon.

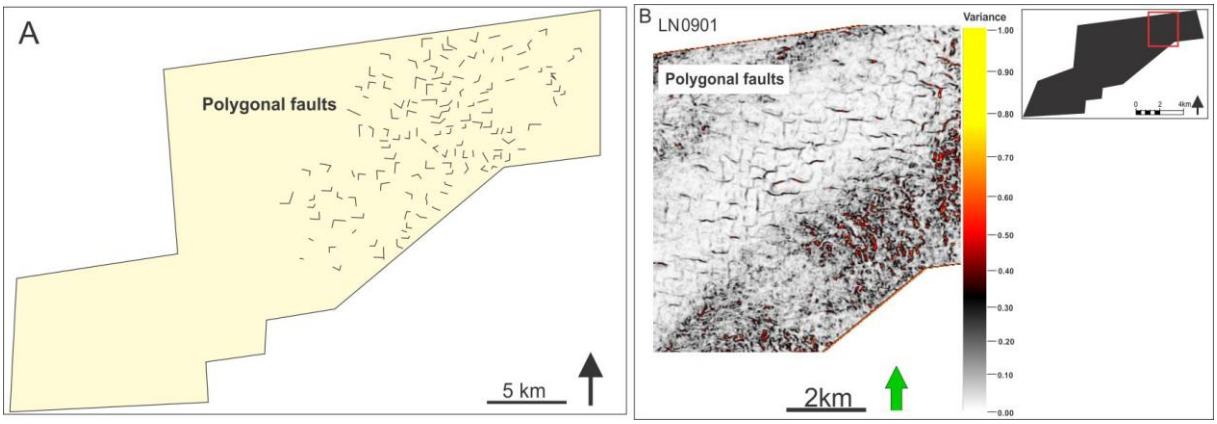

Figure 4- 8A: Overview map for the polygonal faults. *B*: Time section through a variance cube at -1664 ms (TWT) that shows polygonal faults. The red box indicates the area of the variance map.

Shallow normal faults

Shallow faults occur mainly within the LN0901 survey. However, it is more difficult to map them in survey ST8320R00 due to poorer quality of the dataset. These shallow faults are normal fault systems with a predominat direction of NNW-SSE and NNE-SSW (figure 4-9). They occur within the dataset as single closely-spaced faults within the Upper Paleocene-Early Eocene, Torsk Formation, where most of the faults occur within the upper 1000 ms (TWT) (figure 4-10*a*). The throw of the faults range between 5-30 ms (TWT) which corresponds to 5-30 m (TVD) assuming a velocity of 1600 m/s (table 3.2). The shallow faults occur throughout the survey except within the middle part (figure 4-10*a*). In the middle/eastern part of the survey the main orientation of the faults is NNW-SSE, but further east the main direction changes to a NNE-SSW orientation. The western are the fault are smaller and the direction varies between NNW-SSE and NNE-SSW. One larger fault (figure 4-10*b*) extends from the deeper-seated fault with an orientation EEN-WWS to WNW-ESE (figure 4-10*a*,*b*). This fault truncates just beneath the URU (figure 4-10*b*).

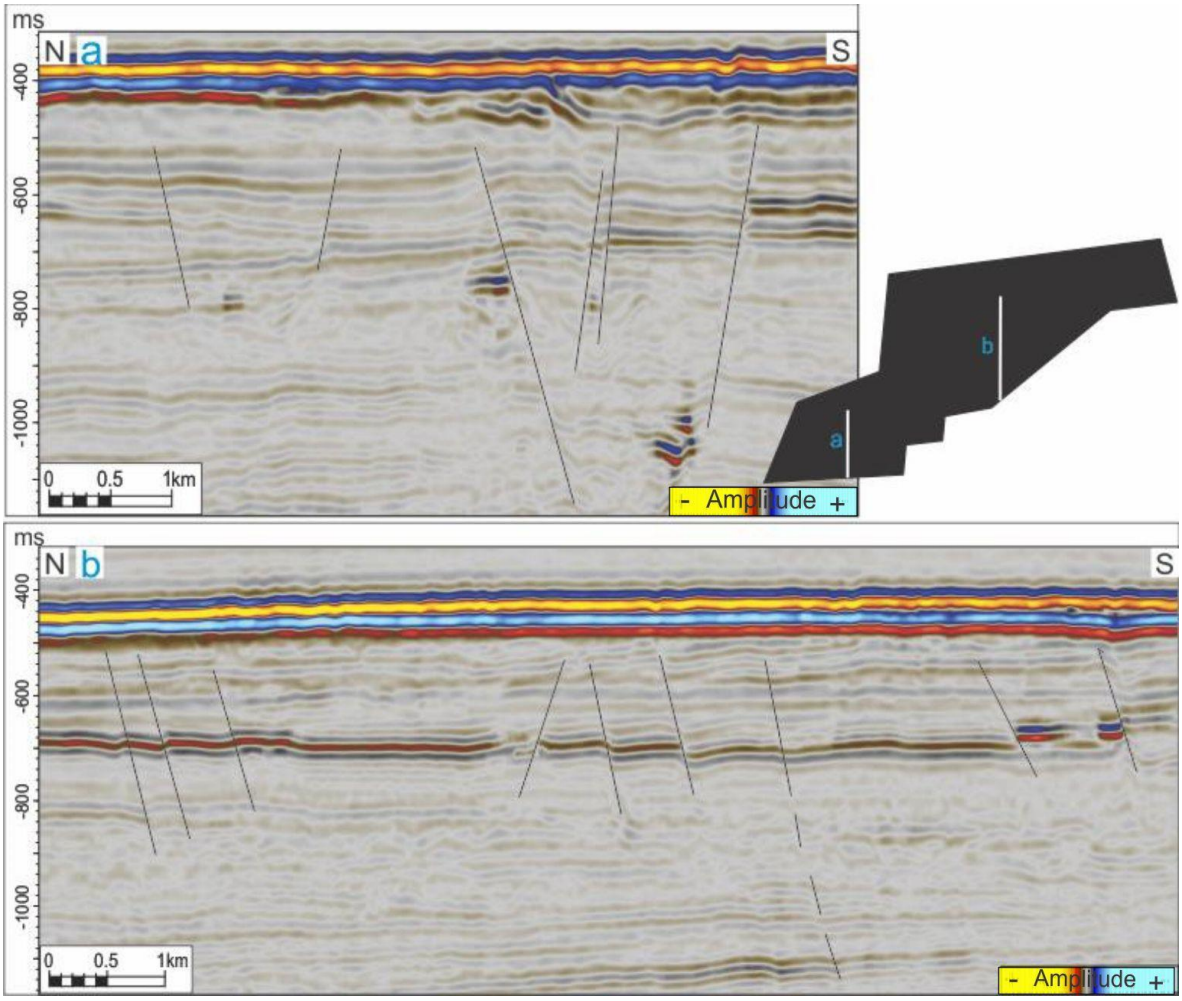

Figure 4- 9a: Seismic cross section from the dataset LN0901 which shows shallow normal faults, where (a) white indicated line in the polygon shows the location. *b*; Seismic cross section which indicates normal shallower faults, the white line in the polygon indicates the location.

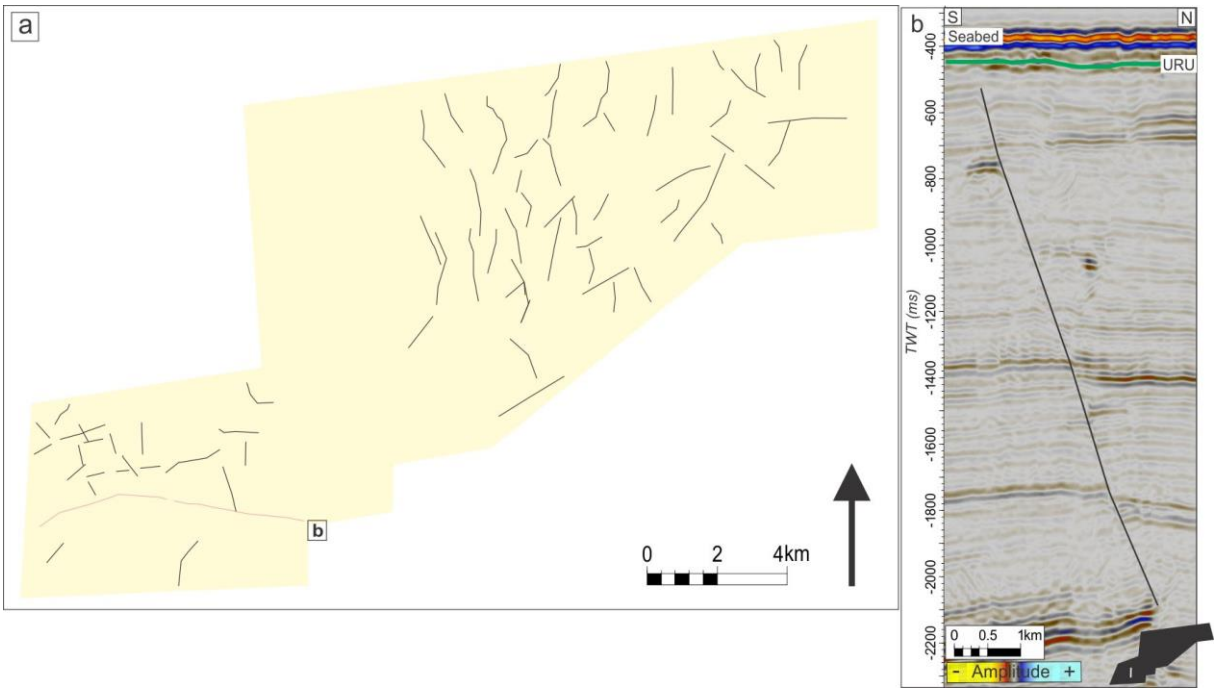

Figure 4- 10. Overview map of the shallower faults within the Upper Paleocene-Early Eocene stratigraphy for the dataset LN0901, with one larger deep-seated fault (b). b. Seismic cross section of the deep-seated fault which extends to the Torsk Formation.

4.3 Shallow gas accumulation

Shallow high amplitude anomalies occur mainly within the impermeable Torsk Formation but can also be recognized within the Kolmule Formation in the two surveys (figure 4-11). They vary in horizontal distribution, shape and vertical extent. The high amplitude anomalies are often associated with a chaotic pattern underneath and in some places show lower reflection amplitudes and push-down effects. I interpret the high amplitude anomalies as shallow gas accumulations comparable with observations in the whole SW Barents Sea (Vadakkepuliyambatta et al., 2013).of particular note is that many of the high amplitude anomalies coincide with one or several faults. These systems can relate to focused fluid migration from deeper to shallower areas.

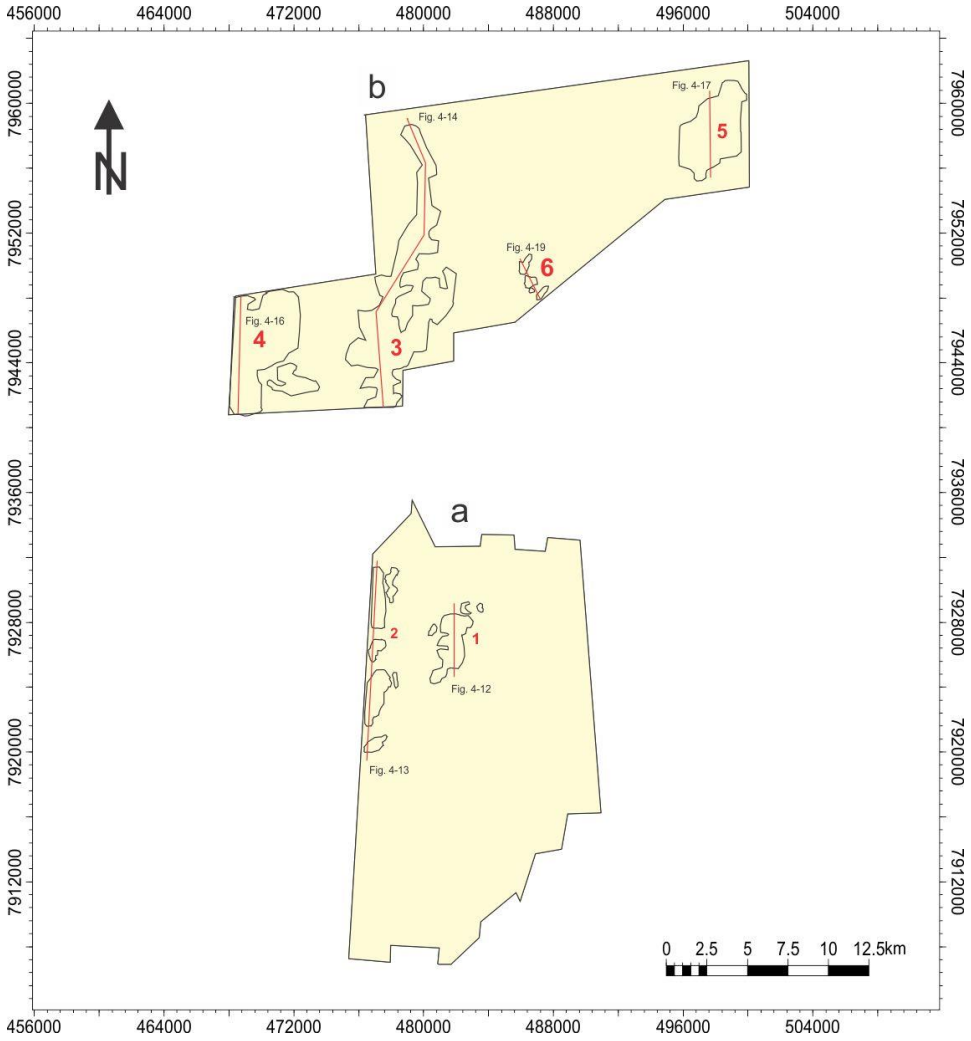

Figure 4-11. An overview map showing the main areas where shallow high amplitudes occur within the two datasets.

4.3.1 Amplitude anomaly 1

Strong reflection amplitudes occurs within the Upper Paleocene stratigraphy, in the northern part of the dataset ST8320R00 (figure 4-11). The high amplitude anomaly occurs as a laterally continuous reflection (figure 4-12), and shows reversed polarity relative to the seabed (figure 4-12). Chaotic reflections occur beneath the bright spot, and acoustic masking is observed next to the faults (figure 4-12). Several deep-seated normal faults with a distinct throw are observed within the Hekkingen Formation and extend into the Upper Paleocene stratigraphy. The top of the high amplitude is located at ~672 ms (TWT) and the base at ~730 ms (TWT). Depth converted data with an apparent velocity of 1800 m/s (chapter 3, table 3.2) shows the vertical extent of the high amplitude anomaly of 58 ms TWT (65 m TVD). The high amplitude anomaly occurs as an elongated object oriented in a south-northward direction. The length of the object is 4.3 km and the width at its broadest is 1.4 km. The amplitude anomaly covers an area of 6.02 km² (figure 4-12).

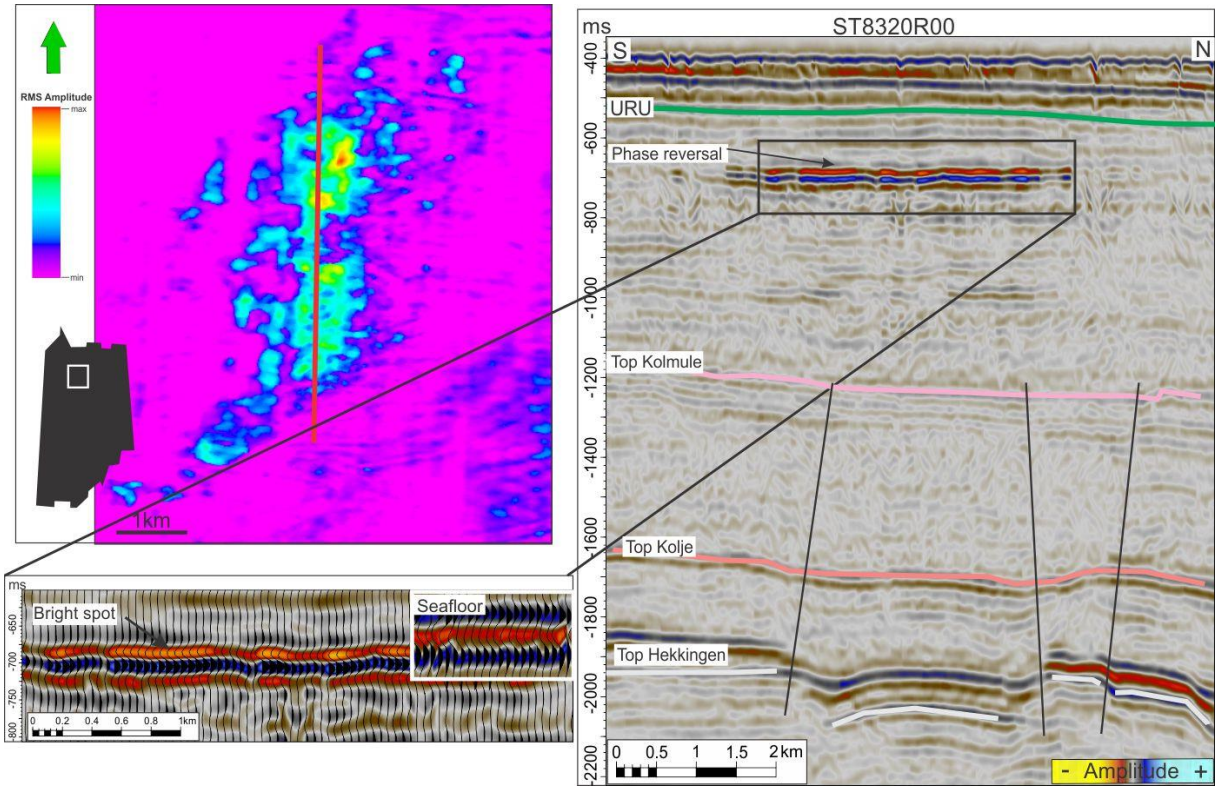

Figure 4-12. Seismic cross section of the amplitude anomaly 1 (figure 4-11), zoomed in seismic section shows phase reversal relative to seafloor. RMS amplitude map including values between 600-850 ms TWT of amplitude anomaly 1 where the red line shows the location of the seismic line.

4.3.2 Amplitude anomaly 2

Amplitude anomaly 2 is located to the north-west part of the dataset ST8320R00 (figure 4-11 and 4-13). The object shows four narrow but separated bodies located in the same layer, just below URU within the Upper Paleocene stratigraphy (figure 4-13). The high amplitude anomaly shows a phase reverse reflection relative to the seafloor. Beneath the bright spot the reflection is chaotic, and acoustic masking occurs next to the faults from the Hekkingen Formation (figure 4-13). The strong reflection has an orientation of south-north direction and is located with a distance from south to north of 1.2 km, 2.2 km, 1.8 km and 1.1 km (figure 4-13). The total length of the four bodies is 12.7 km with an average width of 1.1 km (figure 4-13). The top of the objects are located within the same level at ~700 ms (TWT) and an average base of ~760 ms (TWT). Together they cover an area of 13.97 km².

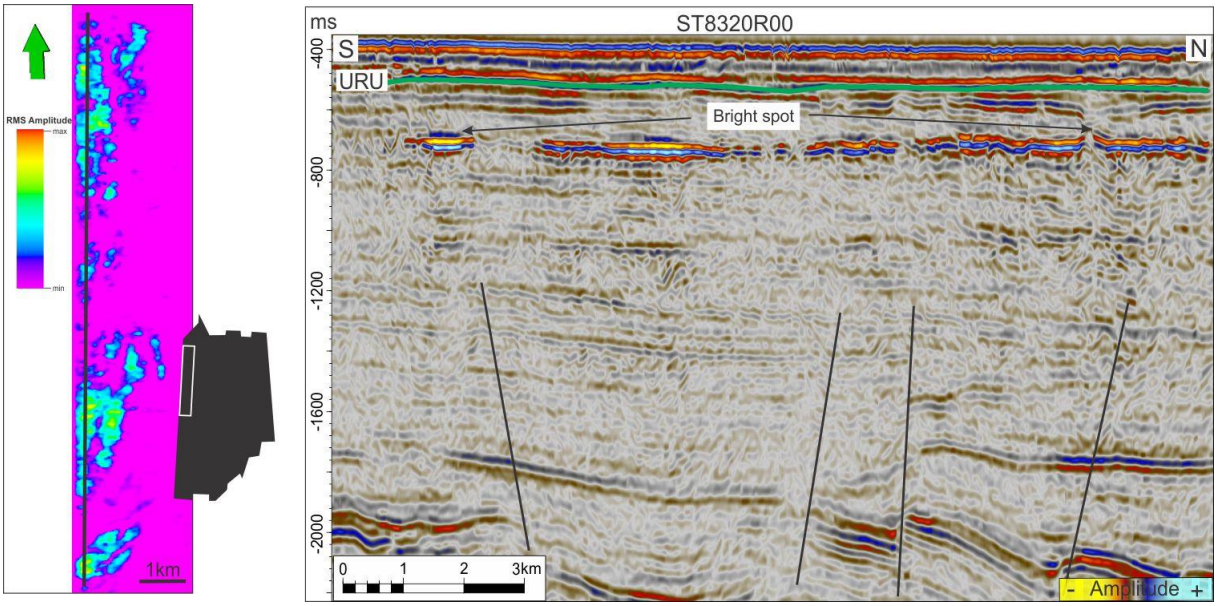

Figure 4- 13. Seismic cross section through amplitude anomaly 2 (figure 4-11). RMS amplitude map is including the values between 600-850 ms TWT of amplitude anomaly 2 where the red line shows the location of the seismic line.

4.3.3 Amplitude anomaly 3

Amplitude anomaly 3 is located within the Upper Paleocene stratigraphy (figure 4-18*a*). Geographical the anomaly is located south-west and stretches out towards north-northeast in dataset LN0901 (figure 4-11). The amplitude anomalies are strongest in the south-western part and pitches out into a meandering shape towards the north (figure 4-14). The southern part of the bright spot is located at a higher level, where the strong reflector occurs 180 ms (TWT) below the seafloor (figure 4-14*a*). Depth converted data shows that the top to be located at 504 m (TVD) beneath the sea level, with apparent velocity of 1800 m/s

(chapter 3, table 3.2) The top of the bright spots is located between 575 ms to 675 ms (TWT) and the base is located between 625 ms to 725 ms (TWT). Depth converted data shows location of a top between 518 m to 608 m (TVD) to, and a base between 563 m to 653 m (TVD) beneath sea level.

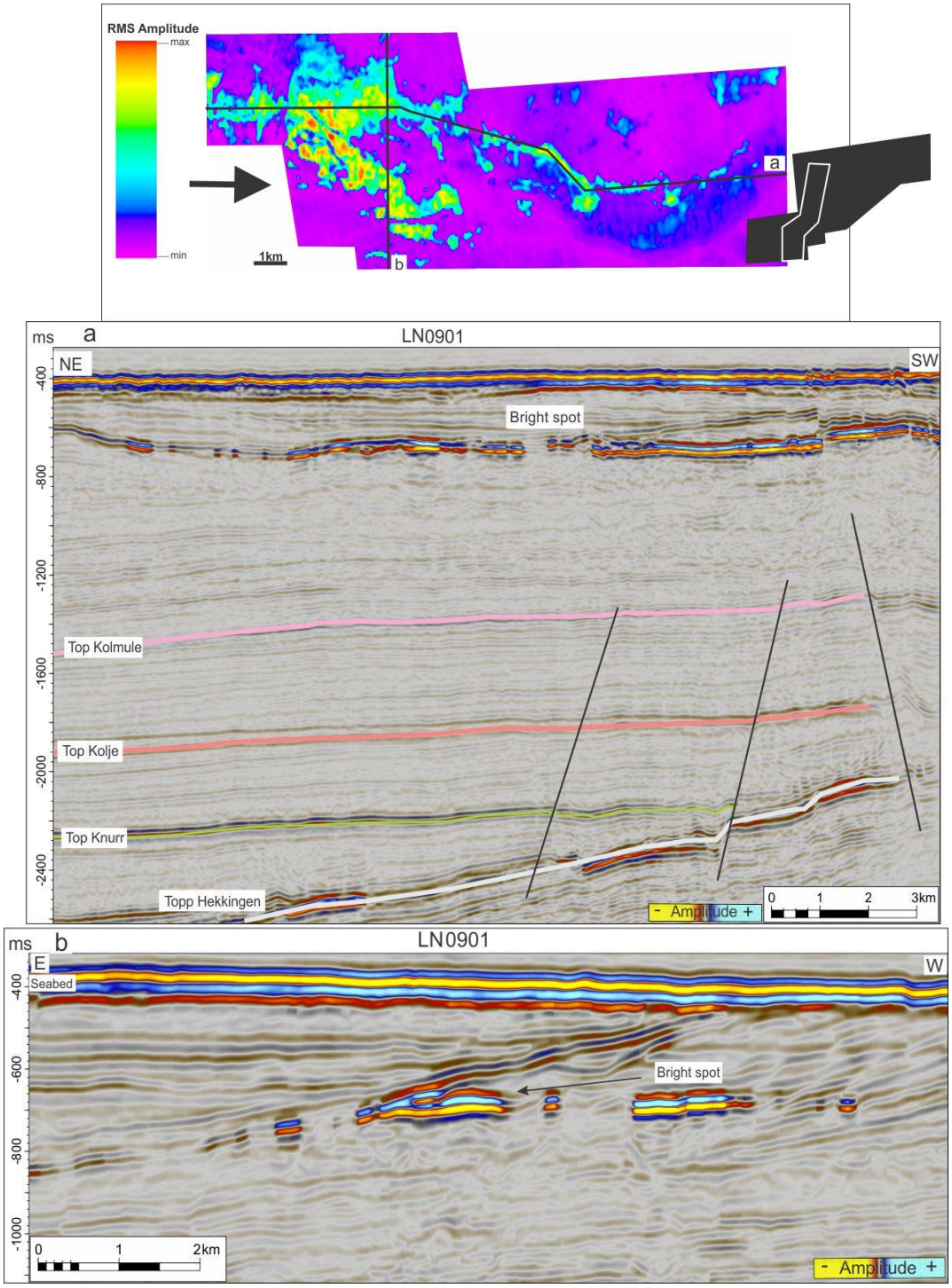

Figure 4- 14. RMS map for amplitude anomaly 3 (figure 4-11), including values between 600-900 ms (TWT). *a*: seismic cross section that shows the relation of the object. *b*: Seismic corss section that shows the high amplitude cutting the dipping strata.

The bright spots show reversed polarity relative to the seabed and flat spots are observed just beneath the amplitudes which show phase reversal from the bright spots (figure 4-15). The total length of the object is 16.9 km and the width varies from 0.3 to 4.7 km. The area of the object is 23.83 km². Beneath the amplitude anomaly an area of acoustic masking occurs horizontally from the south towards north along the high strong reflectors (figure 4-14*a*). Deep-seated faults within the southern area of the bright spots initiate from Hekkingen Formation and extend into Upper Paleocene level. Acoustic masking occurs next the faults (figure 4-14*a*). The strong reflections correspond to a depth from 225 m to 369 m below the seabed, using a velocity 1800 m/s for sediments. The high amplitude reflection is discordant and looks like they are crosscutting the dipping strata (figure 4-14*b*).

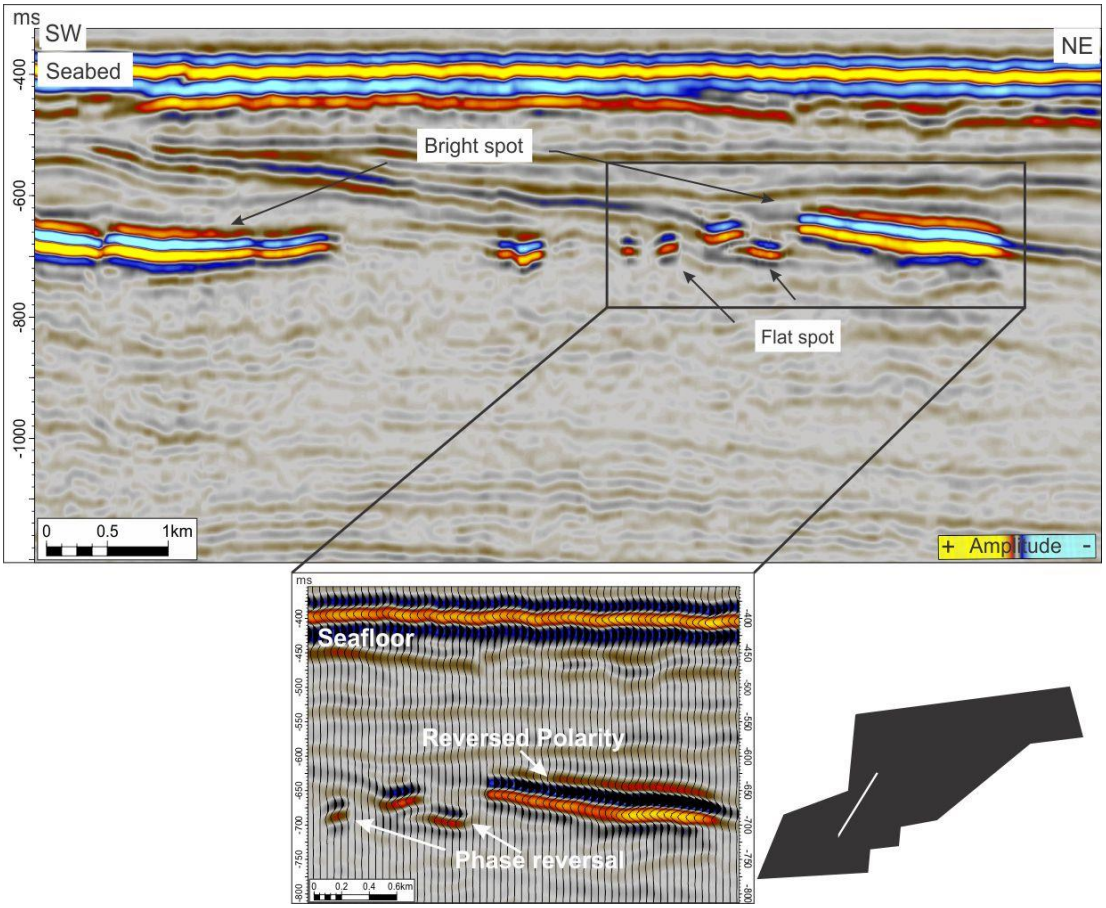

Figure 4- 15. Seismic intersection from south to north through amplitude anomaly 3. Flat spots are observed in the enlarged seismic section just beneath and to the south of the bright spot.

4.3.4 Amplitude anomaly 4

Amplitude anomaly 4 is located within the Torsk Formation in the western part of the dataset LN0901 (figure 4-11 and figure 4-16). The strong reflection is laterally continuous with negative reflection coefficient relative to the seabed (figure 4-16). The top of the continuous negative reflector occurs at ~890 ms (TWT) and the base is traced down to ~930 ms (TWT). The bright spots mimic the seafloor, and acoustic masking occurs below and above the high reflector (figure 4-16). The high amplitude anomaly pitches out in the south-north direction, in an otherwise oval body (figure 4-16). The total length of the object is 7.3 km, and a maximum width of 4 km. The total area the object covers is 32.12 km². There are several deep-seated faults that extend into the high amplitude anomaly, and possibly extend up to the seafloor.

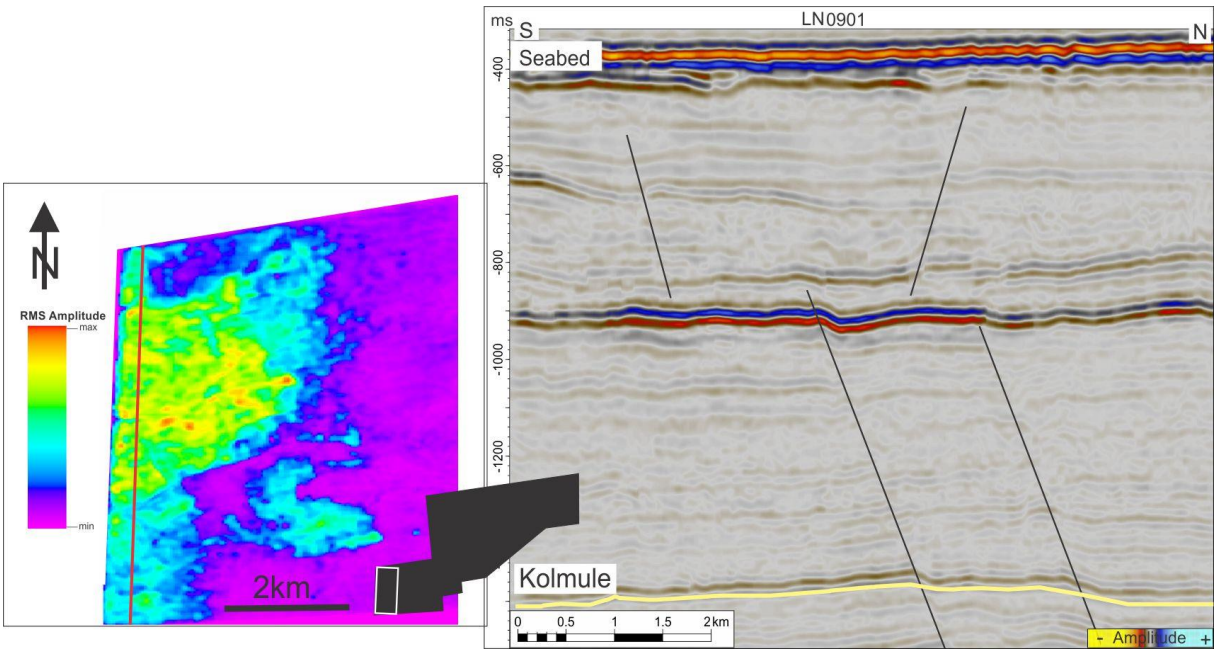

Figure 4- 16. RMS amplitude map which indicates values between 800-1000 ms TWT. To the right seismic cross section (figure 4-11) which shows the high amplitude that is indicated from the red line in the RMS map.

4.3.5 Amplitude anomaly 5

Amplitude anomaly 5 is located in the eastern part of the dataset LN0901 (figure 4-11 and figure 4-17). The bright spot occur within the top of Lower Cretaceous stratigraphy, just below top of Kolmule Formation. The high amplitude anomaly is dipping towards the west-northwest, continuous with the Kolmule Formation (figure 4-18). The top of the high amplitude anomaly, which occur within a much lower level than the other bright spots, has a location of ~1205 ms (TWT) and ~1240 ms (TWT). The bright spot lies within the top of the polygonal faults (figure 4-17). The object shows an oval to elongated shape where it

pitches out in the south and north (figure 4-17). The total length of the object is 5 km and is 3.9 km wide, and covers a total area of 19.5 km². Deep-seated faults extend from the Hekkingen Formation to Kolje Formation.

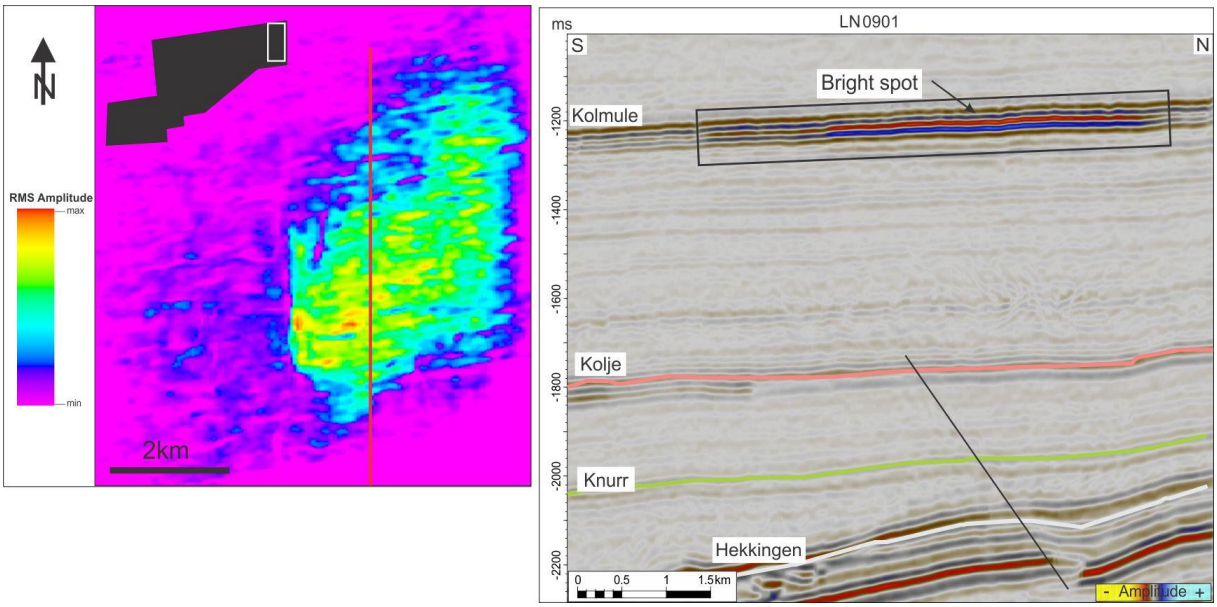

Figure 4- 17. Seismic cross section from dataset LN0901 shows high amplitude anomaly within the Kolmule (figure 4-11) Formation. RMS amplitude map which indicates the values between 1100-1500 ms TWT

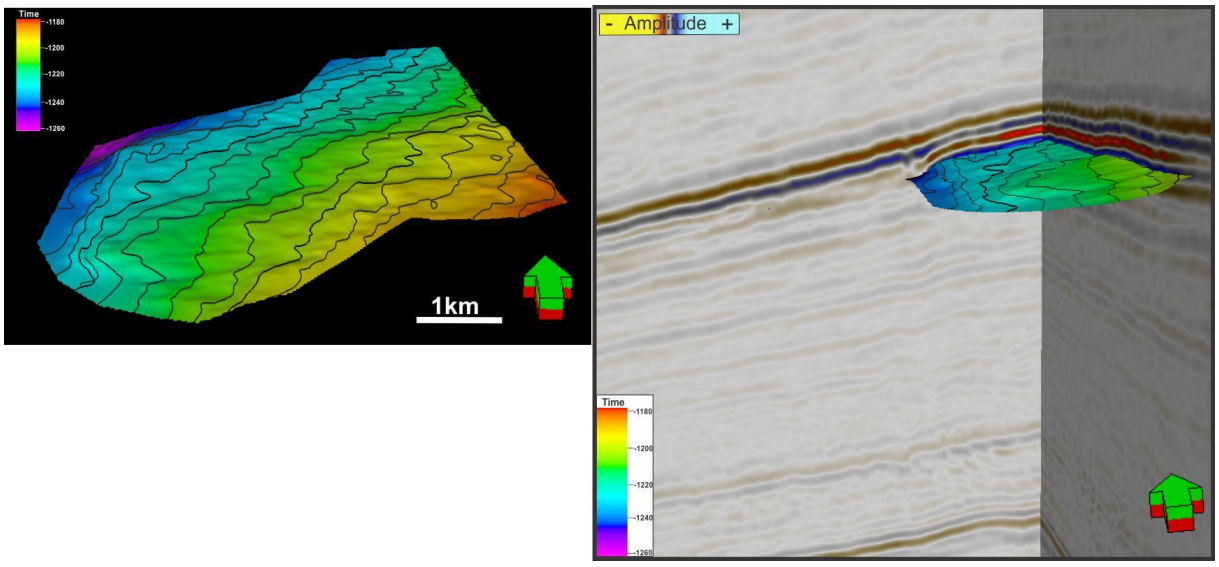

Figure 4- 18. Time-map of the high amplitude reflection, where the dip increases towards the west. Below 3D view of the high amplitude reflection where the time-map shows how the reflection is dipping towards the west.

4.3.6 Amplitude anomaly 6

Amplitude anomaly 6 is located in the southern-middle part of the dataset LN0901 (figure 4-11 and 4-19). There are two small patches of strong reflections with an elongated and oval

shape. They are two narrow, but separated bodies (figure 4-18) within the same layer. They are located within the Upper Paleocene strata within the Torsk Formation. The bright spots have reversed polarity relative to the seabed. The top of the bright spot furthest south is ~650 ms (TWT) and a base of ~680 ms (TWT), while the other object has a top of ~640 ms (TWT) and a base of ~695 ms (TWT). The length of the two objects is ~950 m and ~700 m respectively, and is ~450 m and ~700 m wide. Together they cover a total area of 1.9 km². The lateral extent of high amplitude anomalies occationally coincides with a fault (figure 4-18).

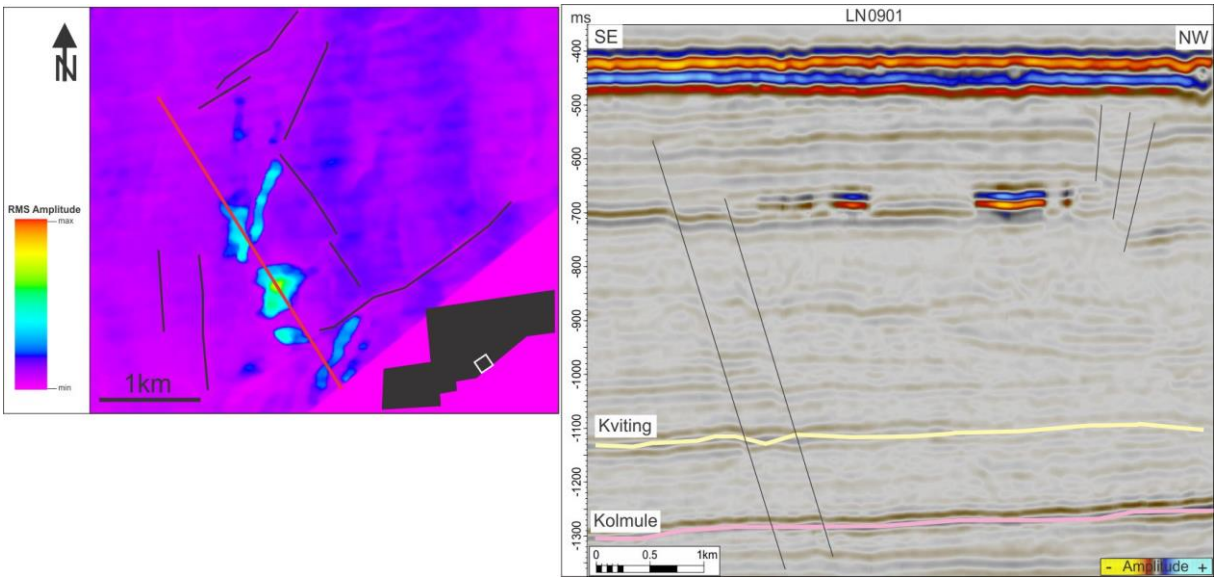

Figure 4- 19. RMS map from dataset LN0901 which includes the values between 600-900 ms TWT. Above shows a seismic cross section with high amplitude (figure 4-11) anomaly which is indicates in the RMS map with a red line.

	Dataset	Shape	Size (km)	Area (km²)	Top (TWT)	Base (TWT)
1	ST8320R00	Elongated body	4.3 x 1.4	6.02	672	730
2	ST8320R00	3x Elongated body	(1.2x0.8) x (2.2x0.35) x (1.8x1.2) x (1.1x1.2)	13.97	700	760
3	LN0901	-	16.9x(4.7x0.3)	23.83	560-640	610-660
4	LN0901	Oval body	7.3x4	32.12	890	930
5	LN0901	Oval body	5x3.9	19.5	1205	1240
6	LN0901	Elongated and oval body	(0.95x0.45) x (0.7x0.7)	1.9	650/640	680/695

Table 4.1 Summarized details for the different amplitude anomaly.

4.4 Vertical fluid migration

There are several areas with acoustic masking in the two datasets. These areas vary in shape horizontal and vertical extent. They can mainly be identified as circular to semi-circular vertical zones of chaotic seismic data, discontinuous reflections and a lower frequency response. These zones are interpreted as focused fluid flow features (Løseth et al., 2002). The seismic indicators of fluid flow occur from deep to shallow strata. Common for these areas with fluid migration is that they truncate into high amplitude anomalies.

In some places a push-down effect occurs. All of the areas with high amplitude anomalies are in contact with one or several faults which may be an indicator that the latter is a fluid migration pathway. There are different fluid migration features which are observed in the two datasets. These will be described in this chapter. Identifying the origin of acoustic masking and its termination may provide a constraint of the top and bottom level of the fluid migration pathway.

4.4.1 Small vertical fluid zone

A small, narrow gas chimney is located in the southern-middle part in dataset LN0901 (figure 4-20). This chimney extends down to ~ 2300 ms (TWT) and has its upper termination at ~1000 ms (TWT) where it terminates in a high amplitude anomaly (figure 4-20). The vertical extent of the acoustic masking area is ~1300 ms (TWT) and assuming a velocity of 2200 m/s (chapter 3, table 3.2) this corresponds to 1430 m (TVD). The chimney penetrates through the Kolje and Kolmule formation and into the Upper Paleocene strata. Sharp boundaries exist to the adjacent layers and there is a clear transition within the chimney with dimmed reflection of the strata outside. Time slice through a variance cube shows that the lateral extent of the chimney is more or less the same in the shallower as is in the deeper level (figure 4-20). Moreover, the chimney structure shows an oval shape in plan view. A deep-seated fault is located just north of the chimney observed (figure 4-4) at ~2200 ms (TWT). This fault can be followed into the Upper Paleocene (figure 4-4). The upper part of the chimney high amplitude lacks the same strong reflection as other high amplitude anomalies (figure 4-20). Push-down effects exist just below the high reflection and in the dimmed area below where some are more difficult to identify than others.

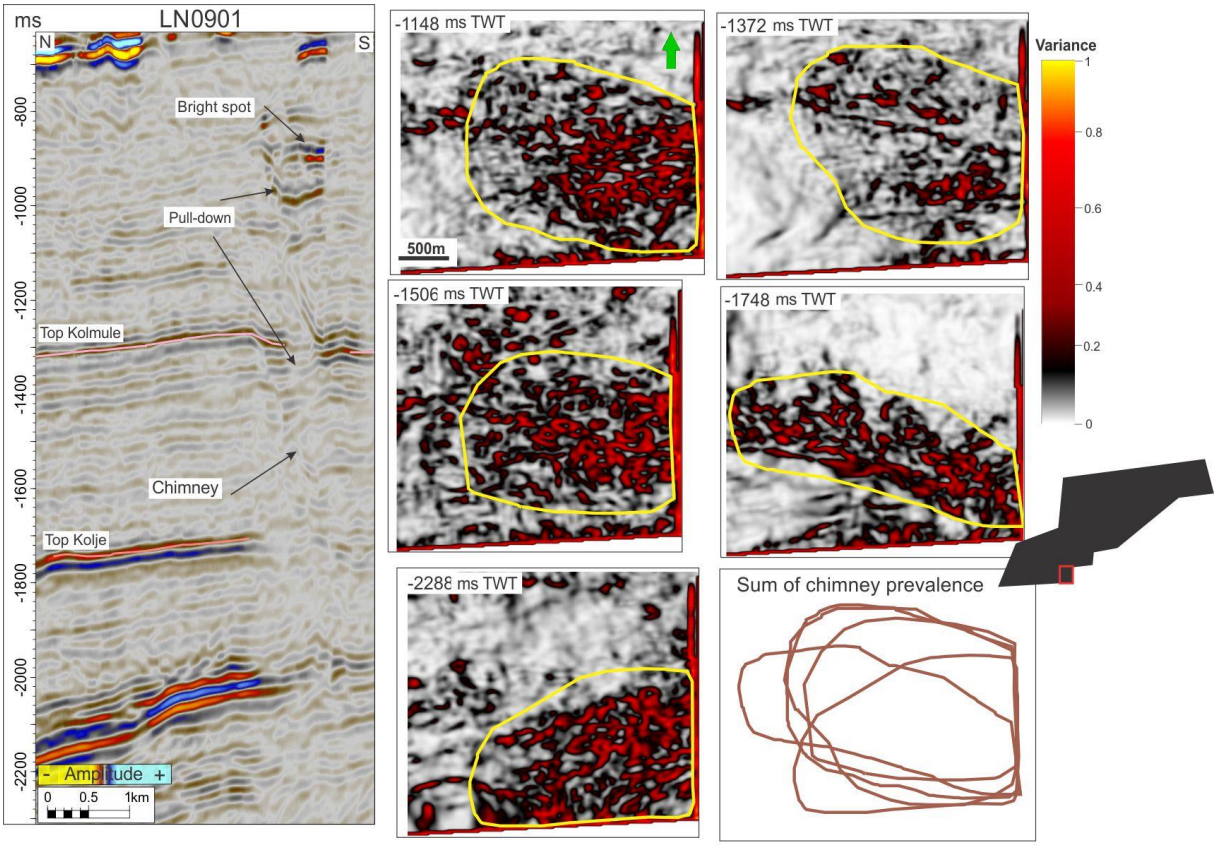

Figure 4- 20. Seismic section through gas chimney, and variance cube that shows different stratigraphic levels. The yellow oval shaped outline is representing the shape of the chimney. Lower right shows a sum of the outline of the chimney from the different stratigraphic levels.

An area of discontinuous patches occurs within the western part of dataset ST8320R00 interpreted and denoted earlier as amplitude anomaly 2 (bright spots) (figure 4-21). Just below these amplitude anomalies chaotic reflection and acoustic masking can be observed (figure 4-21). Acoustic masking occurs next to the faults from the Hekkingen Formation and terminates into the bright spots. These might be small gas chimneys that occur as pathways for fluids. The acoustic masking furthest to the south has a base at an approximately ~1950 ms (TWT) and extends to the Upper Paleocene, Torsk Formation where it terminates into stacked of bright spots at ~1100 ms (TWT). With an expected velocity of 2200 m/s the converted value for the chimney extending vertical is 936 m (TVD). Further to the north acoustic masking occurs over a larger area, it's difficult to give an exact location but it can be followed form the bottom of Hekkingen Formation at ~2400 ms (TWT) and terminates within the high amplitude anomaly at ~750 ms (TWT). The vertical extent of the area with acoustic masking is 1816 m (TVD). Furthest north there is an area with acoustic masking from ~2050 ms (TWT) and extends to the high amplitude anomaly at ~750 ms (TWT). The vertical extent of

the acoustic masking is 1365 m (TVD). The acoustic masking zone may interpret as small gas chimneys. The origin of small gas chimneys coincides with deeper faults indicating that fluid migration originated along fault planes and subsequently formed chimneys where faults terminate. The chimney structures are disturbing the strong reflections of the Knurr and Hekkingen formation. Within one of the small chimneys push-down can be observed located just beneath the top Kviting Formation (figure 4-21). Several deep normal faults are observed with the distinct throw in the Knurr and Hekkingen Formation and terminate in the Upper Paleocene strata, but because of low amplitudes and chaotic reflections it is not possible to locate the faults upper termination accurately.

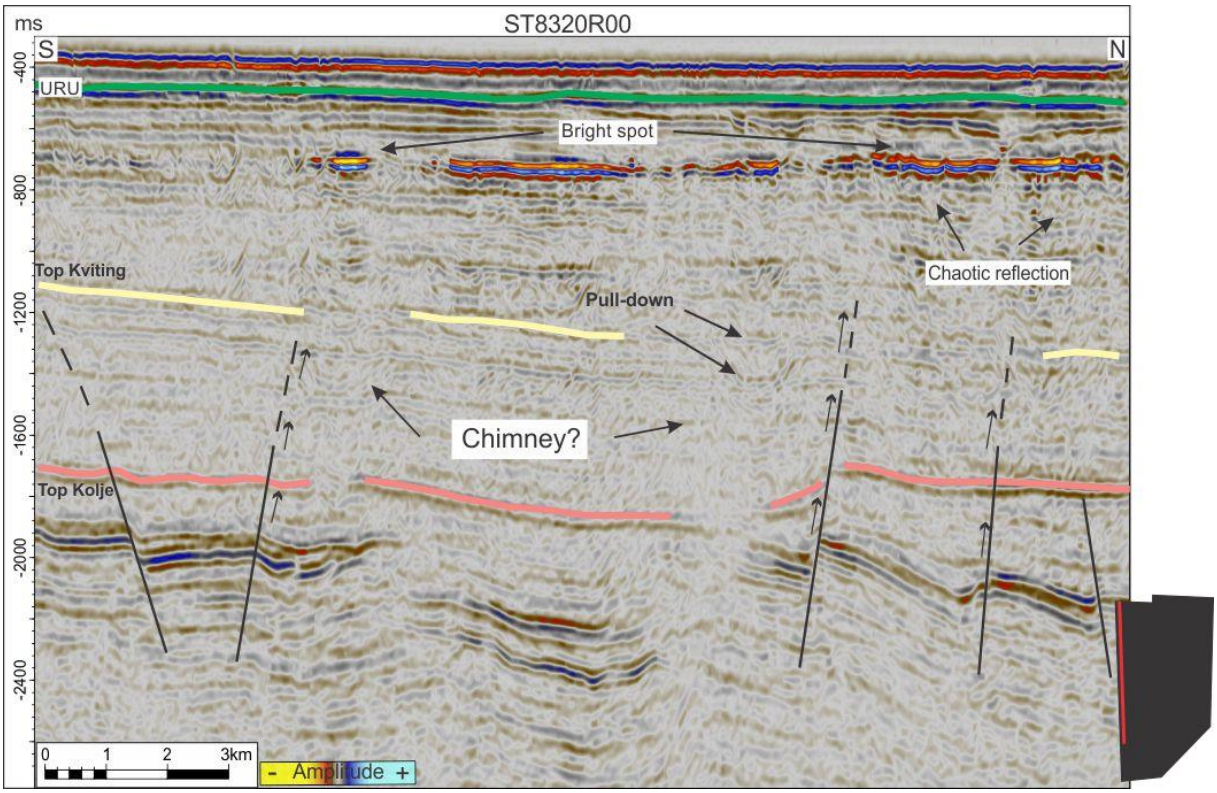

Figure 4-21. Seismic cross section in survey ST8320R00 that is showing fluid migration pathways along faults with chimneys, and shallow gas accumulation. The red line in the polygon indicates the seismic line of ST8320R00

Within the middle-western part of survey LN0901 two thin, sub-vertical structures are observed showing dimmed seismic amplitudes and slight push down (figure 4-22). These structures extend from the Hekkingen Formation into the Upper Paleocene strata and have an orientation of W-E direction. These two structures could be interpreted as pipes and have an upper termination within high amplitude anomalies at ~700 ms (TWT). However, the vertical structures could also result from acoustic masking due to shallow gas accumulation marked

by the bright spot. The transition from the dimmed reflection zone inside the pipes to the reflection outside becomes more distinct with depth. It is clearly observed that they terminate into the Hekkingen Formation (figure 4-22). Just north of the pipe structure there is a deep-seated fault (figure 4-4), and fluids might have emanated along this fault. The amplitude anomaly is cross-cutting the overlying dipping strata

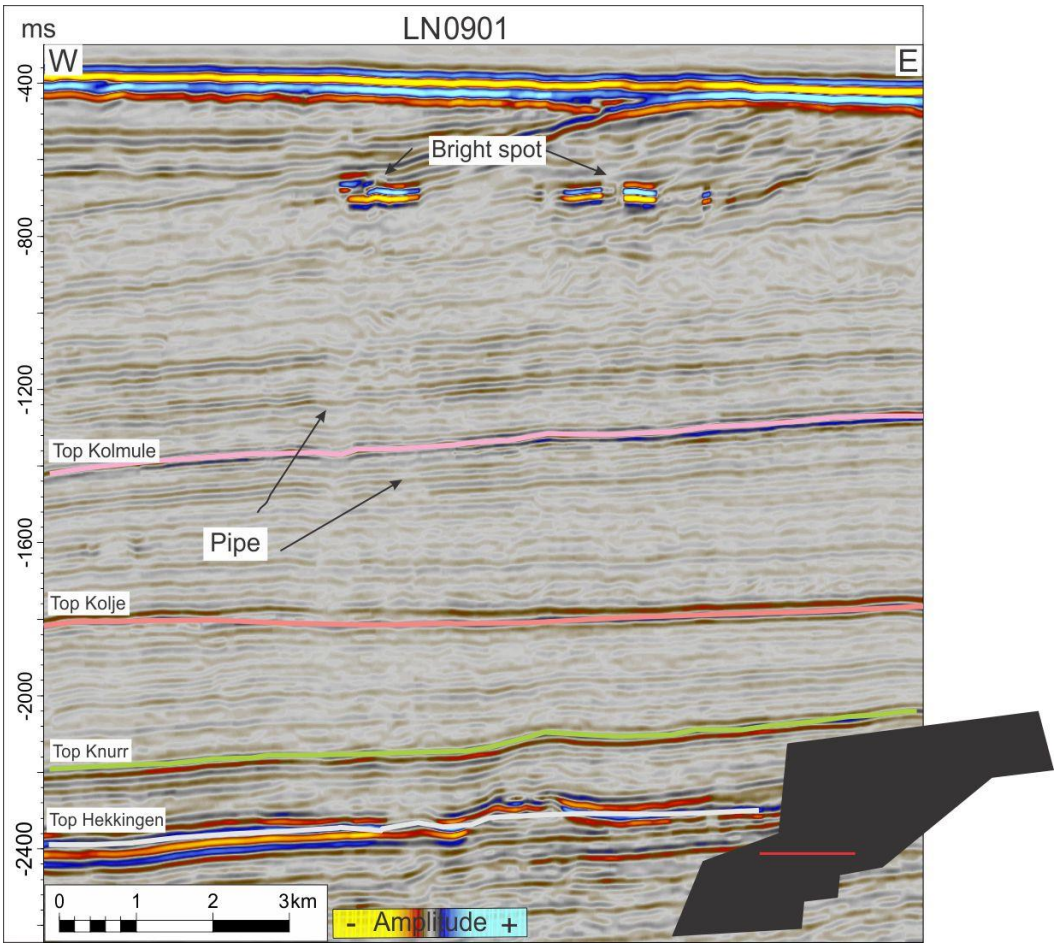

Figure 4-22. Seismic section of dataset LN0901 which shows two pipe structures that penetrate from Hekkingen Formation and terminate at the high amplitude anomaly.

4.4.2 Potential fault related leakage zones

The deep-seated faults seem to have a relation with the shallow high amplitudes, which often coincide with the upper termination of deep-seated faults. This can suggest that hydrocarbons are escaping through these faults. Due to limitation to deeper seismic sections the possible origin of hydrocarbons cannot be detected.

In dataset ST8320R00 high amplitude anomaly 1 occurs in the shallower areas just below URU which has its upper termination at ~680 ms (TWT) (figure 4-23 and table 4.1). Just

below the high amplitude there is an area with chaotic reflection and acoustic masking (figure 4-22). The shallow high amplitudes may be a result from fluid migration from deeper structures and can be a result of accumulation against the faults. There are two deeper normal faults observed in the seismic which are a part of a horst and graben structure. From ~ 2000 ms (TWT) the throw of the faults is very distinct (figure 4-23). It is difficult to see where the faults terminate in the shallower seismic because of discontinuous and chaotic reflections, but they terminate broadly within the Upper Paleocene stratigraphy.

Above the high amplitudes an area with vertical discontinuity is observed that might be fluids moving through low-permeable sediments (figure 4-24) and forming depressions on the seabed. A sub-vertical structure, interpreted to be a pipe that occurs below the high amplitude and penetrates through the amplitude anomaly and towards the seabed. In this pipe structure pull-up is observed above the high amplitude anomaly and can be followed to just below the seabed (figure 4-24).

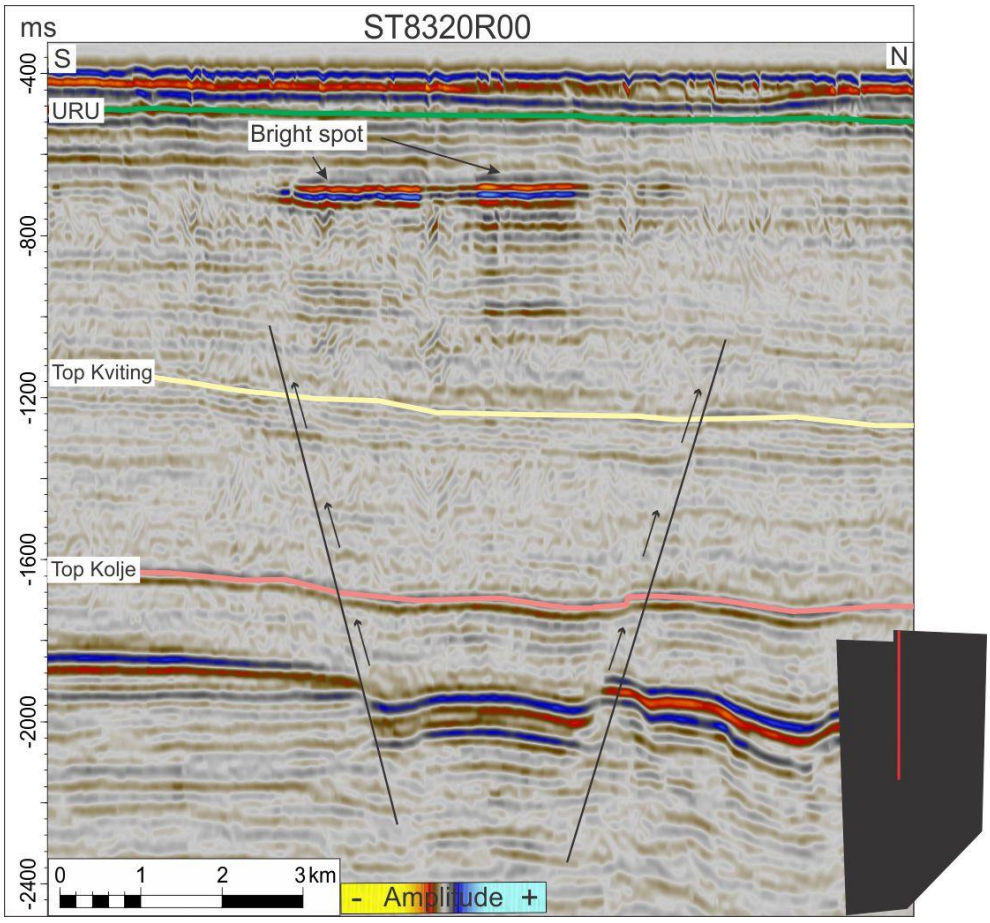

Figure 4- 23. Seismic cross section of survey ST8320R00 which is showing fluid migration pathway along the faults, and shallow gas accumulation. The red line in the polygon indicates the seismic line.

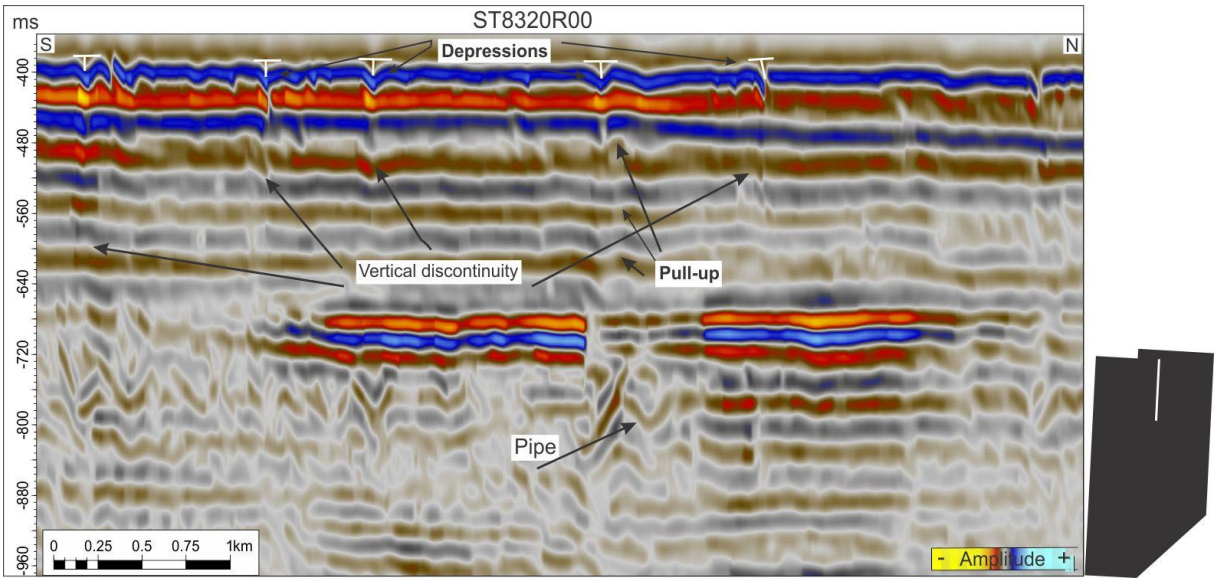

Figure 4- 24. Zoomed in from figure 4-20 which is showing shallow high amplitudes with pipe structure and vertical discontinuity above the bright spot. Pull-up is observed in the pipe structure above the bright spot and towards the seabed, where there occurs depressions.

High amplitude anomaly 4 is located in the eastern part of LN0901, occurring at ~ 900 ms (TWT) (figure 4-25 and table 4.1). A time slice within the variance cube shows that a larger fault can be detected from 2388 ms (TWT) to a upper termination of 600 ms (TWT) (figure 4-25*c*). Other deep-seated faults can be traced to the Lower Cretaceous stratigraphy and Upper Paleocene stratigraphy (figure 4-25). Next to the faults there are reflections with higher amplitude and reversed polarity relative to the seafloor (figure 4-25*a*). This high amplitude may have occurred from leakage when fluid migrated upward along the faults. Acoustic masking can be recognized in deeper levels where the deep-seated faults have the largest throw and just below the high amplitudes. Several smaller faults occur above the high amplitude anomaly. These might pathways for fluid migration into the seafloor (figure 4-25*a*). A sub-circular structure penetrates through the bright spot and is interpreted to be a pipe structure (figure 4-25*b*). Within the pipe structure a push-down effect is observed (figure 4-25*b*).

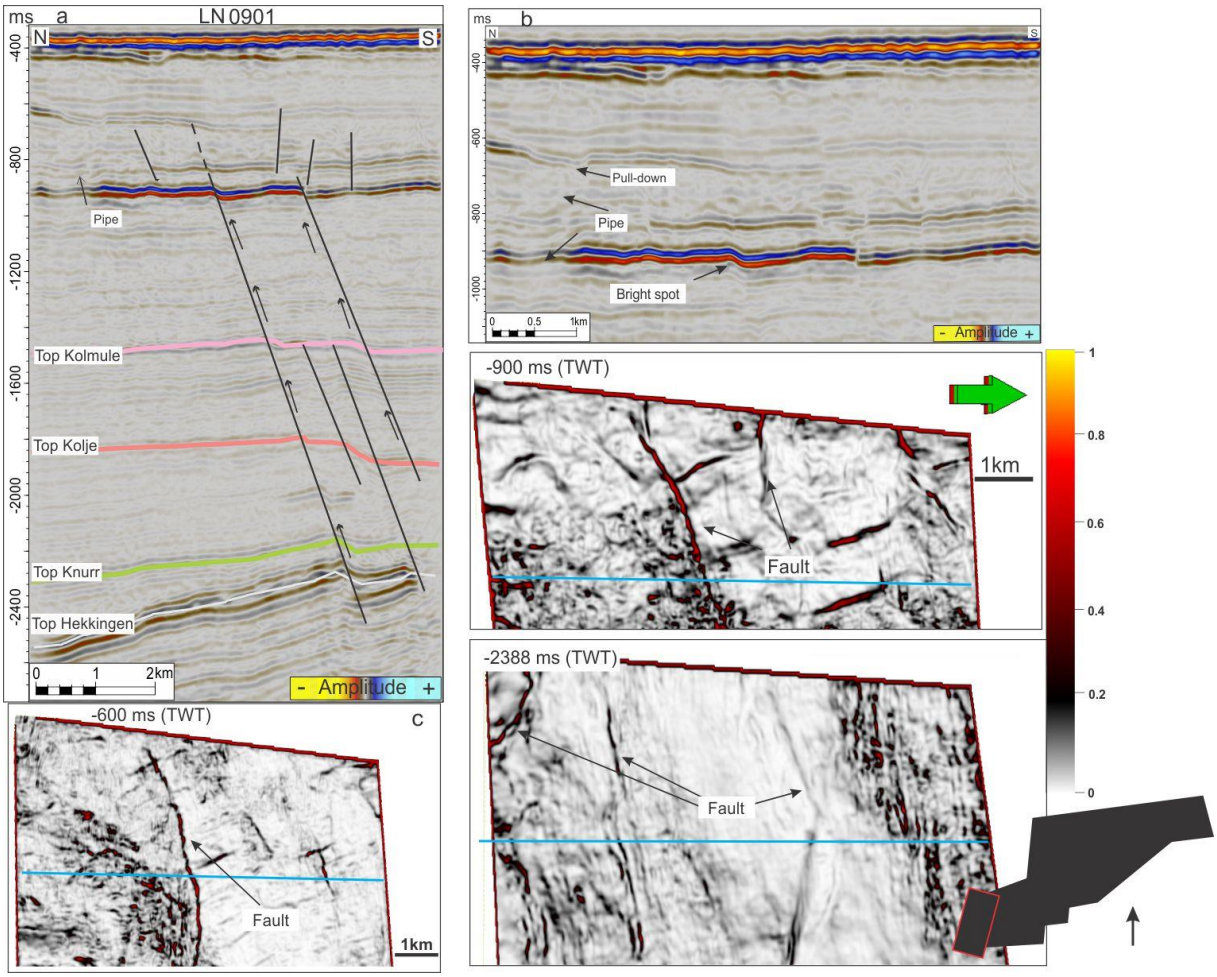

Figure 4- 25. *a*: Seismic cross section of survey LN0901 shows fluid migration pathway along the faults. *b*: A zoomed in section of the high amplitude anomaly which shows a pipe structure and pull-down effect. *c*: Map of a variance cube from -600-, -900, and -2388 ms TWT which shows shallow and deep faults. The red box in the polygon indicates the area.

High amplitude anomaly 6 forms two small patches along mostly continuous reflection amplitudes. Below this anomaly several faults occur. One larger deep-seated fault with an orientation of ENE-WSW occurs within the Hekkingen Formation and terminates within the Lower Cretaceous. In the Lower Cretaceous polygonal faults are observed in the area (figure 4-26) and truncate against the top of Kolmule Formation. These polygonal faults extend with a length of 450 ms (TWT). Shallower faults extend from top Kolmule Formation and also within the same strata as the bright spot occurs. The latter faults might provide fluid migration pathway into the seafloor, where depressions are also observed (figure 4-26). As mentioned in 4.3.6 the faults may limit the high amplitude anomalies to migrate laterally (figure 4-19). The bright spot is located just below the seafloor at ~ 700 ms (TWT) (table

4.1) and just below the reflections are disturbed and weaker. Acoustic masking is observed next to the faults from top Hekkingen Formation to the bright spot.

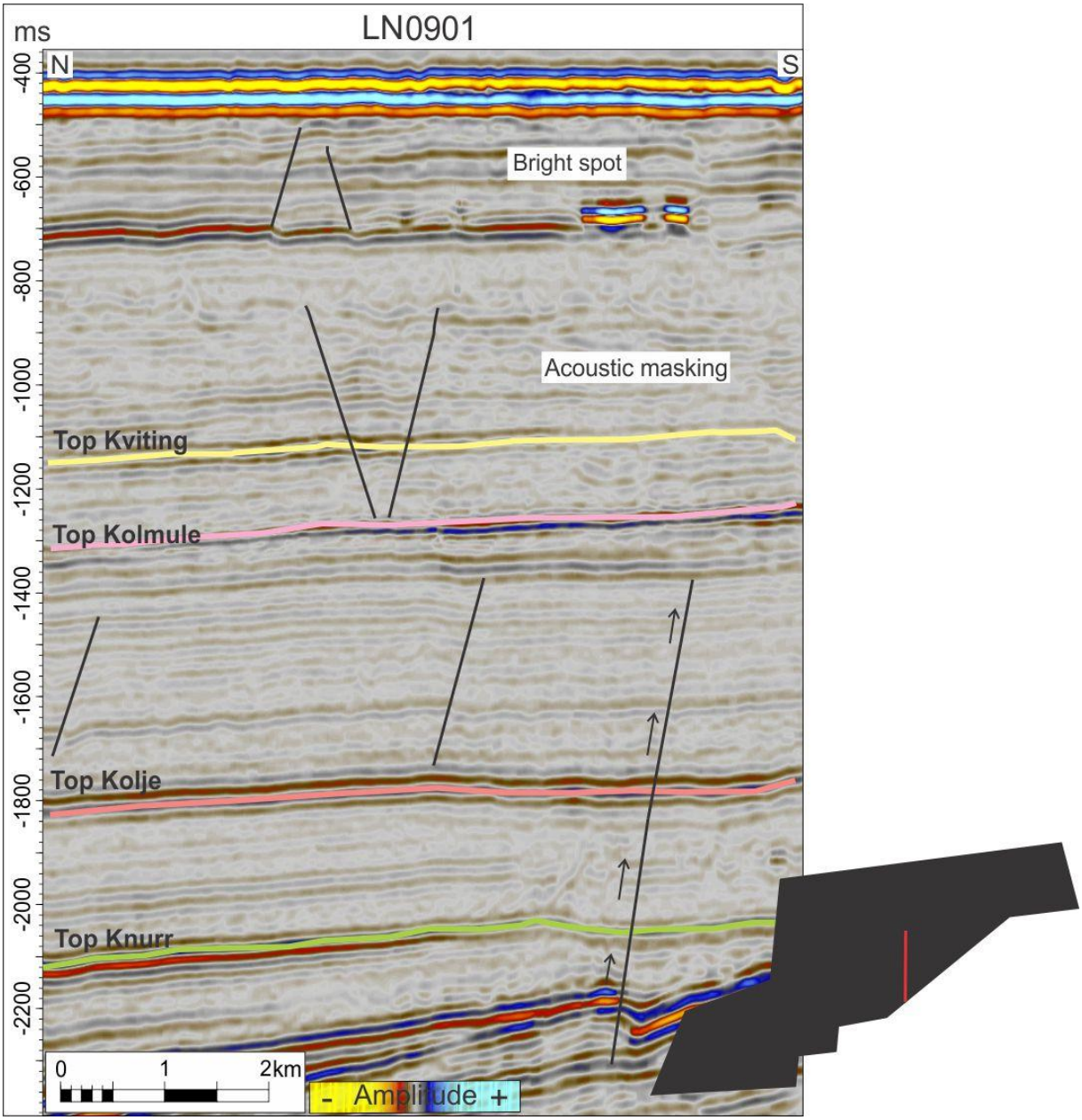

Figure 4-26. Seismic cross section of survey LN0901 shows different types of fault complexes and fluid migration along these faults. The red line in the polygon indicates the seismic line.

In the northeastern section of dataset LN0901 high reflection amplitudes are observed over a larger area of 19.5 km² within the Kolmule Formation (figure 4-18). The high amplitude anomaly occurs just below the top of Kolmule formation at ~ 1200 ms (TWT) (figure 4-27 and table 4.1). It shows reversed polarity compared to the seabed and dips towards the west-northwest. An ENE-WSW trending deep- seated fault at ~ 2300 ms (TWT) is observed and the seismic reflections just above and within the faults are characterized by reflections of

much lower amplitude. The earlier interpreted polygonal fault occur at this depth (figure 4-7) and terminate approximately at the top of Kolmule Formation (4-27). The high amplitude anomaly could be related to the formation of the polygonal faults.

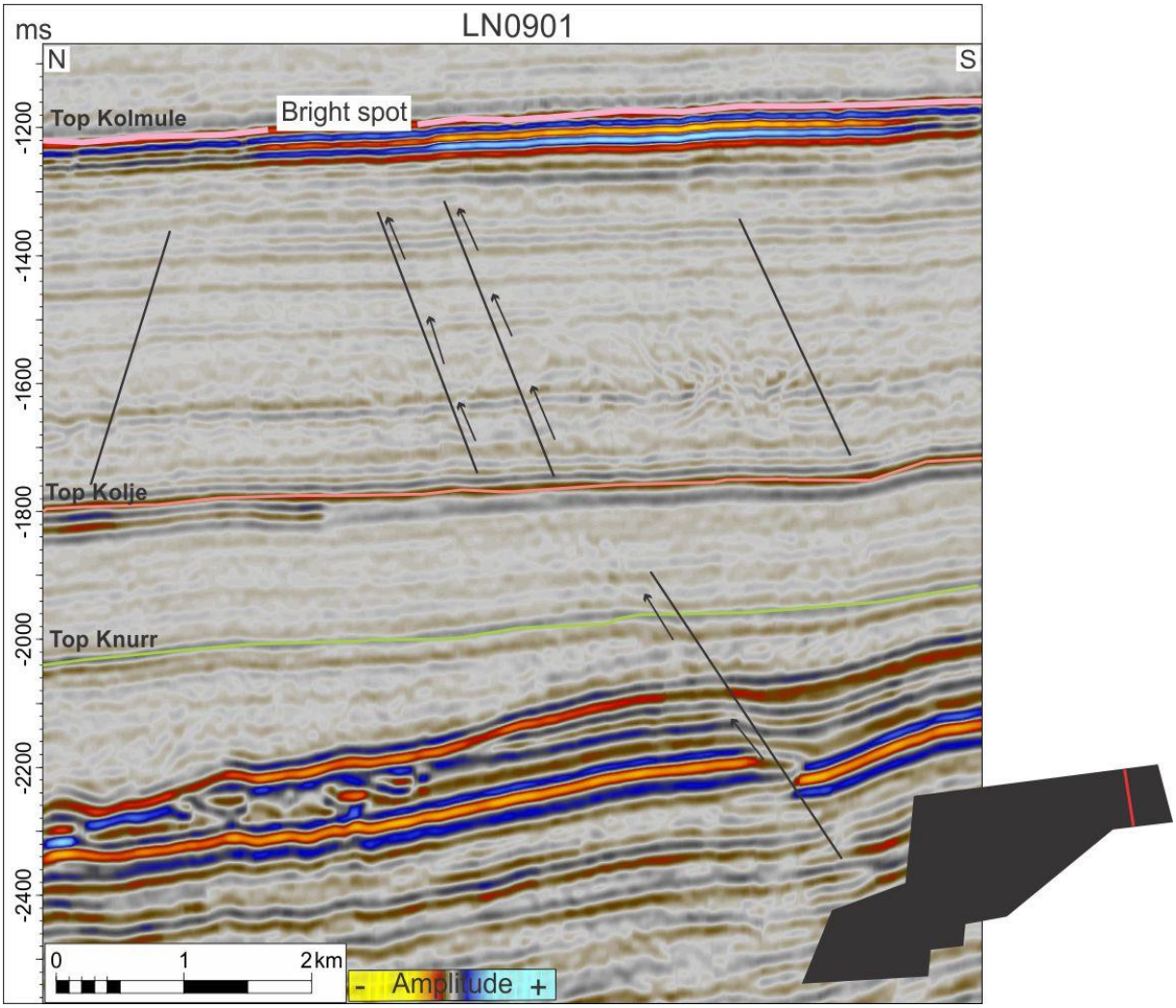

Figure 4- 27. Seismic cross section of survey LN0901 that shows fault complex and possible fluid migration pathway. The red line in the polygon indicates the seismic section.

4.5 Morphological circular to sub-circular depressions on the seabed

During the Plio- Pleistocene the Barents Sea was under glacial influence and large parts of the sea are formed after this period of erosion, deposition and compaction caused by grounded glaciers (Andreasen et al., 2007a; Knies et al., 2009). This created numerous iceberg ploughmarks on the seabed (Andreassen et al., 2007b). The erosion from the iceberg ploughmarks has made it difficult to distinguish the circular to sub-circular depression on the seabed, which are interpreted as pockmarks. These depressions within the plougmarks are observed within both of the datasets (figure 4-28, 4-32), and in some places depressions are observed as chains in these ploughmarks. However, dataset ST8320R00 is to a greater extent dominated by iceberg ploughmarks which is criss-crossing the whole area. The northern and also deeper parts of the seafloor of survey ST8320R00 is increasingly dominated of glacial erosion and ploughmarks. The sub-circular to circular depressions is also randomly distributed.

Artefacts are observed on the seafloor of Survey ST8320R00 as footprints which are coherent noise that is oriented along the direction of the survey (figure 3-8; Bulat, 2005). At the points where the ploughmarks cross the footprints it may apparently appear that depressions occur. Some of these depressions assume to be artefacts and will not be taken into description.

Generally for both of the datasets the depressions have a diameter of ~80-300 m. The depth varies between 5-20 m with a given water velocity of 1500 m/s. The lateral extension varies from 3500 m² to 53000 m². The depressions occur mainly at water depth between 390-420 m (TVD) and 450-460 m (TVD) for survey LN0901 and between 385-425 m (TVD) for survey ST8320R00 (figure 4-28, 4-32). Some of the depressions occur within the same area as the acoustic masking, and above high amplitude anomalies described in section 4.3. Beneath some of the depression faults occur. Faults extending to the seafloor are not observed, but termination into the URU occurs. The pockmarks within the study area formed mostly within ploughmarks varying in shape and these can be placed in different groups based on the classification of pockmarks (Hovland et al., 2002). There are mainly three different categories of pockmarks which occur in the study area. In dataset LN0901 most of the pockmarks occur within the group of normal pockmarks that are circular depressions, measuring from 10 m to 700 m in diameter, and from 1 m to 45 deep (table 4.2, table 4.3). Elongated pockmarks are more or less the same as normal pockmarks, but with one axis much longer than the other. Especially in dataset ST8320R00 there occur strings of pockmarks consist of small normal pockmarks arranged in a curvilinear chains or strings. They are suspected to be a result of focused fluid flow along near-vertical faults (Hovland et al., 2002).

For dataset LN0901 the depressions occur in three different areas of the seabed. Some of the depressions occur in the same area as the high amplitude anomalies occur within the shallower parts of the seabed. Pockmarks are also observed in the deepest part of the seabed where there no high amplitude anomalies but both deep and shallow faults occur.

The first area with depressions 1, 2, 3 and 4 occurs in the southern/western part of the survey LN0901 (figure 4-28). The depressions occur mainly within the erosion ploughmarks, however, sub-circular to circular shapes are observed in these ploughmarks (figure 4-28). The longest axis varies from 130-170 m, except for depression 2 which have an axis of 270 m. the shortest axis vary from 90-120 m, and for depression 2 it is 250 m. The depth for the depressions is from 8-20 m (V_p = 1500 m/s) (table 4.2). The seismic beneath these depressions show pipe structure; faults and disturbed seismic reflections (figure 4-29). Beneath depression 3 and 4 faults are observed. The faults extend to URU. Pull-downs are weak developed below the depressions and a pipe structure occurs in depression 3 (4-22). In the seismic the depressions have steep sidewalls which are either U-formed or V-formed. The larger depressions are mainly more flat-bottomed (figure 4-29).

The second area observed with depression 5, 6 and 7 is on the east-northern part of the survey (figure 4-28). These depressions occur also in a ploughmark, but it is possible to observe single sub-circular depression within the ploughmark (figure 4-31). The longest axis for the depressions is from 100-130 m, and the short axis is from 80-116 m. The depth varies between 6-12 m (V_p= 1500 m/s) (table 4.2). The lateral extension varies from 6280 m² to 14507 m².

Beneath the depression 6 and 7 small faults are observed (figure 4-31), and weak developed push-down within depression 7. These depressions are located above high amplitude anomaly 5 (figure 4-18). All the depressions are U-shaped in the seismic cross-section.

The third area with depression 8 and 9 occurs in the deepest part of the seabed LN0901 that occurs in the middle east and towards the north of the survey (figure 4-28). The depressions occur as single sub-circular forms and the deeper part of the seabed. The longest axis for these two depressions is 80 m and 135 m, and the shortest axis is 60 m and 110 m. Depression 8 has a steep side-wall and is V-shaped and has a depth of 19.5 m (table 4.2: figure 4-32). While depression 9 is more U-shaped with a smaller depth of 5.25 m (table 4.2). Beneath depression 9 small faults are observed (figure 4-31), however, it is difficult to see how far they extend because of acoustic masking just beneath the seabed. A pipe structure is observed just beneath depression 8.

Depression	Long axis (m)	Short axis (m)	Short axis/long axis	Horizontal extension m^2	Depth (ms TWT)	Depth (m,1500 m/s)
LN0901						
1	170	90	0.53	12010	14	10.5
2	270	250	0.93	52988	22	16.5
3	-, 140	-, 120	0.86	13188	14, 22	10.5, 16.5
4	-, 130	-, 115	0.88	11736	11, 26	8, 19.5
5	130	116	0.89	11838	9	6.75
6	110	88	0.8	14507	15	11.25
7	100	80	0.8	6280	12	9
8	80	60	0.75	3768	26	19.5
9	135	110	0.81	11571	7	5.25

Table4.2. Overview of depressions on the LN0901 seafloor

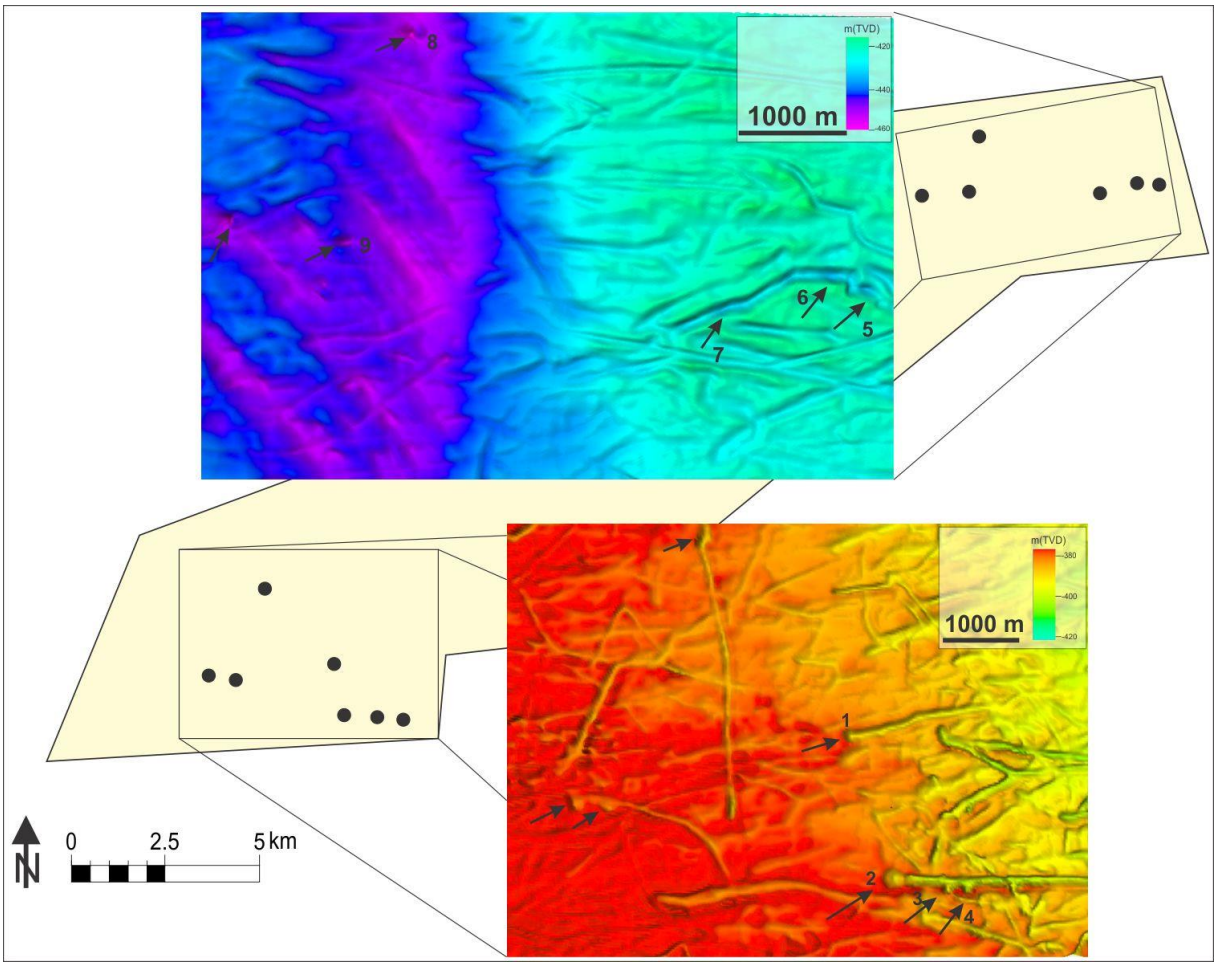

Figure 4- 28. Overview figure of the depression in dataset LN0901. The depressions are numbered from 1-9.

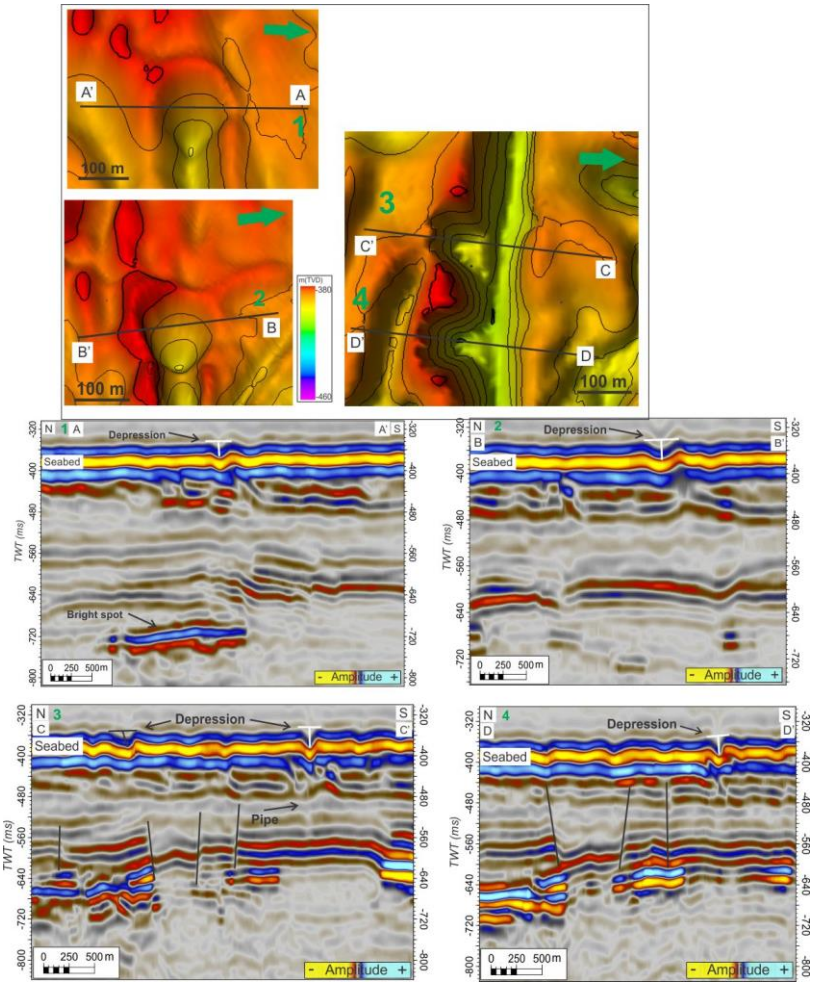

Figure 4-29. 3D map of the depressions. Black line indicates the seismic cross section. 1: Seismic cross section of A-A' through the depressions. 2: Seismic cross section B-B'. 3: Seismic cross dection C-C'. 4: Seismic cross section D-D'.

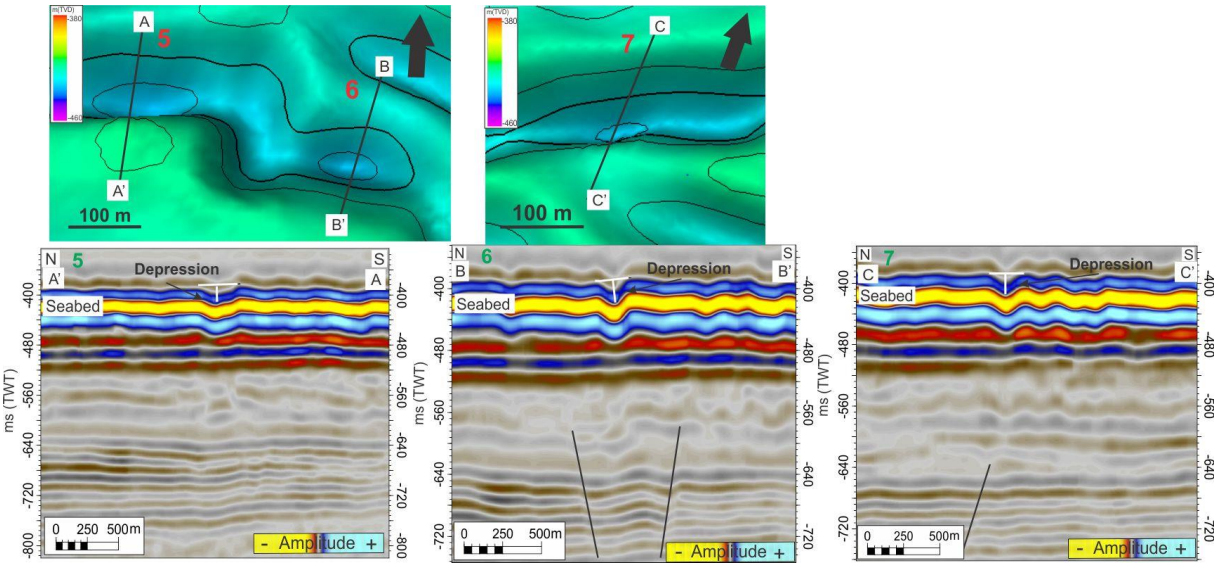

Figure 4-30. Figure 4- 3010. 3D map of the depression 5-7. The black line indicates the seismic cross section of the depressions. 5: Seimic cross section A-A' through the depression. 6: Seismic cross section of B-B'. 7: Seismic cross section of C-C'.

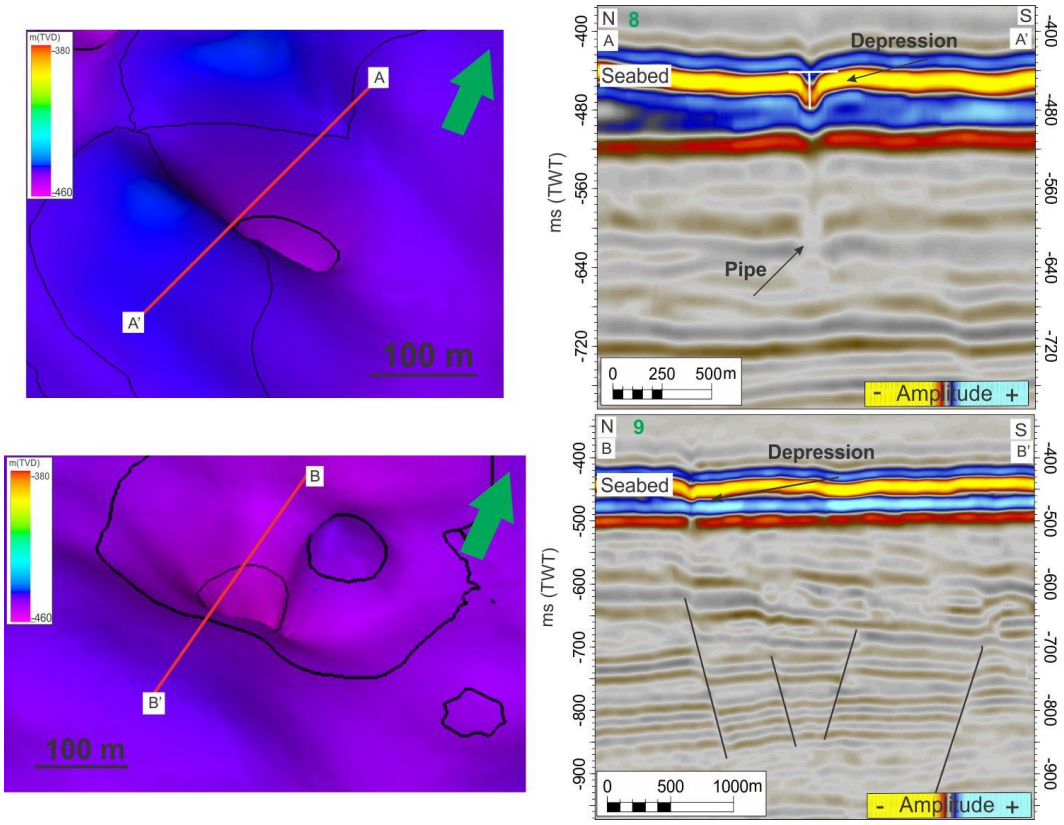

Figure 4-31. 3D map of the depression 8 and 9. Red line indicates the seismic section of the depressions. 8: Seismic cross section of A-A' of depression 8. 9: Seismic cross section of B-B'.

Depressions occur more frequently within dataset ST8320R00. They are mostly observed in the north and also deeper part of the seafloor, within curvilinear furrows but also as single depressions. In some of these curvilinear furrows distinct sub-circular to circular depressions are observed.

Depressions 1, 2, 3, and 4 occur within the same area, in the south-west part of survey ST8320R00 (figure 4-32, 4-33) All the depression has a sub-circular shape with a longest axis from 90-200 m, and shortest axis from 80-125 m (table 4.3). The depth is measured to be between 7-14 m. The depressions occur above the high amplitude anomaly 2, where deep-seated faults and vertical zones with acoustic masking have been documented in section 4.4.1. Weak push-down effect is observed just beneath depression 1 and 4. In seismic cross section all depression are U-shaped.

Depression 4, 5 and 6 occur in the middle part of survey ST8320R00 (figure 4-32, 4-34). Depression 6 occurs as a single, sub-circular depression within a group of several single

depressions. Depression 4 and 5 occur within curvilinear furrows as sub-circular depressions. The longest axis is from 100-160 m and a short axis from 75-136 m. The depth is measured to be between 6-12 m, with a water velocity of 1500 m/s. Depression 4 and 5 occurs above high amplitude anomaly 1, where it has also been documented deep-seated fault (section 4.4.2). Two narrow, sub-circular structures are observed extending towards the depressions and push-down is observed within these structures. The depressions are U-shaped in the seismic cross section.

Depression	Long axis (m)	Short axis (m)	Short axis/long axis	Horizontal extension m²	Depth (ms TWT)	Depth (m,1500 m/s)
ST8320R00						
1	90	85	0.94	6075	18	13.5
2	105	80	0.76	6656	11	8
3	100	90	0.9	7065	14	10.5
4	200	125	0.624	19468	10	7.5
5	115	95	0.87	6990	8	6
6	100	75	0.75	3611	11	8
7	160	135	0.84	16831	15	11.25

Table 4.3. Overview map of depression which occur in dataset ST830R00.

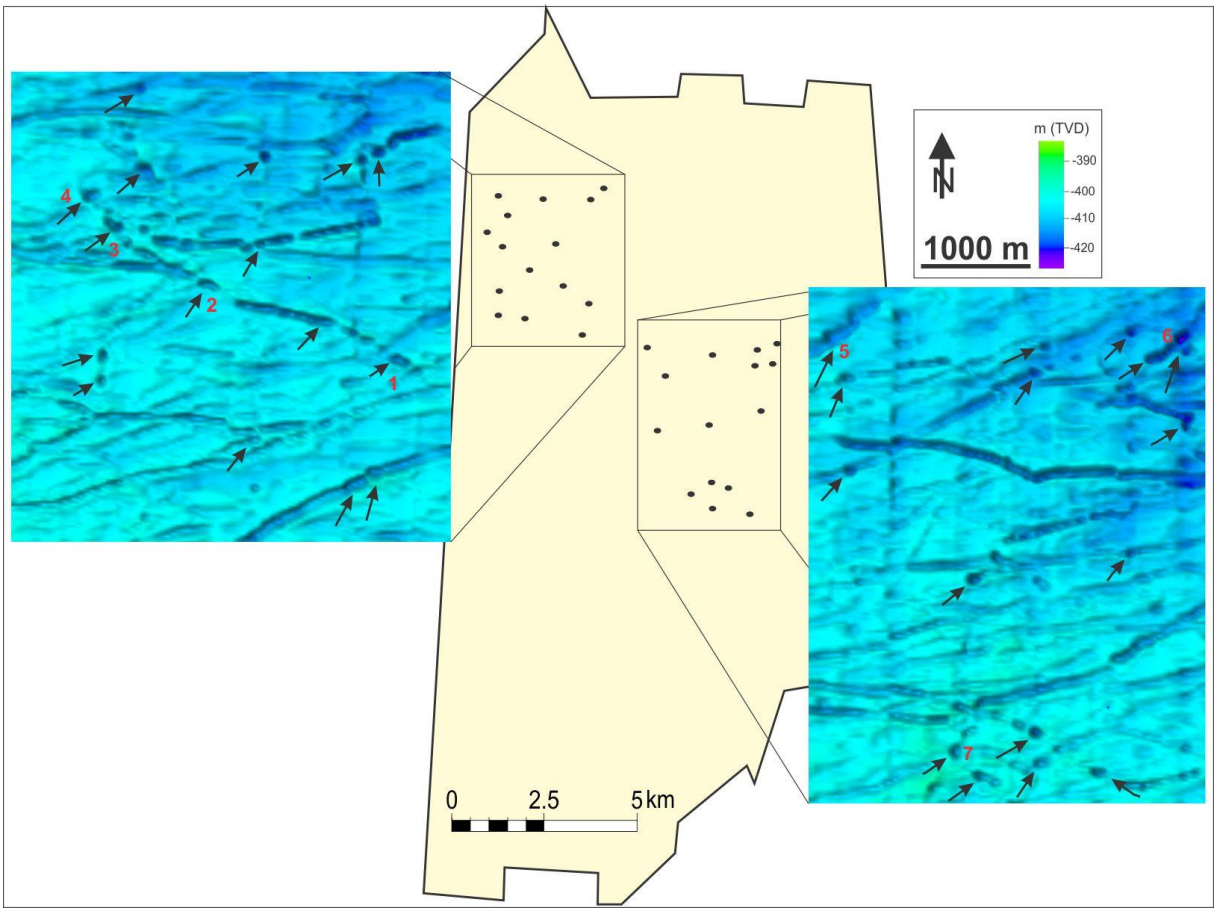

Figure 4- 32. Overview map of depressions locolized within the middle and western part of the seafloor in survey ST8320R00. Depressions are numbered from 1-7. The black arrow indicates depressions, and the circle indicates the location.

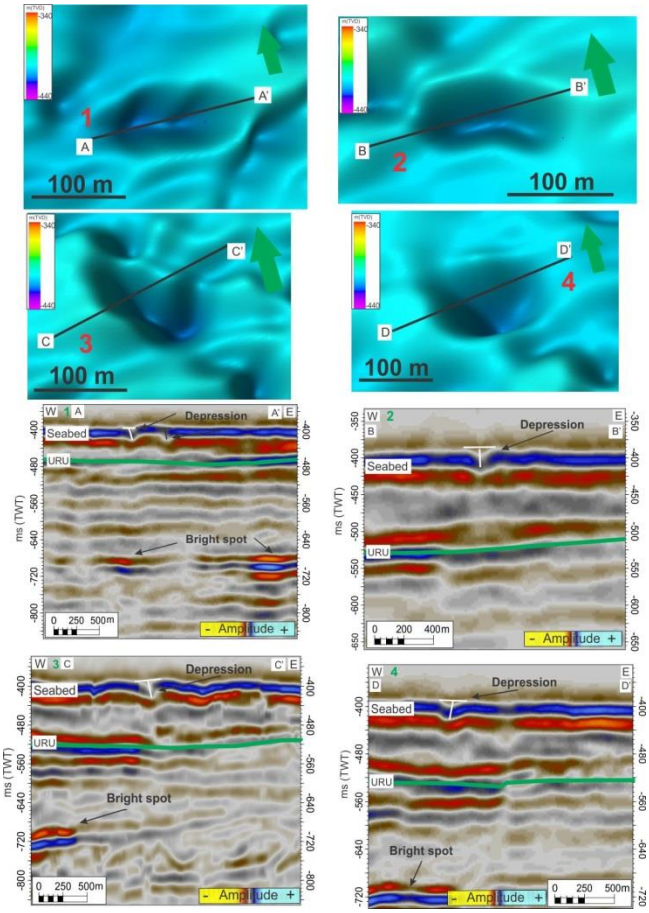

Figure 4-32. 3D map of depression 1-4 in survey ST8320R00. Black line indicates the seismic cross section. 1: Seismic cross section of A-A' through depression 1. 2: Seismic cross section of B-B'. 3: Seismic cross section of C-C'. 4: Seismic cross section of D-D'.

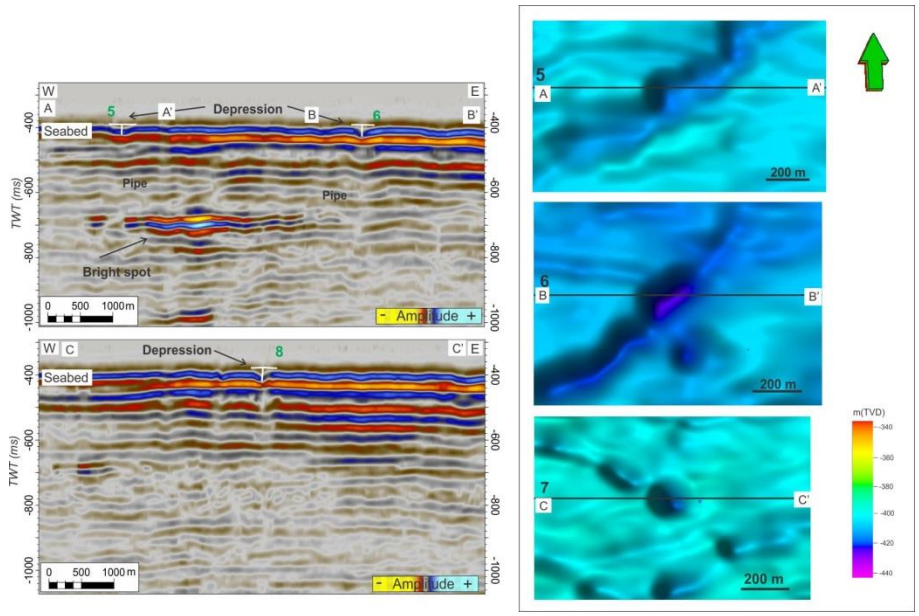

Figure 4-33. 3D map of depressions 5-7 in survey ST8320R00. Black line indicates the seismic cross sections for the depressions. 5,6: Seismic cross section of A-A' and B-B' through depressions 5 and 6. 7: Seismic cross section og C-C'.

5. Discussion

In the result chapter I presented a stratigraphic and structural interpretation and also interpreted high amplitude anomalies as fluid accumulations as well as chaotic and transparent zones as fluid migration zones. The discussion chapter integrates these observations and interpretations aiming at an understanding of the relationship between shallow accumulations, fluid migration and the structural setting. Fluid leakages may have been caused from the Cenozoic uplift and erosion which is calculated to be ~1000 m in the Hammerfest Basin (Nyland et al., 1992; Henriksen et al., 2011; Ohm et al., 2008; Rodriguens Duran et al., 2013).

5.1 Faults

The Barents Sea has been influenced by several tectonic events and has been tectonically active since the Paleozoic time (Gabrielsen, 1984). Hammerfest basin is therefore surrounded by larger fault complexes bordered to the W and N by the Senja Ridge and by the Loppa High, respectively, and the Troms-Finnmark Fault Complex to the S. The Ringvassøy-Loppa Fault Complex separates the Hammer fest Basin from Tromsø Basin (Gabrieslen et al., 1984; Gabrielsen, 1990). In the SW Barents Sea, post-caledonian rifting lead to development of rift basins and later several rifting episodes took place until the final breakup of the Atlantic in Late Cretaceous (Smelror et al., 2009).

The Hammerfest Basin has been interpreted as a failed rift in a triple junction (Talleraas, 1979) with a part of an older rift system overexposed by a younger system (Hanish, 1984; Gabrielsen, 1984). The Hammerfest Basin itself is also characterized by the post-caledonian tectonic activity with the main faulting occurring during the Jurassic period, Kimmeridgian stage. Tectonic movements in the area at that time where dominated by transtensional strike slip movements and updoming along the Asterias Fault Complex. The latest tectonic activity within the basin occurred in the Torsk Formation during Paleocene-Early Eocene age in Cenozoic (Faleide et al., 1984; Gabrielsen, 1984; Ostanin et al., 2012).

The faults presented in the result chapter, especially within the Hekkingen Formation seems to play an important role as a migration pathway, as gas indicators such as acoustic masking often occur along the fault planes and high amplitude anomalies tend to truncate the faults towards shallower depths. The tectonic formation of the different faults systems will be discussed in this chapter.

Table 5.1 Classification of fault system into first, second and third classes (Gabrielsen, 1984)

First class	Basement involved	regional significance	Reactivated	Separate areas of different tectonic outline
Second class	Basement involved	Semi-regional	Reactivated/ not reactivated	Separate areas of different tectonic outline
Third class	Basement detached	Local significance	Not reactivated	Does not separate areas of different tectonic outline

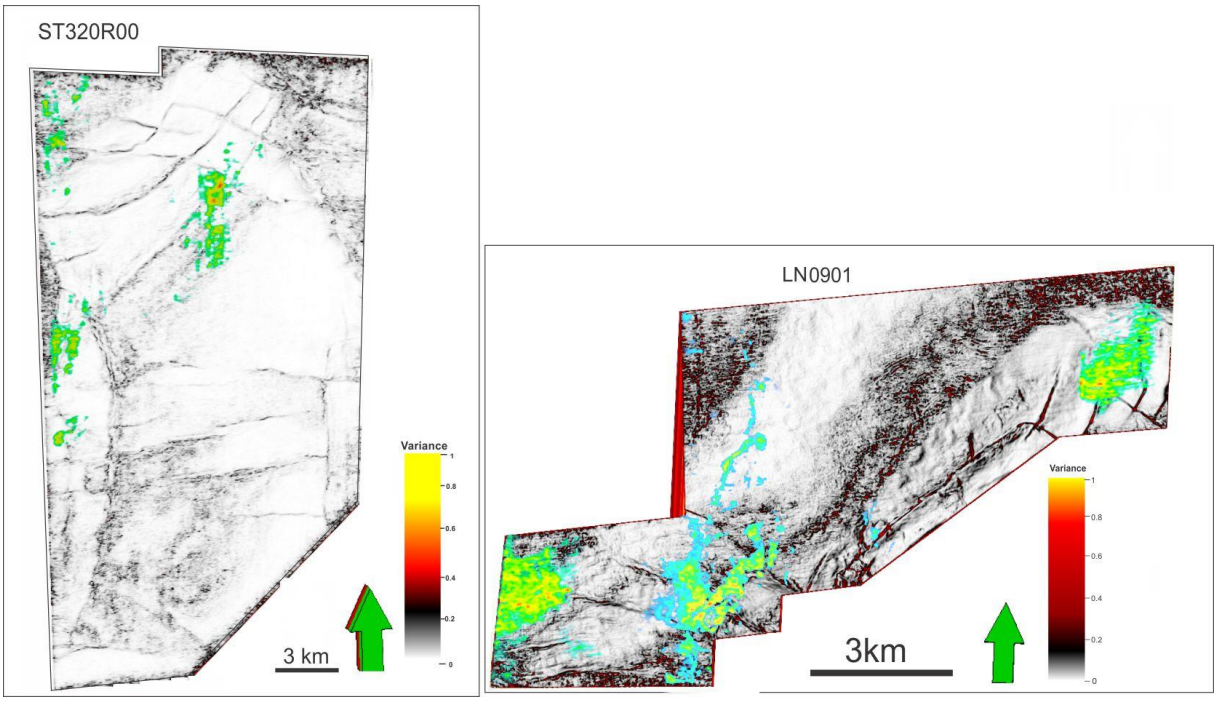

Figure 5- 1. ST8320R00: variance cube at 2000 ms (TWT) that shows the deep-seated fault with high amplitudes from RMS map between -600-850 ms (TWT). LN0901: variance cube at 2200 ms (TWT) with high amplitude anomalies from a RMS map between -600-900 ms and 1100-1500 ms (TWT).

Deep-seated faults occur in both datasets with the main direction WNW-ESE to NNW-SSE, ENE-WSW to NNE-SSW. However, in dataset ST8320R00 the deep-seated faults are mainly Oriented E-W (figure 4-4 and figure 5-2a). Often the located of high amplitude anomalies coincide with deep-seated is shown in a composite image of variance and RMS amplitude map (figure 5-1).

Due to their subsurface location, the WNW-ESE to NNW-SSE oriented faults (figure 4-5*a*, 4-6*a* and figure 5-2*a*) have likely been formed during the regional extension and strike slip adjustments along old lineaments during the Middle-late Jurassic (figure 5-2*b*) (Faleide et al., 1993; Ostanin et al., 2012). This major fault group belongs to the 1st order fault group (table 5.1). The orientations of these faults have their origin from Troms-Finnmark or Ringvassøy-Loppa Fault Complexes connected to the Late Devonian shear (Rønnevik et al., 1982) being dreactivated during the Kimmerian tectonic period.

The Hammerfest Basin has an ENE-WSW striking axis (figure 5-2; Gabrielsen et al., 1990). The major structural NE-SW trending basin can be traced back to Late Devonian to Early Carboniferous times (Rønnevik & Jacobsen, 1984). It is believed that the Late Devonian?-Carboniferous shear was succeeded by an E-W transition regime in the Middle to Late Permian as there occurred a situation through the Mesozoic (Gabrieslen, 1984). During this period the pronounced NE-SW was probably superimposed by a NNE-SSW trending fault

system (figure 5-2*a*; Gabrielsen, 1984). During the main Kimmerian, Rønnevik et al. (1982) speculated an already active strike-slip motion W of Tromsø Basin of compressional features associated with the NE-SW trending fault zones. The faults are linked to the first and second class fault complexes, where the second class is formed in response to movements of the primary features (table 5.2; Gabrielsen, 1984).

The E-W trending fault complexes (figure 5-2*a*) may have been related to the Kimmeridgian tectonic phase which resulted in a transtensional regime and updoming along the Asterias fault complex. The dome-shaped, elongated structures occurring in the central part of the Hammerfest Basin are previously suggested to be associated with an E-W trending swarm of faults in the Hammerfest Basin Fault System (HBFS) (figure 5-2*b*; Gabrielsen, 1984; Ostanin et al., 2012). The main faults are best defined in the Jurassic level but can also be localized in deeper levels. The E-W trending faults which were generated by local deformational events (doming) are third class faults (table 5.1) which have developed inside fault blocks (Gabrielsen, 1984).

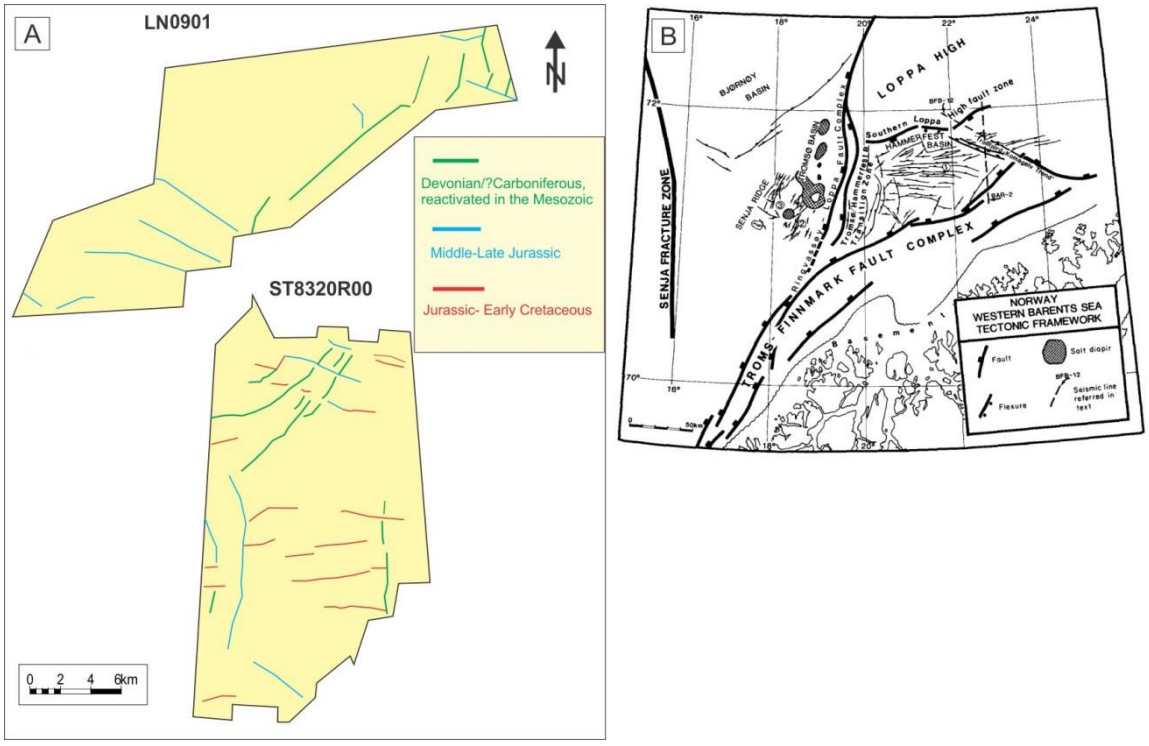

Figure 5- 2. Tectonic activity during different periods within the two datasets, the NE- SW to ENE-WSW trending fault labeled in green, the WNW-ESE trending faults labeled in blue and the E-W trending faults labeled in red. B. Tectonic framework of the SW Barents Sea. Figure from Gabrielsen (1984).

The shallow faults appear as polygonal faults within the Lower Cretaceous Kolmule Formation and shallow normal faults within the Upper Paleocene Torsk formation. These fault complexes are mainly observed in dataset LN0901.

The polygonal faults have three different orientations, WNW-ESE, NE-SW and W-E (figure 4-7) but are only observed within the eastern part of the survey. Polygonal faults are developed in passive margin basins and are normal non-tectonic and non-gravitational faults (Cartwright et al., 2007; Ostanin et al., 2012). The polygonal faults in the studied dataset LN0901 are most distinguished in the Kolmule Formation deposited in early Cretaceous. The faulting is likely to have occurred during the Lower Cretaceous, as the sea level transgressed; shelf starvation and later uplift occurred (Ostanin et al., 2012).

The shallow normal faults are oriented NNW-SSE and NNE-SSW (figure 4-9)and are likely to have developed during Paleocene-Early Eocene time during deposition of Torsk Formation, which was controlled by plate tectonic movements and uplift of highs prior to the opening of the Norwegian-Greenland Sea (Faleide et al., 2008; Ostanin et al., 2012).

Faults occur often where there is acoustic masking and can be related to fluid migration features (Vadakkepuliyambatta et al., 2013). Faults have been proven to be an important factor for migration acting as a seal bypass system (Cartwright et al., 2007). Studies from the Barents Sea show that there is a connection between fluid migration and faults (Andreassen et al., 2007a; Chand et al., 2009; Ostanin et al., 2012).

5.2 Vertical migration of fluids

Acoustic masking along a fault indicates that the fault is, or has been open for vertical fluid migration (Ligtenberg, 2005). Ligthenberg et al. (2003) states further that detection of acoustic masking can give a better understanding of hydrocarbon`s potential source and their migration system which can enhance areas of hydrocarbon expulsion, assist in evaluating the sealing quality of faults and can provide information on charge, leakage and spillage from reservoirs.

5.2.1 Potential source rock

During the extension of the Norwegian-Greenland rifting in the Cenozoic, the Barents Sea has undergone late Cenozoic uplift. As a result of this, many source rocks were supposed to be buried deeper and thermally more mature than expected from the present depth (Dore and Jensen, 1996; Linjordet & Olsen, 1992).

To understand the migration processes and the origin of the hydrocarbons it is important to have knowledge about the quality of the present source rock in the area. In the Barents Sea there are different source rocks present between the Carboniferous and Cretaceous age (figure 5-3). Figure 5-3 gives an indication that the most prolific source rock is located within the Upper Jurassic Hekkingen Formation. However, there is also source rock potential for oil in the Barents Sea between the lower and middle Jurassic. But also during the Triassic and Carboniferous there is potential for petroleum generation in some areas (Ohm et al., 2008). There are large variations in the maturity of source rocks within the Barents Sea. From observations from drilled wells maturity is seen to be higher than the average in Haltenbanken and the North Sea (figure 5-4) (Ohm et al., 2008). The higher temperature gradient in the Barents Sea might have a connection with higher maturities. The mature source rocks within the Barents Sea occur on shallower levels than expected, and the source rock may have been exposed to high temperature before uplift and erosion occurred. It may therefore be overmature (Henriksen et al., 2011).

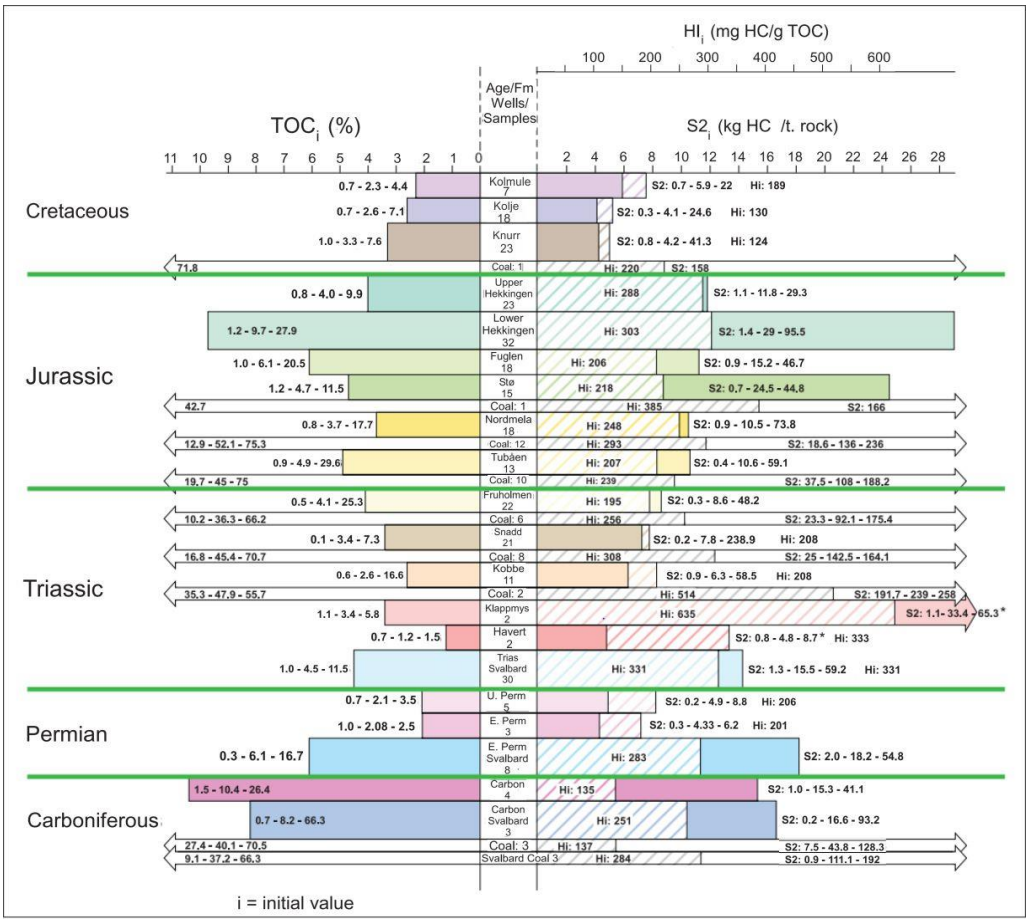

Figure 5- 3. Source rock characteristic diagram from Carboniferous to Cretaceous showing back-calculated initial total organic carbon (TOC), S2, and hydrogen index (HI). The Hekkingen Formation is most profiled source rock and widespread source rock interval generating petroleum both in western and eastern Barents Sea. Few wells have penetrated pre-Triassic source rock intervals, and the extent is also less known. Figure from Ohm et al. (2008).

The uplift and erosion can also explain the high maturities due to the current depths of burial (Ohm et al., 2008). Figure 5-4 shows a fairly similar maturity trend versus depth. However, some places show elevated maturity with depth (Ohm et al., 2008). This might reflect that the uplift level varies within different parts of the Barents Sea (Ohm et al., 2008). Figure 5-5, based on the maturity data from figure 5-4, illustrates which parts of the SW Barents Sea lies within the oil window for the Upper Jurassic Hekkingen Formation, Triassic and Permian. The mature source rocks occur progressively in older sequences towards the east where the uplift and erosion have been greatest (Ohm et al., 2008). Figure 5-4 gives a general indication of the location of mature source rocks in the Barents Sea. Taking the uplift into account, the Hekkingen source rock is deeply buried in the Tromsø Basin and is overmature in the area. In the Hammerfest Basin the uplift has been greater and the oil generation for Hekkingen shale is mature (Dore & Jensen, 1996; Ohm et al., 2008). There are three potential source rocks in the Hammerfest Basin. The Late Jurassic anaerobic shales of Hekkingen Formation, the Early

Jurassic Nordmela Formation and the Triassic shales (Ohm et al., 2008). The Triassic source rock is buried deeply in the basin and may have generated considerable volumes of gas. The Hekkingen and Nordmela formations are mainly within the oil window towards the northwest of the Hammerfest Basin (Linjordet & Olsen, 1992). The Fuglen- and Hekkingen Formation within the Hammerfest occur in dense shale intervals with high content of organic material (Linjordet & Olsen, 1992; Dore, 1995; NPD 2014). Well 7121/4-1 is located a bit north of the Snøhvit gas field, where the Nordmela Formation consists of alternating very fine to fine-grained sandstones, siltstones and mudstones accompanied by thin coal and shales (Linjordet & Olsen, 1992). The Nordmela Formation has poor reservoir quality but forms a good cap rock for gas discovery in the lower Tubåen formation. The Nordmela Formation was deposited in a coastal or delta plain environment with possible active feeder channels or tidal channels. This formation becomes more marine towards the west within well 7120/5-1 (figure 5-5) (Linjordet & Olsen, 1992). Well 7120/8-1 within the dataset ST8320R00 is located in the Snøhvit Field area (figure 5-6), where relatively dry gas was discovered in sandstone of the Middle to Early Jurassic Stø Formation (NPD, 2014). In early Cretaceous clay was deposited and forms mudstones with good source rock potential. The shales within Late Jurassic Hekkingen Formation also have good potential for generating gas and oil (NPD, 2014).

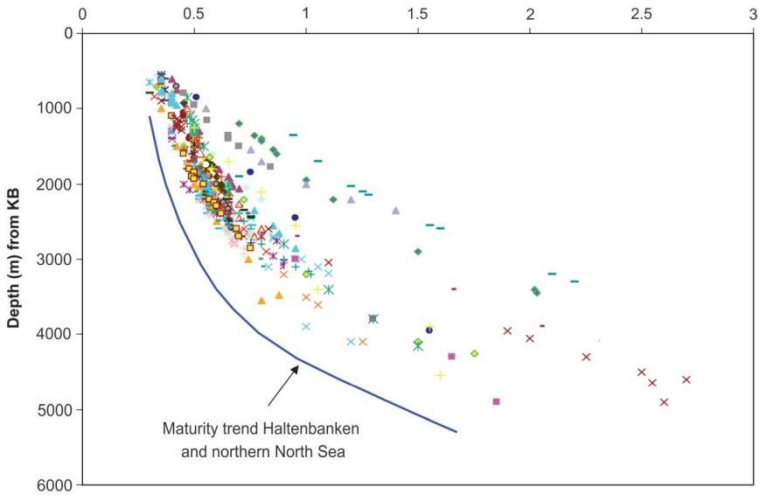

Figure 5-4. Development of the maturity of the source rocks from the northern North Sea and Haltenbanken compared to the maturity from well data in the Barents Sea. Figure from Ohm et al. (2008).

The geological history of the Barents Sea has most likely resulted in re-migration of hydrocarbons over larger areas. This may have caused hydrocarbons to migrate away from the source rock and into new accumulation areas together with hydrocarbons coming from other source rocks, typically suggesting that one is not able to trace back to one type of source rock (Ohm et al., 2008; Henriksen et al., 2011).

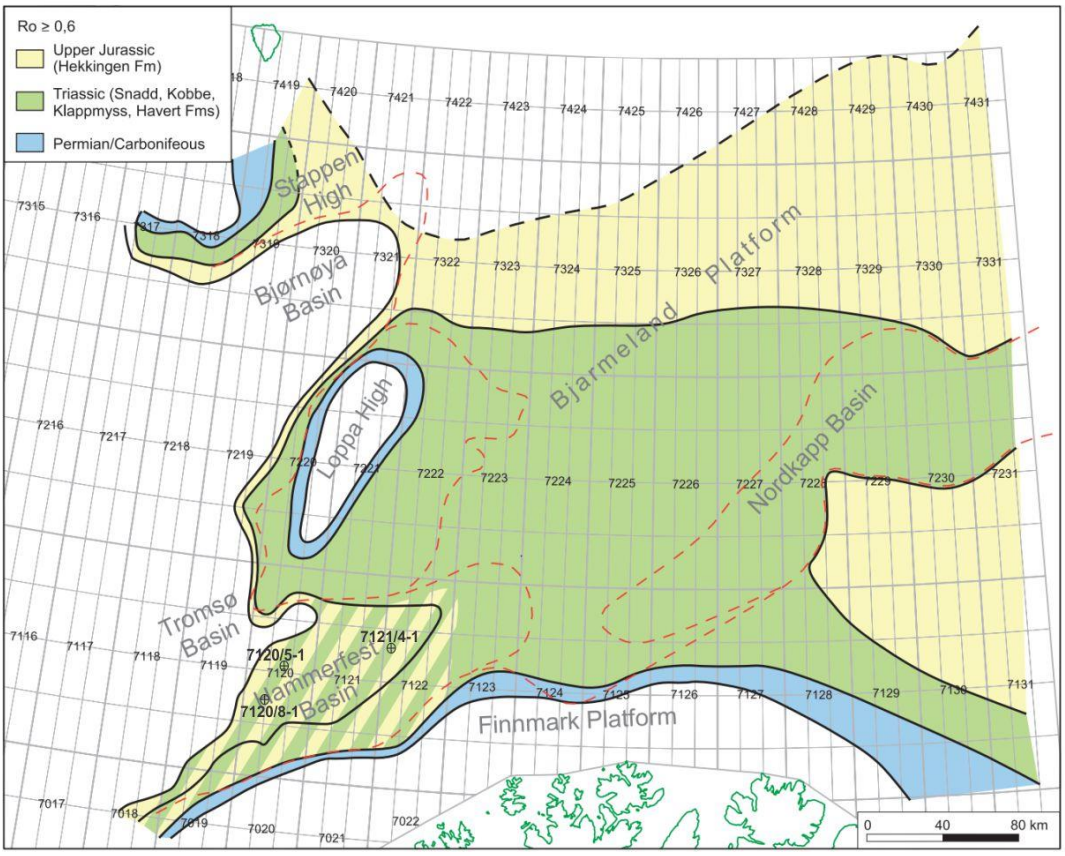

Figure 5- 5. Tentative maturity map where the Permian, Triassic, and Jurassic strata are oil mature, given that such are present in the source quality. The map is based on data from the maturity from wells and semiregional maturity trends, and depth maps. Well within the Hammerfest Basin. Figure is modified from Ohm et al. (2008)

As mentioned, there is a tendency for source rocks to be overmature within the Barents Sea. However, due to the uplift and erosion within the Hammerfest Basin the source rocks are within the oil and gas window. Within well 7120/8-1 in dataset ST8320R00 the source rocks of kerogen II were mature in the lower part of the Hekkingen Formation (NPD, 2014). Further west within dataset ST8320R00, well 7120/7-2 is located where the different formations are buried a bit deeper. The shale within in the Hekkingen Formation shows good potential source rocks for gas and condensate but the well was immature all through. Hydrocarbon accumulations where discovered in sandstone of the Middle Jurassic Stø Formation where potential fluid migration could have occurred (NPD, 2014; Ohm et al., 2008). The well 7120/5-1 just south for survey LN0901 also shows good source rock potential for gas and oil within shale of the Hekkingen Formation. The Stø and Nordemela Formations were water bearing but with good oil shows (NPD, 2014). The observations from the wells within the study area show potential source rocks and reservoirs which match the explanation of uplift and erosion as well as the re-migration of fluids due to tilting (Ohm et al., 2008).

5.2.2 Fluid flow along chimneys

Acoustic masking in seismic data may be an important indicator of the occurrence of the fluid migration (Løseth et al., 2009; Vadakkepuliyambatta et al., 2013). Gas is scattering energy that can result in low amplitude and acoustic wipe-out zones as in figure 4-20 and 4-22. Areas with acoustic masking zones can be observed within different levels of high amplitude anomalies with limited lateral distribution. The interpreted acoustic masking in the datasets have a lower termination within the Hekkingen- and Knurr Formation, between ~1900 ms (TWT) and ~2200 ms (TWT) for survey ST8320R00 (figure 4-20 and 4-22), and between ~2100 ms (TWT) to ~2300 ms (TWT) for survey LN0901 (figure 4-23 and 4-25) These coincide with the loctation of faults within Hekkingen. However the exact lower termination is difficult to determine because of acoustic masking that occurs below many of the larger faults (figure 4-20, 4-21). As described in section 5.2.1 the source rock in the Hammerfest Basin mainly occurs within the Hekkingen Formation, Nordmela and the Triassic deposits. However, the acoustic masking in the Hekkingen Formation may not be the source for fluid migration; the source may have originated from deeper buried units as the Nordmela or Triassic shales.

Many of the vertical zones of acoustic masking coincide with faults, which I will discuss further below. However, few of the acoustically masked zones have a semi-circular to elliptical shape in plan view, interpreted as chimneys and vertical focused fluid flow structures (figure 4-20, 4-21). The internal structure and extent of acoustic masking varies both in size and shape. The chimney in figure 4.20 shows a near oval-shape in lateral extent, slightly varying with depth. The chimneys in figure 4-21 show a vertical zone of acoustic masking with push-down effects.

The push-down effects observed within the chimney structures decreasing size from shallow to deeper stratigraphic levels. This may indicate changes in the amount of gas within the chimney (figure 4-20). The largest push-down effect is observed near high amplitude anomalies in the upper part of the chimney which may suggest that gas accumulates at top of the chimney. In the uppermost sequence of the leakage zone, high amplitudes are observed laterally adjacent to the acoustic masking (figure 4-20). This might indicate that the vertical migration stops due to sealing in the lithologies and the fluids accumulating at this point may be forced to migrate laterally. The shallowest accumulation zone was found at ~560 ms (TWT) (figure 4-20) and at ~700 ms (figure 4-21). This indicates that the fluid migration has most likely occurred after the Torsk Formation was deposited in the Upper Paleocene time.

The upper part of the Torsk Formation acts as a seal where no high amplitudes are observed above, but there may have have occurred limited migration to the seafloor since pockmarks are occasionally observed (4-14b, 4-29).

Smaller narrower seismically blanked zones might be interpreted as pipe structures (Løseth et al., 2009) but could also be the result of acoustic masking beneath high amplitude anomalies in shallow strata (figure 4-22). The high amplitude anomalies are interpreted as bright spots and indicate the presence of fluids and/or gas in the system. The pipes also originate at a fault at the top of the Hekkingen Formation and reach up to the upper part of Torsk Formation.

5.2.3 Fluid flow along faults

As previously mentioned the SW Barents Sea has been affected by the Cenozoic uplift and erosion where several faults have been reactivated. Faults may act as a seal or a fluid migration pathway. Fault zones may be filled with cement or ductile clay where they occur as good seals, but can act as migration pathway if the fluid pressure increases (Løseth et al., 2008). During faulting granular material causes cataclasis and the porosity changes. This process may affect the quality on the reservoir rocks and fluid flow may occur (Antonellini & Aydin, 1994). If cementing is caused by fluids that contain minerals along the fault plane it can cause the faults to clog up and migration will stop. This may cause a change in the pressure in the reservoir and if the pressure exceeds the fracture pressure new zones with cracks will be formed that can cause a new fluid migration (Roberts and Nunn, 1995).

The deep-seated faults that were reactivated during the Upper Jurassic and the Hekkingen Formation can be the source for the fluid migration (figure 5-1). The orientation and the vertical length of the faults vary. Some faults truncate within the Lower Cretaceous formations, the Kolje or Kolmule Formation while others may penetrate into Upper Paleocene and Torsk Formation or even to the seabed. An indication for fluid migration here is the presence of acoustic masking in a narrow zone along the fault planes. Other evidence of fluid migration includes high amplitude anomalies along the faults, structure fitting high amplitude anomalies within the fault hanging walls and bright spots in shallower strata where the faults terminate. Thus, I hypothesize that these fault are most likely active vertical fluid migration pathways.

The fluid leakage has its source in the deeper-seated faults but may branch into shallower faults at the top of Lower Cretaceous (figure 5-6) which is observed mainly in the LN0901 survey (figure 4-26).This indicates a link between the 1st order faults and the source of

migration to the shallow bright spots. The reactivated 1st order faults ascend the fluids from the leaking Hekkingen Formation into the Upper Paleocene strata where they can relocate vertically or laterally via the shallow normal faults into the seabed or along the permeable carrier beds of the Torsk Formation.

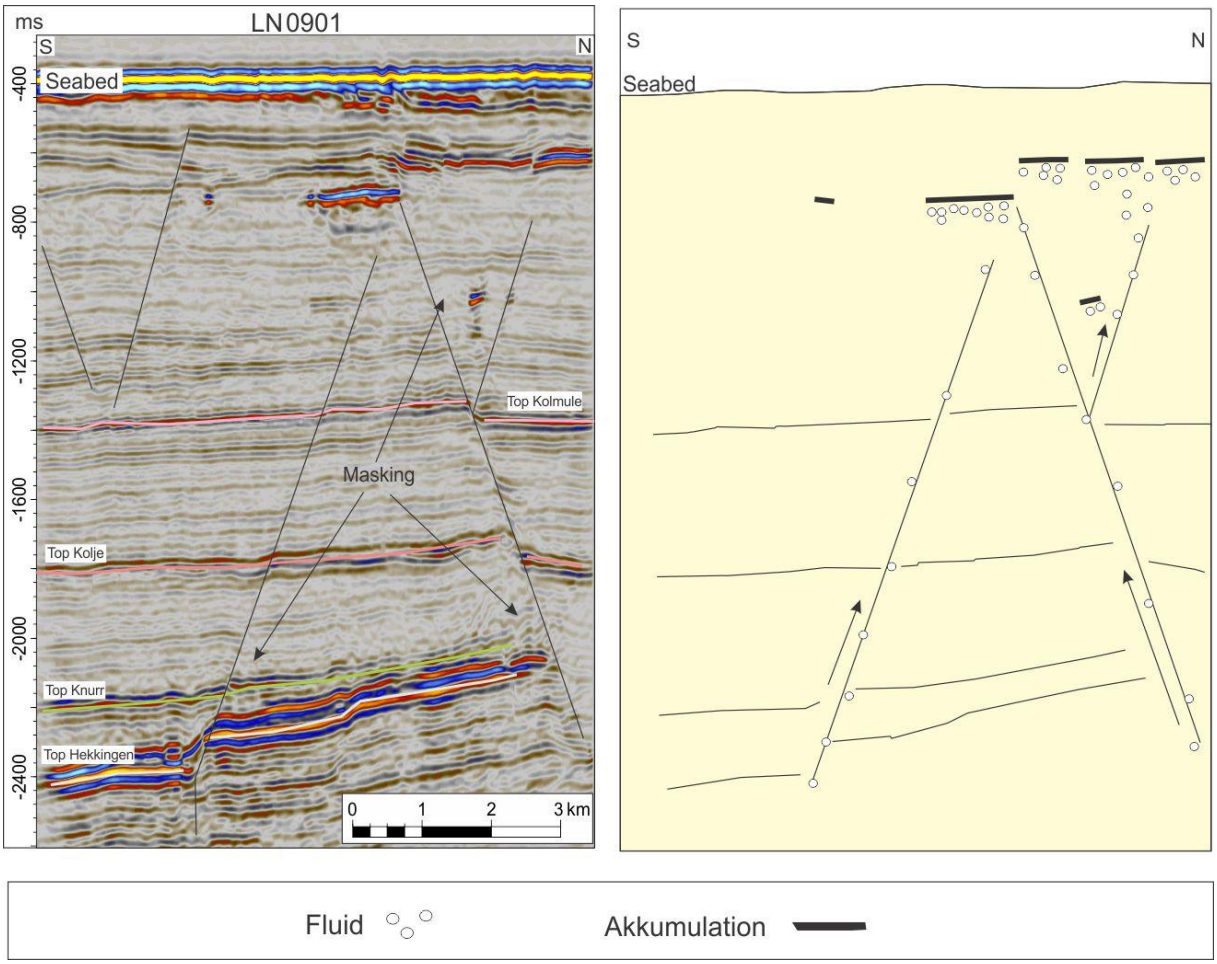

Figure 5-6. Schematic presentation of fault related migration within the fault there occurs acoustic masking that terminates into amplitude anomalies. The example is from section of amplitude anomaly 3 from the result chapter.

The polygonal faults may also be a migration pathway for the ascending fluids linking with the deep-seated faults (figure 4-26, 4-27; Berndt et al., 2003). The polygonal faults were formed during the Cenomanian-Campanian burial followed by the Late Cretaceous uplift (Dallmann, 1999; Ostanin et al., 2012). During the mid-Paleocene deposition of sediments of clastic material came from erosion of topographical highs (figure 5-7). Due to sediment loading the polygonal faults might have been reactivated, with dewatering fluids from the Cenomanian-Campanian interval migrating into younger, Paleocene-Early Eocene strata (Ostanin et al., 2012). Tectonic activity from the Norwegian-Greenland Sea opening (Late Eocene) triggered uplift and reactivation of the 1st order faults. Removal of overburden during the Oligocene-Miocene uplift and the Pliocene-Pleistocene glaciations stressed the

reservoir with gas expansion and phase changes which resulted in episodes of leakage (figure 5-7; Ostanin et al., 2012). The fluids from Hekkingen Formation can migrate through the reactivated 1st order faults and into the Paleocene where open polygonal faults are able to focus fluids to higher stratigraphic levels (figure 5-8; Ostanin et al., 2012). The polygonal faults occur only within the eastern part of dataset LN0901. There is hardly any high amplitude anomalies present within the Torsk Formation above the polygonal faults (figure 4-26). Fluids might have migrated to the seabed (figure 4-31) and formed pockmarks on the seabed.

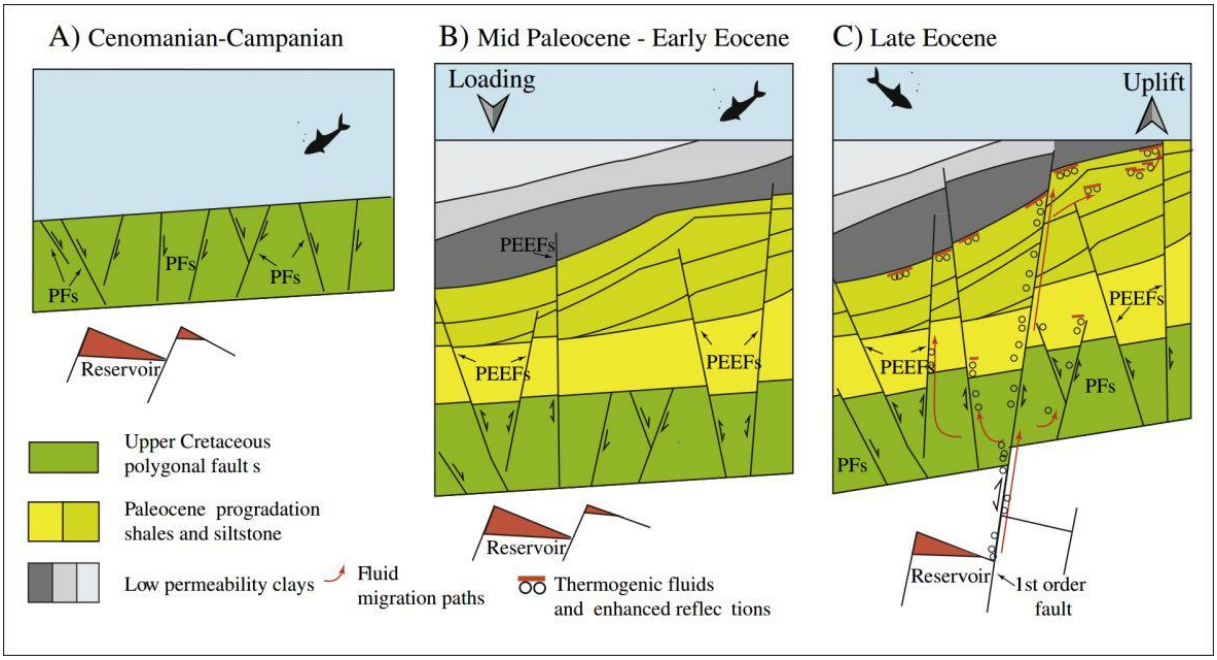

Figure 5- 7. Schematic presentation of the development between polygonal faults and fluid flow. A(Cenomanian-Campanian formation of polygonal faults, followed by uplift and erosion. B) Paleocene-E. Eocene sediments loading results in preferential reactivation of the polygonal faults forming the Paleocene-Early Eocene Faults (PEEF). C) Late Eocene uplift and reactivation of the 1st order faults result in further PEEF reactivation. Fluid migration ascend from deeper seated-faults. From Ostanin et al. (2012)

5.3 Lateral mechanism

The upper part of the Torsk Formation consists of prograding dipping strata representing clinoforms (figure 4-14b). Similar prograding clinoforms were observed by Martens (2009) in the Snøhvit field and Kristiansen (2010) in the south-western flank of Loppa High. In the study area the clinoforms are prograding towards the northwest and increasing seismic amplitudes can be observed stratigraphically upwards (figure 4-14b). The clinoforms terminates either at URU where it occurs or they terminate just beneath the seafloor. In the

middle to upper part of the Torsk Formation the unit is characterized by low angle, shingled clinoforms dipping towards the northwest (figure 5-8; Vorren et al., 1991). Most likely the clinoforms are formed in response to sediment transport from areas north-east of the Hammerfest Basin, indicating that these areas were still uplifted at this time (Vorren et al., 1991). The sedimentation of the Hammerfest Basin was concurrent with the initiation of a marine environment due to a transgression of the central part of the basin. A south-southwesterly progradation occurred from the platform areas north-northeast of the Hammerfest basin, possibly combined with high biogenic rates leading to high accumulation rates. The clinoforms can be a possible migration pathway for fluid and gas through the

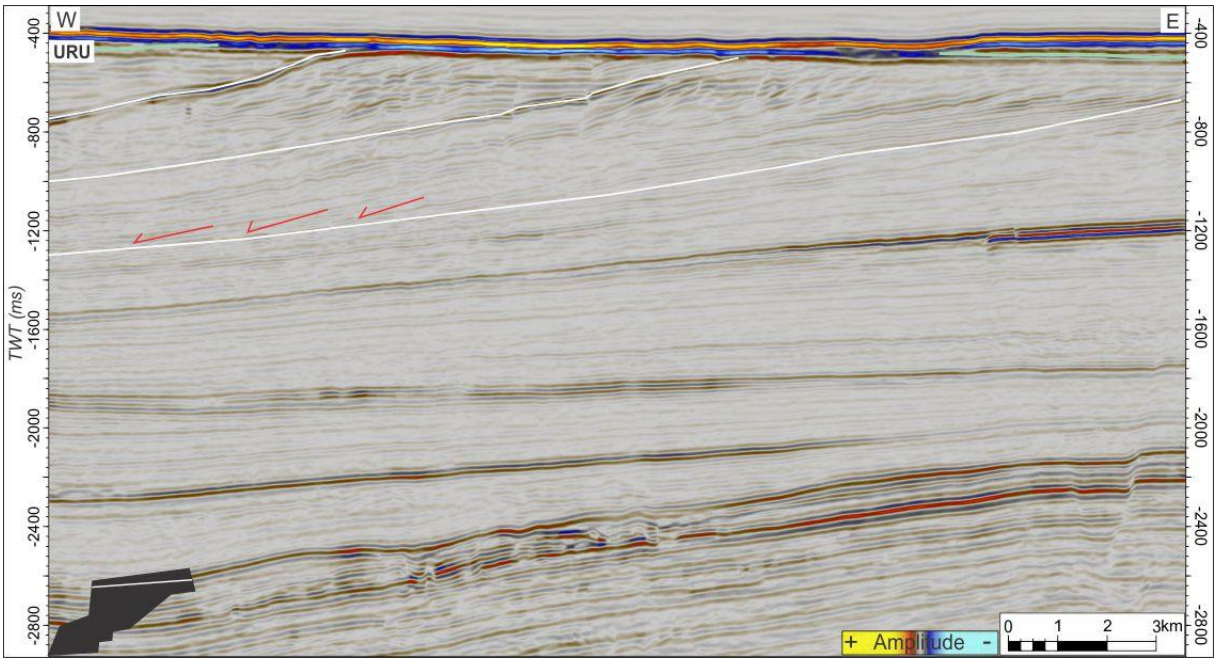

Figure 5-8. Example of prograding strata from the study area (dataset LN0901) which represents clinoforms. The red arrows indicate down-lap of the west-northerly prograding clinoforms.

sediments and lead to shallow gas accumulations. The fluids may originate from the deeper Tromsø Basin and migrate on a continuous permeable bed in contact with impermeable seals. Clinoforms or foresetted reflection configurations originate from prograding slope systems (Veeken, 2007). The shape and angle of the sediments deposited in these slope systems can be influenced by: sedimentation rate, energy level of environment of deposition, position of sealevel and the subsidence rate. The clinoforms observed within dataset as mentioned are prograding towards the northwest with an oblique form. It is suggested that thhis represents a somewhat high-energy slope system and coarser sediments may be incorporated due to high deposition rate (Veeken, 2007)

5.3.1 Lateral fluid migration and fluid accumulation

A large area within the upper part of the Torsk Formation in the middle part of dataset LN0901 is dominated by a zone of high amplitude anomalies (figure 4-14). The southern part of the strong reflections there coincide with larger deep-seated faults (figure 4-4, 4-14) and a chimney structure furthest south of the area (4-20). The acoustic masking occurs from Hekkingen Formation to Torsk Formation where it terminates into high amplitude anomalies. The structure of the area with high amplitude anomalies may suggest that focused fluid flow occurs along the strata and migrates laterally towards northeast and northwest. The bright spots most likely occur beneath impermeable layers. The fluid accumulation from the depth might be larger than the permeable layers can accommodate, so the focused fluid flow may flow laterally at the top of the continuous permeable beds, in contact with impermeable seals. The Late Paleocene to Early Eocene succession is dominated by silt- and claystone, and locally there might be some sandstone horizons (Laberg &Andreassen, 1996; Knutsen & Vorren, 1991). Most likely these are porous and permeable sediments which form the main lateral migration pathways for fluids

Below the high amplitude anomalies in the northeastern and northwestern part shows a zone of acoustic masking with weak but continuous reflection amplitudes occurs (figure 4-14a), which is quite different from the acoustic masking within the chimney structure where it is more chaotic (figure 4-20). The northwestern part shows a channel structure. It might consist of sandy sediments since high amplitudes are observed within the sides and base. Low-permeability, clayey glacial till and/or marine sediments might act as a seal for the hydrocarbon accumulating in the more permeable sand (Andreassen et al., 2007a).

The Torsk formation represents the accumulation area for fluids with the deepest high amplitude anomaly occuring at ~700 ms (TWT). This indicates the migration of fluid occurring after the deposition of the Paleocene-Early Eocene Torsk Formation.

5.3 Presence of gas hydrates

Gas hydrates occur within regions of permafrost and seafloor sediments along the continental margin. There are several areas in the Barents Sea that show development of gas hydrate zones. These systems have been influenced by glacial-interglacial changes, sea-level changes, bottom water temperature, erosion and gas expansion (Chand et al., 2008; Mienert et al.,

2005; Chand & Minshull, 2003). The gas hydrate stability zone (GHSZ) thickness depends mainly on pressure and temperature conditions. Within the Barents Sea the geothermal gradient can be highly variable due to different factors, which are: (1) structures of mud diapirs or salt domes, (2) inversion of the basin resulting in shallow basement rocks, and (3) the presence of faults causing focused fluid flow (Chand et al., 2008).

The stability of gas hydrates are affected by several parameters such as the bottom water temperature, the geothermal gradient, seabed depth, composition of the gas and pore water salinity (Slaon, 1998b). Chand et al. (2008) estimated that the Barents Sea lies within the stability field for gas hydrate of structure II (96% methane, 3% ethane and 1% propane). The GHSZ can vary with a thickness between 50 to 900 m depending on the geothermal gradient and gas composition (Chand et al., 2008). In the study area, the observation of a reflection that runs parallel to the seafloor and cross-cuts other reflections indicates a BSR related to the possible occurrence of gas hydrates. This reflection which lies at a depth between 515 m to 659 m beneath sea level (figure 4-14b). The water depth is 290 m, which would result in a possible GHSZ thickness from 170 m to 250 m below the seafbed (figure 4-14b). These observations occur within the GHZS thickness calculated by Chand et al. (2008).

The heat flow (geothermal gradient) can affect the BGHSZ if the gradient decreases with depth, the thermal conductivity increases with depth, if there is a significant advective of heat transport, or if the seabed temperature decreases (Minshull & Keddie, 2010). The thermal gradient will increase with depth if rapid sedimentation has occurred or the seabed temperature has recently decreased (Minshull & Keddie, 2010). The average geothermal gradient that is observed in the Barents Sea is ~30˚C/km (Laberg et al., 1998).

5.3.1 GHSZ modeling

Vadakkepuliyambatta (2014) has improved the GHSZ modeling in the SW Barents Sea, which shows a much shallower (up to ~400m) GHSZ thickness than previously estimated by Chand et al. (2008). The knowledge of the gas composition can play a major role in increasing the GHSZ thickness. The gas composition data is from exploration wells (figure 5-9) within the Barents Sea (Vadakkepuliyambatta, 2014). Biogenic gases forming the gas hydrates is unlikely since the fluid flow is widespread and related to deep-seated faults (Vadakkepuliyambatta et al., 2013) and gas is predominantly of thermogenic origin.

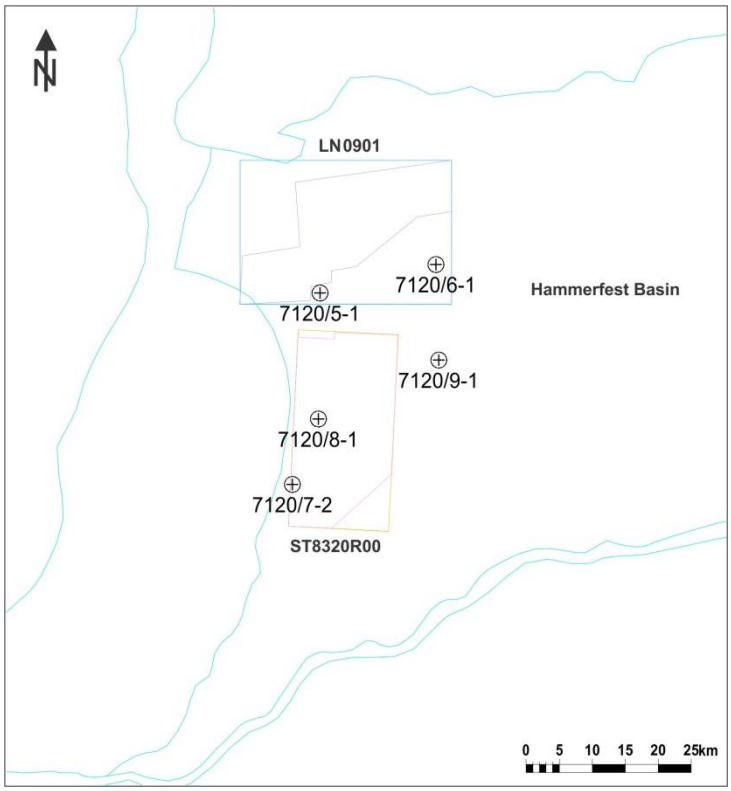

Figure 5- 9. Overview map of the two datasets within the Hammerfest Basin, and five wells in the area.

The thickness of the gas hydrates stability zone has been modeled by using the CSMHYD program from Sloan (1988). The gas composition, pore water with a salinity similar to the seawater (35 SU) and temperature (bottom water temperature of 5˚C) was used from well data (7120/5-1, 7120/6-1, 7120/7-2, 7120/8-1 and 7120/9-1) within the study area (Vadakkepuliyambatta, 2014). The geothermal gradient was based on data collected by Vadakkepuliyambatta, (2014) and is 35˚C/km, which is the average of what has been observed in the five wells listed above.

Five different gas compositions as basis for a gas hydrate formation from the well data have been tested (diagram 1).

- 7120/5-1- 89.96% methane, 2.48% ethane, 0.37%propane, 0.09% i-butane, and 5.32% CO_2.
- 7120/6-1- 82.18% methane, 4.82% ethane, 2.11% propane, 0.66% i-butane, and 10.23% CO_2.
- 7120/7-2- 83.82% methane, 6.26% ethane, 2.6% propane, 0.59% i-butane, and 6.73% CO_2.

- 7120/ 8-1- 87.51% methane, 3.91% ethane, 1.26% propane, 0.30% i-butane, and 6.10% CO_2.
- 7120/9-1- 83.84% methane, 5.42% ethane, 2.41% propane, 0.80% i-butane, and 7.53% CO_2.

	Pressure (Atm)					Depth (m)				
Temperature (k)	7120/5-1	7120/6-1	7120/7-2	7120/8-1	7120/9-1	7120/5-1	7120/6-1	7120/7-2	7120/8-1	7120/9-1
270	13,69	7,37	6,98	9,17	6,87	136	73,2	69,4	91,1	68,3
274	20,28	11,14	10,51	13,71	10,36	201,5	110,7	104,4	136,2	103
278	32,07	17,95	16,91	21,88	16,7	318,6	178,3	168	217,4	166
282	51,98	29,2	27,38	35,47	27,1	516,5	290,1	272	352,4	269,2
286	88,93	49,42	45,78	60,13	45,39	883,6	491	454,9	597,4	451
290	159,79	94,26	84,35	114,86	84,1	1587,6	936,5	838	1493,3	835,6
294	271,47	213,29	188,65	238,23	190,47	2697,3	2119,2	1874,4	2367	1892,5

Table 5.2. Results from the gas hydrate stability modeling from the five wells. The temperature is given in kelvin and the pressure in atmosphere. A graphic outline of the variation of the gas hydrate stability with varying gas compositions is shown in diagram 1.

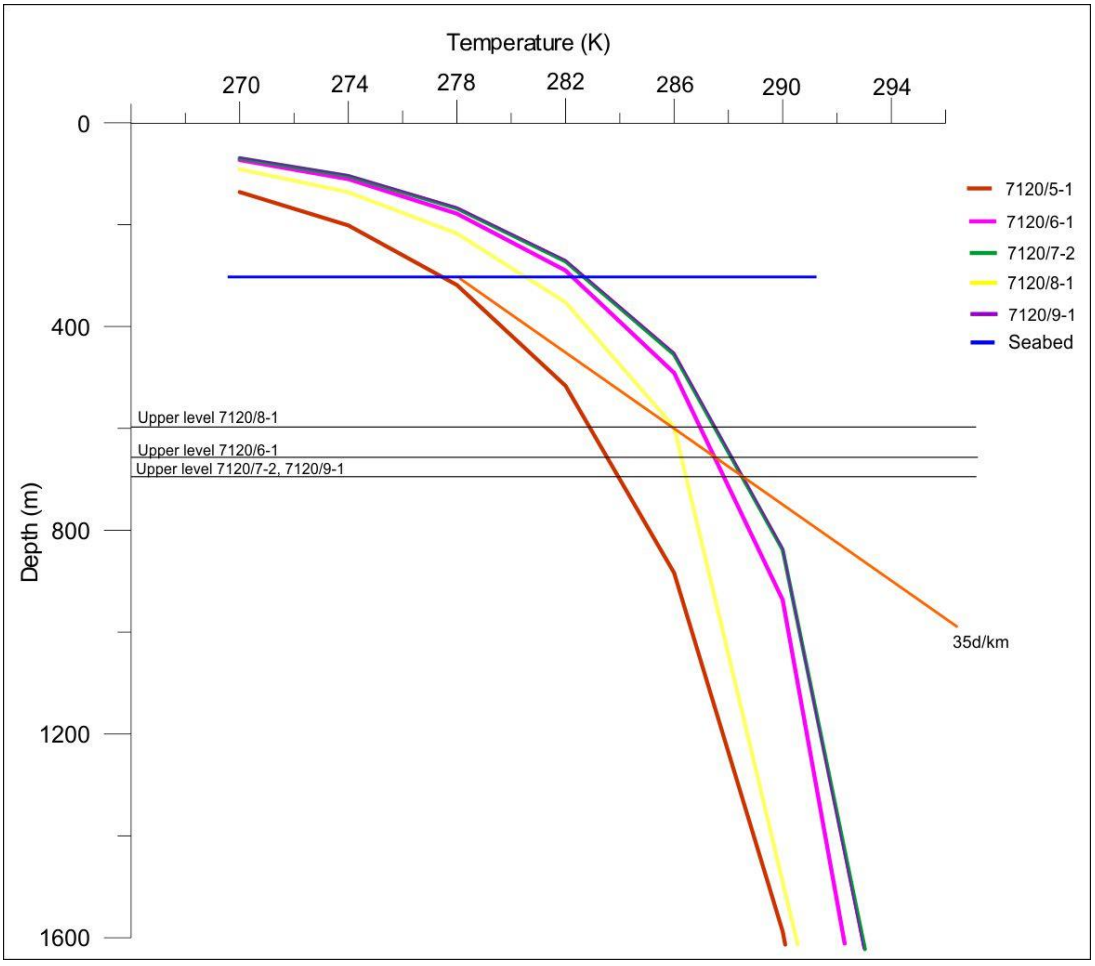

Diagram 1. Gas hydrate stability curves with gas composition from the five different wells using the estimated values of temperature/pressure from the program CSMHYD by Sloan (1998). Gas composition from well data based on Vadakkepuliyambatta et al. (in press). The geothermal gradient was based on data from Vadakkepuliyambatta, (2014) to 35˚C/km.

In diagram 1 the gas compositions from the different wells show that gas hydrates of gas composition from well 7120/5-1 are not stable at today's pressure and temperature (~5˚C and water depth of ~280 m). The possible BSR observed within dataset LN0901 (figure 4-14b) lies very close this well. Given the gas composition, the geothermal gradient of 35˚C/km, bottom water temperature and the water depth, gas hydrates are not stable within this area. Hence the bright spot may be related to another accumulation mechanism. The high amplitude anomalies from this area are mostly likely free gas that is trapped within permeable layers in the upper Torsk Formation.

The gas compositions within the four remaining wells produce a GHSZ from 600 m to 680 m below the sea surface (diagram 1). High amplitude anomalies (figure 4-12, 4-13) with reversed polarity compared to the seafloor are observed within this depth range and may be a gas-hydrate related BSR. Reflections found beneath possible BSRs (figure 4-12, 4-13) show a disturbed, chaotic reflection pattern that are characteristic of gas accumulations. Above the possible BSR, dimmed reflections occur (figure 4-13). Deep-seated faults may have been a conduit for the free gas to migrate to the GHSZ. The upper level of the theoretically predicted BSR is located just on the top of the bright spot (figure 5-10). A small wipe-out zone is observed that intercepts the high amplitude anomaly in the centre (figure 5-10).

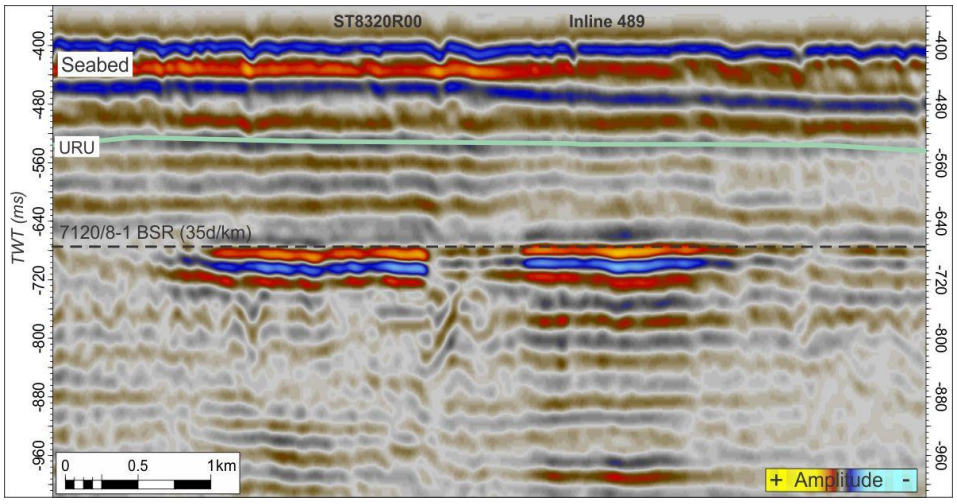

Figure 5-10. The top area of the geothermal gradient of 35d/km is located above the high amplitude anomaly (possible BSR).

5.5 Indication of fluid leakage on the seafloor

Depressions are observed on the seafloor in both of the datasets. In the following, I will discuss occurrence and potential timing.

5.5.1Formation of the depressions

Different processes may have formed the sub-circular to circular depressions occurring on the seafloor.

Glacial erosion

The Barents Sea has been influenced by glacial erosion and deposition several times during the Cenozoic. Icebergs which were detached from glaciers may have been dragged by winds and currents for distances before melting. During transport such icebergs may erode the seafloor with their base, and create iceberg ploughmarks (Andreassen et al., 2007b; Andreassen et al., 2008). These ploughmarks are often curved, V-or U-shaped in cross-profile. They can be followed by long distances, up to tens of km. They are between 100-300 m wide, with a relief of 3-10 m up to 20 km (Andreassen et al., 2008). Such features are also observed in the study area section 4.4.5. Circular depressions where observed within these ploughmarks interpreted as pockmarks (figure 4-29, 4-30, 4-32). Pockmarks can have been created after the ploughmarks occurred, since ploughmarks releases pressure form the subsurface, something that might trigger gas to migrate (figure 5-12; Hovland and Judd, 1988).

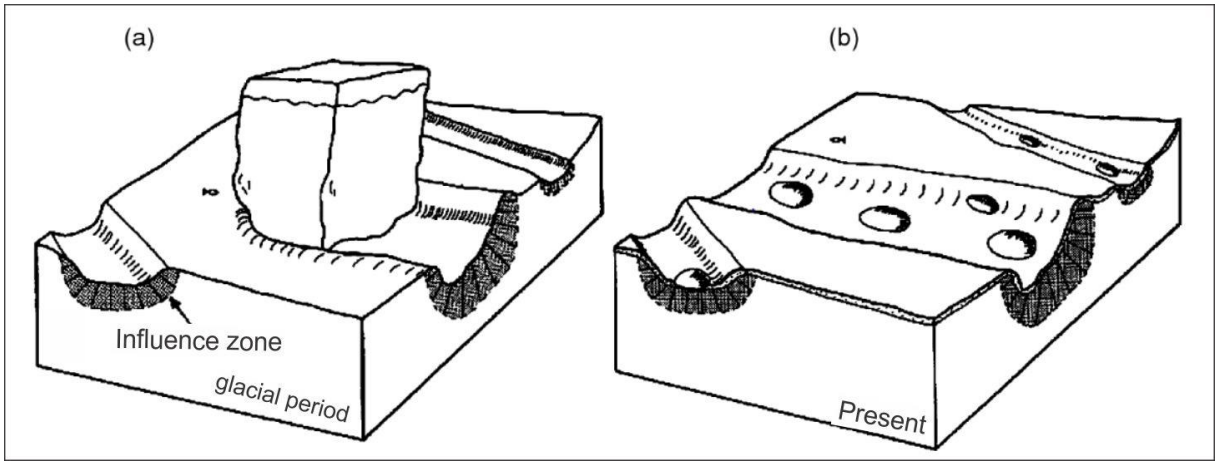

Figure 5-11. (a) An iceberg ploughing through the seabed during glacial time. (b) Present-day situation, with a thin layer of fine-grained sediments drapes over the ice-scoured surface, and pockmarks formed mainly within the furrows. Modified from Hovland and Judd (1988).

Freshwater

Pockmarks can be formed by freshwater streaming through impermeable units. Freshwater can be conducted from land to the seafloor through porous deposition within permeable units (Whiticar and Werner, 1981). This is most unlikely within the study area because of the distance from land.

Pore-water

Pockmarks may be caused by dewatering in soft cohesive sediment on the seafloor. A pressure can build up as it triggers pore-water to stream up to the seafloor and form a depression (Harrington, 1985). This would not cause acoustic masking, however, which is observed in the datasets. Depressions observed are also in general larger in size compared to earlier observed pockmarks (30-40 m diameter, and 2-3 m deep) formed from such dewatering process (Harrington, 1985).

Gas from deeper levels

The Barents Sea is known to have large number of reactivated, open faults due to removal of the overburden by glaciers and the resulting uplift (Nøttvedt et al., 2008; Chand et al., 2012). Fluids from deeper levels are also suggested to follow permeable formations and may be released to the seafloor through pipe-like structure (Chand et al., 2008). There are observed several pipe-like structures just below observed depression at the seafloor. The pipe structures may act as migration pathway within the datasets (figure 4-29, 4-31, 4-34). Most of the depressions within the study are in contact with one or several faults (figure 4-29, 4-30, 4-31). These faults penetrated from deeper levels but some observed shallower faults that possibly terminate at the seafloor. The faults may act as the fluid migration pathway. Chains of pockmarks are often related to such migration (Hovland et al., 2002). The pockmarks within dataset LN0901 occur mostly as single depressions, while in dataset ST8320R00 the pockmarks are more prevalent and occur both as singles and groups (figure 4-32) Single depressions occur within the deepest part of survey LN0901 (figure 4-31). The identified leakage features within this area are connected to seismic pipes, deep-seated as well as polygonal- and shallow faults (4-4, 4-8, 4-10 and 4-31). The deep-seated faults act as migration pathway, ascending fluids from the Jurassic-reservoir, which are then transported through the Lower Cretaceous polygonal- and shallow intra-Paleocene-early Eocene faults (Ostanin et al., 2013). Since no high amplitude anomalies are observed, fluids are possibly ascending directly to the seabed.

Acoustic masking and bright spots are observed beneath several of the pockmarks (figure 4-29 to 31, 4-33 to 34). Below three of the depressions push-down effects are also observed (figure 4-29, 4-30, 4-32). These observations may indicate existence of gas just beneath the pockmarks.

Pockmarks associated to gas anomalies

The upper level of high amplitude anomaly 1, interpreted as a potential BSR indicating the base of GHSZ (figure 5-10), and composed from deep-seated faults as a migration pathway and leads to a seismic pipe above the amplitude anomaly and into the seabed and forms a pockmark (figure 4-28, 4-32). The acoustic pipes may have formed as a result of capillary seal failure (Cathles et al., 2010; Ostanin et al., 2013). Since leakage along faults may occur periodically, some faults may have been leaking and conducting fluids more than once (Ostanin et al., 2013). This might cause repeated overpressure buildups which could have triggered the fluid escape events observed on the seafloor (4-29, 4-34, 5-12; Ostanin et al., 2013). Within the southern part of amplitude anomaly 3, depressions on the seabed are formed within the ploughmark (figure 4-14b and 4-29). Shallow and reactivated deep-seated faults penetrate the amplitude anomaly and leads to seismic pipes (figure 4-29, 5-12). The location of the shallow faults relative to the pipes may indicate that they have served as conduits for fluids originating from the underlying free gas zone (figure 4-29, 5-12; Ostanin et al., 2013). Some of the seismic pipes can be traced to the seabed and leading to pockmarks. This implies that amplitude anomalies 1 and 3 are active today (Ostanin et al., 2013). The frequency shadows within the pipes may indicate absorption of high frequencies due to the presence of fluids or gas accumulation (Ostanin et al., 2013).

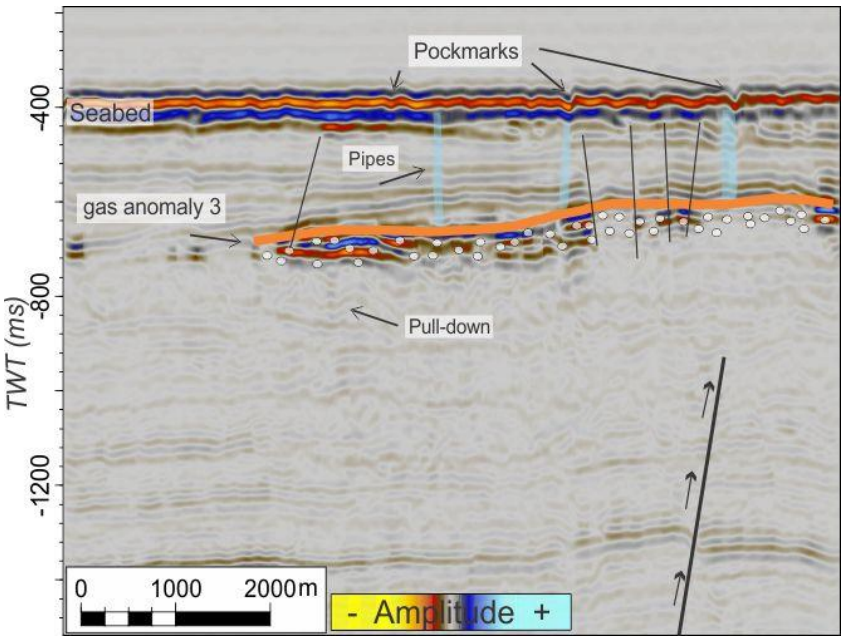

Figure 5-12. Seismic cross section based on figure 4-14b and 4-29 which shows small shallow faults and pipe structure that migrates to the seafloor.

Gas hydrates

The thermodynamic stability of gas hydrates might have been influenced by large scaled erosion and litho- and hydrostatic pressure fluctuated during multiple glacial cycles (Figure 5-13; Laberg et al., 2012; Cavanagh et al., 2006; Ostanin et al., 2013). Since the last glacial period, pockmarks might have formed due to melting of gas hydrates. Rapid destabilization of gas hydrates can make large depressions (figure 5-13; Solheim & Elverhøi, 1993). If gas hydrates are stable they are known to act as good seals but this may change by influence of temperature or pressure (Solheim & Elverhøi, 1993). During the deglaciation the pressure was decreasing and the temperature increasing which may largely have reduced the stable gas hydrate zone (figure 5-13; Chand et al., 2008). Fluids may have migrated through deep-seated faults and may have created a thick layer of gas hydrates which were dependent on the pressure conditions created by the glacier. During deglaciation the pressure conditions decreased and bottom water temperature increased. Gas hydrates were dissociated and migrated to the seafloor to form pockmarks within soft sediments infilling the pockmarks (Hovland & Judd, 1988).

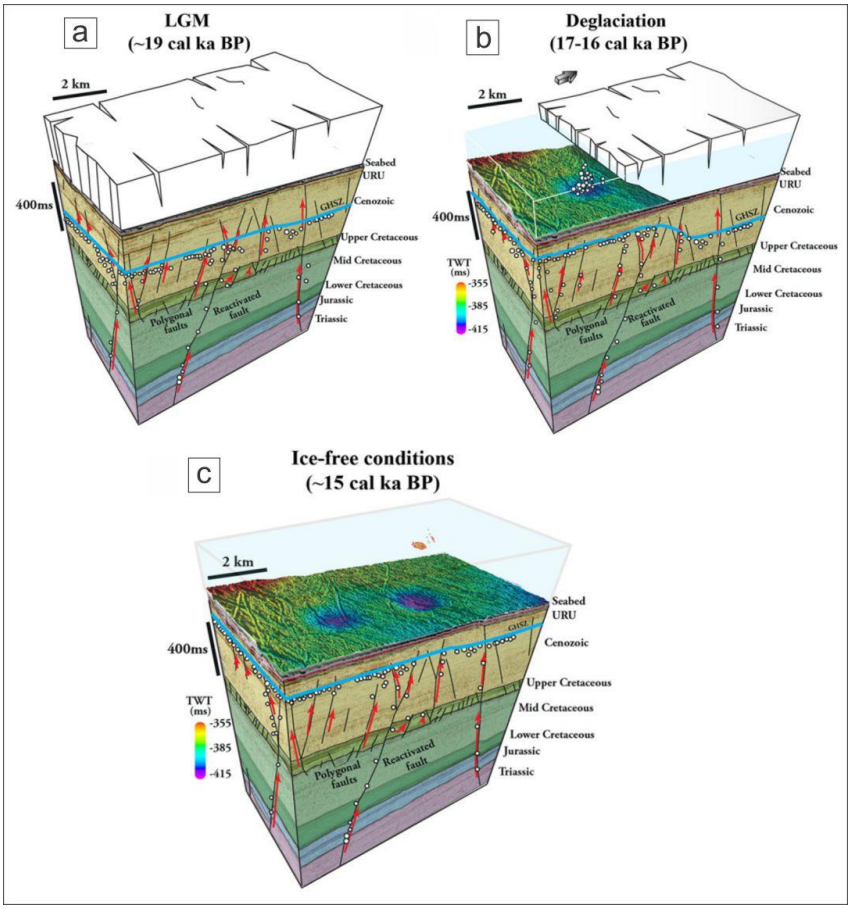

Figure 5-13. a) The ice sheet increases the pressure and formation of gas hydrates. b) The ice sheet retreats, the pressure decreases. c) Gas hydrates destabilise and fluid migration occurs to the seabed. Figure from Ostanin et al. (2013)

Timing of fluid escape due to formation of pockmarks

The main filling from the Triassic source rocks took place between 65 and 30 Ma, while the Jurassic sources contributed between 40 and 2.5 Ma (Rodrigues et al., 2011; Ostanin et al., 2013). Remigration of hydrocarbons where most likely active during this time due to gas expansion, reservoir structure tilt and caprock fracturing in the SW Barents Sea (figure 5-13; Ohm et al., 2008). The reactivation of faults during the Paleocene- early Eocene may have played a larger role for hydrocarbon leakage as the reservoir structures already where filled by this time (Ostanin et al., 2013). As mentioned earlier the preglacial uplift could have generated significant overpressure in the Cenozoic strata due to western margin tilting (Faleide et al., 2008). Due to the preglacial uplift the deep-seated fault may have been reactivated and providing a vertical migration pathways for deeper gas accumulations (figure 5-13; Ostanin et al., 2012; Ostanin et al., 2013). The glaciations might cause the effect of ice loading and unloading of further leakage of water and hydrocarbons due to overpressure development and spill from structures (Cavanagh et al., 2006; Ostanin et al., 2013). Pockmarks are formed within ploughmarks, and from their shape they are interpreted to have been formed after the glacier had melted. The study area became ice-free from 17 to 16 cal ka BP (figure 5-13; Ruther et al., 2011). This implies that the glacial retreat occurred during a time span of thousands of years. Over this time a large flux of thermogenic gas may have been released into the hydrosphere resulting in the observed pockmarks (figure 4-29-32, figure 5-13; Ostanin et al., 2013). The seabed horizons hold evidence that the iceberg ploughmarks and mega scale lineations, which would imply that fluid venting occurred after the ice retreated (figure 4-32; Ostanin et al., 2013).

5.6 Model of fluid migration and accumulation

During the Cenozoic evolution the Barents Sea was affected by the opening of the Norwegian-Greenland Sea, tectonic uplift and erosion, and the onset of glacial cycles (Dimakis et al., 1998: Vorren et al., 1991; Rodrigues Duran et al., 2013). Some of the major consequences of these events may have resulted in: (1) Cessation of petroleum generation, expulsion and migration from source rocks, (2) phase changes including the expansion of gas in reservoir which may result in early spilling of trapped oil, (3) reactivation of faults and breaching seals associated with the reduction of overburden and pressure fluctuations, and (4) leakage of hydrocarbons from the reservoirs to the surface, with possible formation of gas

hydrates and pockmarks (Larssen et al., 1992; Chand et al., 2009, 2012; Ostanin et al., 2012, 2013; Rodrigues Duran et al., 2013). The glacial process led to significant erosion in the Barents Sea and the possible effect of loading and unloading on the petroleum system may have influenced the reservoirs temperature-pressure conditions and potentially risking trap integrity (Cavanagh et al., 2006; Rodrigues Duran et al., 2013). During the erosion up to 1 km of sediments were removed from the Hammerfest Basin. This resulted in pressure changes within the existing reservoirs leading to gas expansion and gas/oil to spill out of the trap (Nyland et al., 1992). Within the study area the reactivation of faults during late Paleocene-Early Eocene (Faleide et al., 2008), fractures in the cap rock and gas expansion gives potential migration pathways into shallower strata. In shallower strata, specially within the Torsk Formation fluids are trapped in porous sediments. The upper Torsk Formation has acted and still acts as an effective caprock.

During the tectonic uplift the main loss of oil occurred due to tilting of the reservoirs. In the Pleistocene, the main loss of hydrocarbons is associated with glacial-interglacial cycles and concomitant erosion (Rodrigues Duran et al., 2013).

The pressure decreases due to ice sheet removal during the deglaciations would have been enhanced as the temperature increased (Laberg et al., 2012; Cavanagh et al., 2006; Ostanin et al., 2013). Gas expansion and overburden erosion may lead to leakage of hydrocarbons and result in fluid escape events due to increased overpressure buildup (Ostanin et al., 2013). The zones of acoustic masking could be a result of fluid leakage through the deep-seated faults. The reactivated faults reaching up to the Cenozoic sediments may have resulted in fluid migration up to the GHSZ.

As discussed in 5.1 the main tectonic events occurred during the Late Jurassic (mainly during the Kimmeridgian tectonic phase) and Early Cretaceous time in the Hammerfest Basin. At this time the Early Jurassic main reservoir units had already been filled (Ostanin et al., 2012). Several events of reactivation of the deep-seated fault occurred from the Late Jurassic to the Upper Eocene, within the Late Cretaceous uplift, and most likely also during the Cenozoic due to uplift and erosion. It is difficult to constrain the timing of faulting within the Paleocene-Eocene period due to denudation history of the Barents Sea. However, as the shallow faults and deep-seated faults appear to be sealed below URU-, fault activity must have ceased by this time (Ostanin et al., 2012). Reactivation may also have occurred during phases of uplift at the end of Eocene and Late Miocene (Bernal, 2009). The fluid may have

migrated due to the reactivation of the deep-seated faults into the Paleocene-Early Eocene strata, where they can then be transferred vertically and laterally via the shallow normal fault and horizontally along the permeable carrier beds of the Torsk Formation (Ostanin et al., 2012).

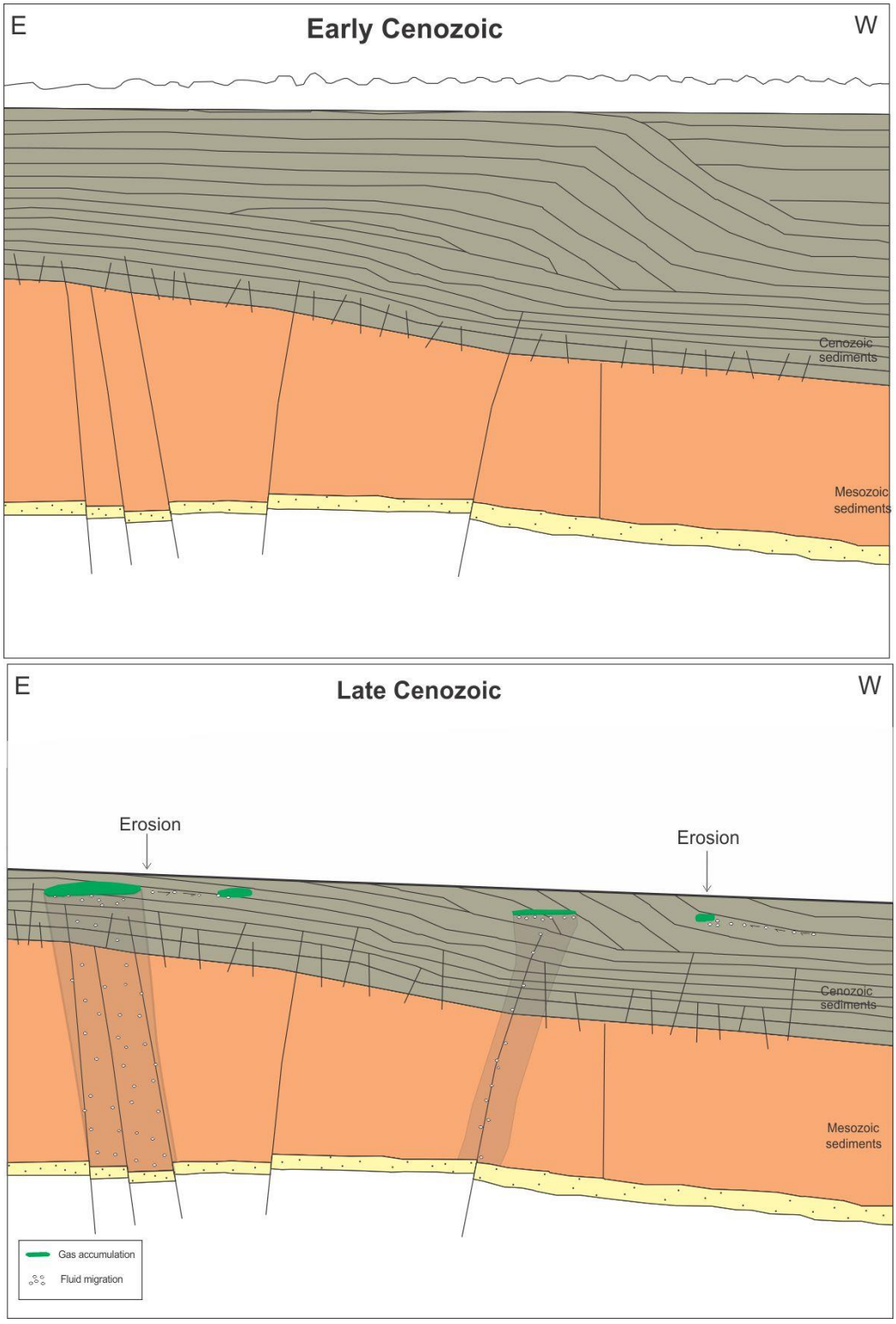

Figure 5-14. Interpretative sketch that shows the situation within the study area in Early Cenozoic and Late Cenozoic, due to profound erosion

6. Conclusion

- Interpretation of 3D seismic data LN0901 and ST8320R00 allowed me to map fluid migration structures, fluid accumulations and fault complexes in the western part of Hammerfest Basin in SW Barents Sea. Both fluid migration features and fault structures show a close link to each other.
- Overall, three generations of faulting events are identified; 1) large deep-seated faults, 2) polygonal faults and 3) smaller shallow faults. The large deep-seated faults are a result of reactivation from tectonic movement in the Late Jurassic- Early Cretaceous period (from c. 160 Ma). The reactivation of fault continued through the Cretaceous and into Cenozoic as a result of the opening of the Norwegian-Greenland Sea. Polygonal faults were caused by reactivation from the dewatering of Late Cretaceous deposits penetrating into lower Paleocene strata. The smaller shallow faults resulted from tectonic activity and/or from unloading and isostatic rebound related to glacial growth and decay.
- High amplitude anomalies at shallower depth and acoustically masked areas are indicators for the presence of fluids, most likely gas, in subsurface sediments. Most of the vertical migration occurs along faults. Gas migrations through the Lower Cretaceous sediment sequences, and mostly accumulates in the Paleocene-Eocene permeable layers (of the Torsk Formation).
- The high amplitude anomalies are observed in the Tertiary succession just below the URU. These anomalies are interpreted to be free gas accumulations. The Quaternary sediments directly above URU are likely acting as an impermeable barrier, trapping the gas here.
- Gas hydrate modeling in this area suggests that gas hydrates occur within the study area. The GHSZ was estimated from bore hole temperatures and the upper level of the BSR was estimated from ~600-700 m below the sea surface. High amplitude anomalies occurring within this zone might potentially be related to gas hydrates and free gas accumulating beneath the hydrates.
- Pockmarks are observed on the seabed above areas with amplitude anomalies. Pockmarks can form by several processes; however, observations suggest that these pockmarks are formed by gas migrating to the seabed from the underlying gas accumulations. They typically occur within the iceberg ploughmarks suggesting that

these are zones of weakness where the gas penetrates to the seabed. Soft sediments draping the ploughmarks could enhance the pockmark formation.

- The acoustically masked structures and migration fluids seem to be connected to faults and origin from the source rock within the Hekkingen Formation between 2000 ms to 2200 ms TWT in the study area.

7. Referencec

Andreassen, K., Laberg, J. S., & Vorren, T. O. (2008). Seafloor geomorphology of the SW Barents Sea and its glaci-dynamic implications. *Geomorphology, 97*(1-2), 157-177.

Andreassen, K., Nilssen, E. G., & Odegaard, C. M. (2007). Analysis of shallow gas and fluid migration within the Plio-Pleistocene sedimentary succession of the SW Barents Sea continental margin using 3D seismic data. *Geo-Marine Letters, 27*(2-4), 155-171.

Andreassen, K., Odegaard, C. M., & Rafaelsen, B. (2007). Imprints of former ice streams, imaged and interpreted using industry three-dimensional seismic data from the south-western Barents Sea. *Seismic Geomorphology: Applications to Hydrocarbon Exploration and Production, 277*, 151-169.

Antonellini, M., & Aydin, A. (1994). Effect of Faulting on Fluid-Flow in Porous Sandstones - Petrophysical Properties. *Aapg Bulletin-American Association of Petroleum Geologists, 78*(3), 355-377.

Arntsen, B., Wensaas, L., Loseth, H., & Hermanrud, C. (2007). Seismic modeling of gas chimneys. *Geophysics, 72*(5), Sm251-Sm259.

Badley, M.E. (1985). *Practical seismic interpretation*. Boston: International Human Resources Development Corporation.

Bernal, A. (2009). *Controls on Economical Hydrocarbon Accumulations in the Askeladd Field, Barents Sea–A Post-mortem Fault Seal Analysis.* Paper presented at the Fault and Top Seals: from Pore to Basin Scale.

Berndt, C. (2005). Focused fluid flow in passive continental margins. *Philosophical Transactions of the Royal Society a-Mathematical Physical and Engineering Sciences, 363*(1837), 2855-2871. doi: DOI 10.1098/rsta.2005.1666

Berndt, C., Bunz, S., & Mienert, J. (2003). Polygonal fault systems on the mid-Norwegian margin: a long-term source for fluid flow. *Subsurface Sediment Mobilization, 216*, 283-290. doi: Doi 10.1144/Gsl.Sp.2003.216.01.18

Bjørlykke, K. (2010). *Petroleum Geoscience: from Sedimentary Environments to Rock Physics*. Berlin, Heidelberg: Springer-Verlag Berlin Heidelberg.

Brown, A. R. (1999). *Interpretation of three-dimensional seismic data*: American Association of Petroleum Geologists and the Society of Exploration Geophysicists.

Bulat, J. (2005). Some considerations on the interpretation of seabed images based on commercial 3D seismic in the Faroe-Shetland Channel. *Basin Research, 17*(1), 21-42. doi: DOI 10.1111/j.1365-2117.2005.00253.x

Bunz, S., Mienert, J., & Berndt, C. (2003). Geological controls on the Storegga gas-hydrate system of the mid-Norwegian continental margin. *Earth and Planetary Science Letters, 209*(3-4), 291-307. doi: Doi 10.1016/S0012-821x(03)00097-9

Caine, J. S., Evans, J. P., & Forster, C. B. (1996). Fault zone architecture and permeability structure. *Geology, 24*(11), 1025-1028.

Cartwright, J. A., & Dewhurst, D. N. (1998). Layer-bound compaction faults in fine-grained sediments. *Geological Society of America Bulletin, 110*(10), 1242-1257. doi: Doi 10.1130/0016-7606(1998)110<1242:Lbcfif>2.3.Co;2

Cartwright, J., Huuse, M., & Aplin, A. (2007). Seal bypass systems. *Aapg Bulletin, 91*(8), 1141-1166. doi: Doi 10.1306/04090705181

Cathles, L. M., Su, Z., & Chen, D. F. (2010). The physics of gas chimney and pockmark formation, with implications for assessment of seafloor hazards and gas sequestration. *Marine and Petroleum Geology, 27*(1), 82-91. doi: DOI 10.1016/j.marpetgeo.2009.09.010

Cavanagh, A. J., Di Primio, R., Scheck-Wenderoth, M., & Horsfield, B. (2006). Severity and timing of Cenozoic exhumation in the southwestern Barents Sea. *Journal of the Geological Society, 163*, 761-774. doi: Doi 10.1144/0016-76492005-146

Chand, S., Mienert, J., Andreassen, K., Knies, J., Plassen, L., & Fotland, B. (2008). Gas hydrate stability zone modelling in areas of salt tectonics and pockmarks of the Barents Sea suggests an active hydrocarbon venting system. *Marine and Petroleum Geology, 25*(7), 625-636. doi: DOI 10.1016/j.marpetgeo.2007.10.006

Chand, S., & Minshull, T. A. (2003). Seismic constraints on the effects of gas hydrate on sediment physical properties and fluid flow: a review. *Geofluids, 3*(4), 275-289. doi: DOI 10.1046/j.1468-8123.2003.00067.x

Chand, S., Rise, L., Ottesen, D., Dolan, M. F. J., Bellec, V., & Boe, R. (2009). Pockmark-like depressions near the Goliat hydrocarbon field, Barents Sea: Morphology and genesis. *Marine and Petroleum Geology, 26*(7), 1035-1042. doi: DOI 10.1016/j.marpetgeo.2008.09.002

Chand, S., Thorsnes, T., Rise, L., Brunstad, H., Stoddart, D., Boe, R., . . . Svolsbru, T. (2012). Multiple episodes of fluid flow in the SW Barents Sea (Loppa High) evidenced by gas flares, pockmarks and gas hydrate accumulation. *Earth and Planetary Science Letters, 331*, 305-314. doi: DOI 10.1016/j.epsl.2012.03.021

Cooper, A. K., & Hart, P. E. (2002). High-resolution seismic-reflection investigation of the northern Gulf of Mexico gas-hydrate-stability zone. *Marine and Petroleum Geology, 19*(10), 1275-1293. doi: Pii S0264-8172(02)00107-1.Doi 10.1016/S0264-8172(02)00107-1

Dalland, A, Worsley, D, & Ofstad, K. (1988). *A Lithostratigraphic Scheme for the Mesozoic and Cenozoic and Succession Offshore Mid-and Northern Norway*: Oljedirektoratet.

Dallmann, Winfried K. (1999). *Lithostratigraphic lexicon of Svalbard: review and recommendations for nomenclature use: Upper Palaeozoic to Quaternary bedrock*: Norsk Polarinstitut.

Dimakis, P., Braathen, B. I., Faleide, J. I., Elverhoi, A., & Gudlaugsson, S. T. (1998). Cenozoic erosion and the preglacial uplift of the Svalbard-Barents Sea region. *Tectonophysics, 300*(1-4), 311-327. doi: Doi 10.1016/S0040-1951(98)00245-5

Dore, A. G. (1995). Barents Sea Geology, Petroleum Resources and Commercial Potential. *Arctic, 48*(3), 207-221.

Dore, A. G., & Jensen, L. N. (1996). The impact of late Cenozoic uplift and erosion on hydrocarbon exploration: Offshore Norway and some other uplifted basins. *Global and Planetary Change, 12*(1-4), 415-436. doi: Doi 10.1016/0921-8181(95)00031-3

E., Rodrigues D., di Primio, R., Anka, Z., Stoddart, D., & Horsfield, B. (2013). Petroleum system analysis of the Hammerfest Basin (southwestern Barents Sea): Comparison of basin modelling and geochemical data. *Organic Geochemistry, 63*, 105-121.

England, W.A., Mackenzie, D.M., Mann, D.M., Quigley, T.M. (1987). The movement nad entrapment of petroleum fluids in the subsurface. *Journal of the Geological Society, 144*, 327-347.

Faleide, J. I., Gudlaugsson, S. T., & Jacquart, G. (1984). Evolution of the western Barents Sea. *Marine and Petroleum Geology, 1*(2), 123-150.

Faleide, J. I., Solheim, A., Fiedler, A., Hjelstuen, B. O., Andersen, E. S., & Vanneste, K. (1996). Late Cenozoic evolution of the western Barents Sea-Svalbard continental margin. *Global and Planetary Change, 12*(1-4), 53-74. doi: Doi 10.1016/0921-8181(95)00012-7

Faleide, J. I., Tsikalas, F., Breivik, A. J., Mjelde, R., Ritzmann, O., Engen, O., . . . Eldholm, O. (2008). Structure and evolution of the continental margin off Norway and Barents Sea. *Episodes, 31*(1), 82-91.

Faleide, J. I., Vagnes, E., & Gudlaugsson, S. T. (1993). Late Mesozoic-Cenozoic Evolution of the South-Western Barents Sea in a Regional Rift Shear Tectonic Setting. *Marine and Petroleum Geology, 10*(3), 186-214. doi: Doi 10.1016/0264-8172(93)90104-Z

Fisher, Q. J., & Knipe, R. J. (2001). The permeability of faults within siliciclastic petroleum reservoirs of the North Sea and Norwegian Continental Shelf. *Marine and Petroleum Geology, 18*(10), 1063-1081. doi: Doi 10.1016/S0264-8172(01)00042-3

Fossen, H., Dallman, W., and TB., A.,. (2006). Fjellkjeden går til grunne. Kaledonidene brytes ned; 405-359 millioner år,. In I. B. Ramberg, Bryhni, I., Nøttvedt, A. (Ed.), *Landet blir til-Norges Geologi* (pp. 230-257). Trondheim: Norsk Geologisk Forening.

Gabrielsen, R. H. (1984). Long-Lived Fault Zones and Their Influence on the Tectonic Development of the Southwestern Barents Sea. *Journal of the Geological Society, 141*(Journal of the Geological socity), 651-662. doi: DOI 10.1144/gsjgs.141.4.0651

Gabrielsen, Roy H, Faerseth, Roald B, & Jensen, Lars N. (1990). *Structural Elements of the Norwegian Continental Shelf. Pt. 1. The Barents Sea Region*: Norwegian Petroleum Directorate.

Gabrielsen, Roy H, Grunnaleite, Ivar, & Rasmussen, Eigil. (1997). Cretaceous and tertiary inversion in the Bjørnøyrenna Fault Complex, south-western Barents Sea. *Marine and Petroleum Geology, 14*(2), 165-178.

Gay, A., Lopez, M, Cochonat, P., Séranne, M, Levaché, D, & Sermondadaz, G. (2006). Isolated seafloor pockmarks linked to BSRs, fluid chimneys, polygonal faults and stacked Oligocene–Miocene turbiditic palaeochannels in the Lower Congo Basin. *Marine Geology, 226*(1), 25-40.

Gudlaugsson, S. T., Faleide, J. I., Johansen, S. E., & Breivik, A. J. (1998). Late Palaeozoic structural development of the South-western Barents Sea. *Marine and Petroleum Geology, 15*(1), 73-102. doi: Doi 10.1016/S0264-8172(97)00048-2

Guzzetta, G., & Cinquegrana, R. E. (1987). Fluid Tectonics - a Little Appreciated Facet of Buoyancy Tectonics. *Tectonophysics, 139*(3-4), 321-324. doi: Doi 10.1016/0040-1951(87)90106-5

Han, De-hua, Nur, A, & Morgan, Dale. (1986). Effects of porosity and clay content on wave velocities in sandstones. *Geophysics, 51*(11), 2093-2107.

Hanisch, J. (1984). The Cretaceous opening of the northeast Atlantic. *Tectonophysics, 101*(1), 1-23.

Harland, WB. (1970). Tectonic Evolution of Barents Shelf and Related Plates: ABSTRACT. *AAPG Bulletin, 54*(12), 2484-2485.

Harrington, P. K. (1985). Formation of Pockmarks by Pore-Water Escape. *Geo-Marine Letters, 5*(3), 193-197. doi: Doi 10.1007/Bf02281638

Heggland, R. (1997). Detection of gas migration from a deep source by the use of exploration 3D seismic data. *Marine Geology, 137*(1-2), 41-47. doi: Doi 10.1016/S0025-3227(96)00077-1

Heggland, R. (1998). Gas seepage as an indicator of deeper prospective reservoirs. A study based on exploration 3D seismic data. *Marine and Petroleum Geology, 15*(1), 1-9. doi: Doi 10.1016/S0264-8172(97)00060-3

Henriksen, E, Bjørnseth, HM, Hals, TK, Heide, T, Kiryukhina, T, Kløvjan, OS, . . . Sollid, K. (2011). Uplift and erosion of the greater Barents Sea: impact on prospectivity and petroleum systems. *Geological Society, London, Memoirs, 35*(1), 271-281.

Henriksen, E, Ryseth, AE, Larssen, GB, Heide, T, Rønning, K, Sollid, K, & Stoupakova, AV. (2011). Tectonostratigraphy of the greater Barents Sea: implications for petroleum systems. *Geological Society, London, Memoirs, 35*(1), 163-195.

Hindle, Andrew D. (1997). Petroleum migration pathways and charge concentration: A three-dimensional model. *AAPG bulletin, 81*(9), 1451-1481.

Hovland, M, Gardner, JV, & Judd, AG. (2002). The significance of pockmarks to understanding fluid flow processes and geohazards. *Geofluids, 2*(2), 127-136.

Hovland, M, & Judd, AG. (1988). Seabed pockmarks and seepages: Impact on geology, biology and the marine environment: London. *Graham and Trotman, 293*, 293.

Hovland, M. (2003). Geomorphological, geophysical, and geochemical evidence of fluid flow through the seabed. *Journal of Geochemical Exploration, 78-9*, 287-291. doi: Doi 10.1016/S0375-6742(03)00091-8

Hudec, M. R., & Jackson, M. P. A. (2007). Terra infirma: Understanding salt tectonics. *Earth-Science Reviews, 82*(1-2), 1-28. doi: DOI 10.1016/j.earscirev.2007.01.001

Knies, J., Matthiessen, J., Vogt, C., Laberg, J. S., Hjelstuen, B. O., Smelror, M., . . . Vorren, T. O. (2009). The Plio-Pleistocene glaciation of the Barents Sea–Svalbard region: a new model based on revised chronostratigraphy. *Quaternary Science Reviews, 28*(9), 812-829.

Knipe, R. J. (1997). Juxtaposition and seal diagrams to help analyze fault seals in hydrocarbon reservoirs. *Aapg Bulletin-American Association of Petroleum Geologists, 81*(2), 187-195.

Knutsen, S. M., & Vorren, T. O. (1991). Early Cenozoic Sedimentation in the Hammerfest Basin. *Marine Geology, 101*(1-4), 31-48. doi: Doi 10.1016/0025-3227(91)90061-8

Kopf, A. J. (2002). Significance of mud volcanism. *Reviews of Geophysics, 40*(2), 2-1. doi:

Kristensen, L. (2010). *Fluid migration and shallow gas accumulation on the south-western flank of Loppa High, SW Barents Sea.* Universitet i Tromsø, Tromsø.

Kvenvolden, K. A. (1989). Seabed Pockmarks and Seepages - Impact on Geology, Biology and the Marine-Environment - Hovland,M, Judd,Ag. *Science, 244*(4904), 590-591. doi: DOI 10.1126/science.244.4904.590-a

Kvenvolden, K. A. (1993). Gas Hydrates - Geological Perspective and Global Change. *Reviews of Geophysics, 31*(2), 173-187. doi: Doi 10.1029/93rg00268

Laberg, J. S., Andreassen, K., & Knutsen, S. M. (1998). Inferred gas hydrate on the Barents Sea shelf - a model for its formation and a volume estimate. *Geo-Marine Letters, 18*(1), 26-33. doi: DOI 10.1007/s003670050048

Laberg, J. S., Andreassen, K., & Vorren, T. O. (2012). Late Cenozoic erosion of the high-latitude southwestern Barents Sea shelf revisited. *Geological Society of America Bulletin, 124*(1-2), 77-88.

Laberg, Jan Sverre, & Andreassen, Karin. (1996). Gas hydrate and free gas indications within the Cenozoic succession of the Bjørnøya Basin, western Barents Sea. *Marine and petroleum geology, 13*(8), 921-940.

Larssen, GB, Elvebakk, G, Henriksen, Leif B, Kristensen, SE, Nilsson, I, Samuelsberg, TJ, . . . Worsley, D. (2002). Upper Palaeozoic lithostratigraphy of the Southern Norwegian Barents Sea. *Norwegian Petroleum Directorate Bulletin, 9*, 76.

Ligtenberg, J. H. (2003). Unravelling the petroleum system by enhancing fluid migration paths in seismic data using a neural network based pattern recognition technique. *Geofluids, 3*(4), 255-261. doi: DOI 10.1046/j.1468-8123.2003.00072.x

Ligtenberg, J. H. (2005). Detection of fluid migration pathways in seismic data: implications for fault seal analysis. *Basin Research, 17*(1), 141-153. doi: DOI 10.1111/j.1365-2117.2005.00258.x

Linjordet, A., & Olsen, R. G. (1992). The Jurassic Snohvit Gas-Field, Hammerfest Basin, Offshore Northern Norway. *Giant Oil and Gas Fields of the Decade 1978-1988, 54*, 349-370.

Liu, X. L., & Flemings, P. B. (2006). Passing gas through the hydrate stability zone at southern Hydrate Ridge, offshore Oregon. *Earth and Planetary Science Letters, 241*(1-2), 211-226. doi: DOI 10.1016/j.epsl.2005.10.026

Løseth, H., Gading, M., & Wensaas, L. (2009). Hydrocarbon leakage interpreted on seismic data. *Marine and Petroleum Geology, 26*(7), 1304-1319. doi: DOI 10.1016/j.marpetgeo.2008.09.008

Løseth, H., Wensaas, L., Arntsen, B., Hanken, N. M., Basire, C., & Graue, K. (2011). 1000 m long gas blow-out pipes. *Marine and Petroleum Geology, 28*(5), 1047-1060. doi: DOI 10.1016/j.marpetgeo.2010.10.001

Løtveit, IF, Gudmundsson, A, Leknes, L, Riis, F, & Fjeldskaar, W. (2009). *Effects of glacial erosion on reservoir fluid pressure and fault reactivation in the Barents Sea.* Paper presented at the EGU General Assembly Conference Abstracts.

Martens, I. (2009). *Fluidmigrasjon i Snøhvitområdet-drivmekanismer og strømningsprosesser.* Universitet i Tromsø, Tromsø.

Minshull, T. A., & Keddie, A. (2010a). Measuring the geotherm with gas hydrate bottom-simulating reflectors: a novel approach using three-dimensional seismic data from the eastern Black Sea. *Terra Nova, 22*(2), 131-136. doi: DOI 10.1111/j.1365-3121.2010.00926.x

Minshull, T. A., & Keddie, A. (2010b). Measuring the geotherm with gas hydrate bottom-simulating reflectors: a novel approach using three-dimensional seismic data from the eastern Black Sea. *Terra Nova, 22*(2), 131-136.

Mosar, J., Lewis, G., & Torsvik, T. H. (2002). North Atlantic sea-floor spreading rates: implications for the Tertiary development of inversion structures of the Norwegian-Greenland Sea. *Journal of the Geological Society, 159*, 503-515. doi: Doi 10.1144/0016-764901-093

Mørk, A., & Elvebakk, G. (1999). Lithological description of subcropping Lower and Middle Triasic rocks from the Svalis Dome, Barents Sea. *Polar Research, 18*(1), 83-104.

NPD. (2014a). 7120/5-1- wellbore_exploration. Retrieved 20.04.2014, from http://factpages.npd.no/ReportServer?/FactPages/PageView/wellbore_exploration&rs:Command=Render&rc:Toolbar=false&rc:Parameters=f&NpdId=471&IpAddress=129.242.206.193&CultureCode=en

NPD. (2014b). 7120/6-1 - Wellbore_exploration. Retrieved 20.04.2014, from http://factpages.npd.no/ReportServer?/FactPages/PageView/wellbore_exploration&rs:Command=Render&rc:Toolbar=false&rc:Parameters=f&NpdId=456&IpAddress=129.242.206.193&CultureCode=en

NPD. (2014c). 7120/7-2 wellbore_exploration. Retrieved 20.04.2014, from http://factpages.npd.no/ReportServer?/FactPages/PageView/wellbore_exploration&rs:Command=Render&rc:Toolbar=false&rc:Parameters=f&NpdId=18&IpAddress=129.242.206.193&CultureCode=nb-no

NPD. (2014d). 7120/8-1 Wellbore_exploration. Retrieved 20.04.2014, from http://factpages.npd.no/ReportServer?/FactPages/PageView/wellbore_exploration&rs:Command=Render&rc:Toolbar=false&rc:Parameters=f&NpdId=120&IpAddress=129.242.206.193&CultureCode=en

NPD. (2014e). 7120/9-1 wellbore_exploration. Retrieved 20.04.2014, from http://factpages.npd.no/ReportServer?/FactPages/PageView/wellbore_exploration&rs:Command=Render&rc:Toolbar=false&rc:Parameters=f&NpdId=82&IpAddress=129.242.206.193&CultureCode=en

NPD. (2014f). NPD map. Retrieved 10.02.2014, from http://npdmap1.npd.no/website/NPDGIS/viewer.htm

Nyland, B, Jensen, LN, Skagen, JL, Skarpnes, O, & Vorren, T. (1992). Tertiary uplift and erosion in the Barents Sea: magnitude, timing and consequences. *Structural and tectonic modelling and its application to petroleum geology*, 153-162.

Nøttvedt, A., Johannessen, E. P., & Surlyk, F. (2008). The mesozoic of western Scandinavia and East Greenland. *Episodes, 31*(1), 59-65.

Ohm, S. E., Karlsen, D. A., & Austin, T. J. F. (2008). Geochemically driven exploration models in uplifted areas: Examples from the Norwegian Barents Sea. *Aapg Bulletin, 92*(9), 1191-1223. doi: Doi 10.1306/06180808028

Ostanin, I., Anka, Z., di Primio, R., & Bernal, A. (2012). Identification of a large Upper Cretaceous polygonal fault network in the Hammerfest basin: Implications on the reactivation of regional faulting and gas leakage dynamics, SW Barents Sea. *Marine Geology, 332-334*, 109-125. doi: DOI 10.1016/j.margeo.2012.03.005

Ostanin, I., Anka, Z., di Primio, R., & Bernal, A. (2013). Hydrocarbon plumbing systems above the Snohvit gas field: Structural control and implications for thermogenic methane leakage in the Hammerfest Basin, SW Barents Sea. *Marine and Petroleum Geology, 43*, 127-146. doi: DOI 10.1016/j.marpetgeo.2013.02.012

Petersen, C. J., Bunz, S., Huston, S., Mienert, J., & Klaeschen, D. (2010). High-resolution P-Cable 3D seismic imaging of gas chimney structures in gas hydrated sediments of an Arctic sediment drift. *Marine and Petroleum Geology, 27*(9), 1981-1994. doi: DOI 10.1016/j.marpetgeo.2010.06.006

Polteau, S., Mazzini, A., Galland, O., Planke, S., & Malthe-Sorenssen, A. (2008). Saucer-shaped intrusions: Occurrences, emplacement and implications. *Earth and Planetary Science Letters, 266*(1-2), 195-204. doi: DOI 10.1016/j.epsl.2007.11.015

Reemst, p., Cloetingh, S., & Fanavoll, S. (1994). Tectonostratigraphic modelling of Cenozoic uplift and erosion in the south-western Barents Sea. *Marine and Petroleum Geology, 11*(4), 478-490.

Richardsen, G., Vorren, T. O., & Torudbakken, B. O. (1993). Post-Early Cretaceous Uplift and Erosion in the Southern Barents Sea - a Discussion Based on Analysis of Seismic Interval Velocities. *Norsk Geologisk Tidsskrift, 73*(1), 3-20.

Riis, F., Lundschien, B. A., Høy, T., Mørk, A. , & Mørk, M. B. E. (2008). Evolution of the Triassic shelf in the northern Barents Sea region. *Polar Research, 27*(3), 318-338.

Roberts, S. J., & Nunn, J. A. (1995). Episodic Fluid Expulsion from Geopressured Sediments. *Marine and Petroleum Geology, 12*(2), 195-204. doi: Doi 10.1016/0264-8172(95)92839-O

Ronnevik, Hans, Beskow, Bengt, & Jacobsen, Hans P. (1982). Structural and stratigraphic evolution of the Barents Sea.

Ryseth, A., Augustson, J. H., Charnock, M., Haugerud, O., Knutsen, S. M., Midboe, P. S., . . . Sundsbo, G. (2003). Cenozoic stratigraphy and evolution of the Sorvestsnaget Basin, southwestern Barents Sea. *Norwegian Journal of Geology, 83*(2), 107-130.

Rønnevik, H., & Jacobsen, H. P. (1984). Structural highs and basins in the western Barents Sea. In A. M. Spencer (Ed.), *Petroleum Geology of the Nortdh European Margin* (pp. 19-32). Trondheim: Springer.

Schulmberger. (2011). *Interpretation guide to seismic attributes*.

Selley, Richard C. (1998). *Elements of petroleum geology*. Elsevier Science:Academic.

Sheriff, R.E. (2006). *Encyclopedic Dictionary of Applied Geophysics* (Vol. 4). Oklahoma: Society of Exploration Geophysics.

Sloan, E. D. (1998a). *Clathrate Hydrates of Natural Gases*: CRC Press.

Sloan, E. D. (1998b). Gas hydrates: Review of physical/chemical properties. *Energy & Fuels, 12*(2), 191-196. doi: Doi 10.1021/Ef970164+

Smelror, Morten, Petrov, OV, Larssen, Geir Birger, & Werner, SC. (2009). Geological history of the Barents Sea. *Norges Geol. undersøkelse*, 1-135.

Smith, D. S. (1966). The structure of intersegmental muscle fibers in an insect, periplaneta americana l. *29*.

Smith, Derrell A. (1966). Theoretical considerations of sealing and non-sealing faults. *AAPG Bulletin, 50*(2), 363-374.

Storvoll, V., Bjorlykke, K., & Mondol, N. H. (2005). Velocity-depth trends in mesozoic and cenozoic sediments from the Norwegian shelf. *Aapg Bulletin, 89*(3), 359-381. doi: Doi 10.1306/10150404033

Talleraas, E. (1979). *The Hammerfest basin—an aulacogen.* Paper presented at the Proc. Norw. Sea Symp., Tromsø.

Thrasher, J., Fleet, A. J., Hay, S. J., Hovland, M., & Düppenbecker, S. (1996). Understanding geology as the key to using seepage in exploration: the spectrum of seepage styles. In D. A. Shumacher, M.A. (Ed.), *Hydrocarbon migration and its near-surface expression* (pp. 223-241): AAPG Memoir 66.

Vadakkepuliyambatta, S. (2014). *Sub-seabed fluid-flow systems and gas hydrates of the SW Barents Sea and North Sea margins.* Universitet i Tromsø, Tromsø.

Veeken, P. (2007). *Seismic Stratigraphy, basin analysis and reservoir characterisation. Handbook of Geophysical Exploration: Seismic Exploration* (Vol. 37): Elsevier.

Vorren, T. O., Lebesbye, E., Andreassen, K., & Larsen, K. B. (1989). Glacigenic Sediments on a Passive Continental-Margin as Exemplified by the Barents Sea. *Marine Geology, 85*(2-4), 251-272. doi: Doi 10.1016/0025-3227(89)90156-4

Vorren, T. O., Richardsen, G., Knutsen, S. M., & Henriksen, E. (1991). Cenozoic Erosion and Sedimentation in the Western Barents Sea. *Marine and Petroleum Geology, 8*(3), 317-340. doi: Doi 10.1016/0264-8172(91)90086-G

Wikipedia. (2014). Barents Sea. Retrieved 24.01.2014, from http://en.wikipedia.org/wiki/Barents_Sea

Wiprut, D., & Zoback, M.D. (2000). Fault reactivation and fluid flow along a previously dormant normal fault in the northern North Sea. *Geology, 28*(7), 595-598.

Worsley, D, Johansen, R, & Kristensen, SE. (1988). The Mesozoic and Cenozoic succession of Tromsøflaket. *A lithostratigraphic scheme for the Mesozoic and Cenozoic succession offshore mid-and northern Norway. Norwegian Petroleum Directorate Bulletin, 4*, 42-65.

Wyllie, MRJ, Gregory, AR, & Gardner, GHF. (1958). An experimental investigation of factors affecting elastic wave velocities in porous media. *Geophysics, 23*(3), 459-493.
Ziegler, PA. (1978). North-western Europe: tectonics and basin development. *Geologie en Mijnbouw, 57*(4), 589-626.